Spring 2003

Finite element analysis and statistical modeling of pipeline rehabilitation liners with material imperfections

Wei Zhao

FINITE ELEMENT ANALYSIS AND STATISTICAL MODELING OF PIPELINE REHABILITATION LINERS WITH MATERIAL IMPERFECTIONS

By

Wei Zhao, B.S.

A Dissertation Presented in Partial Fulfillment
Of the Requirement for the Degree
Doctor of Philosophy

COLLEGE OF ENGINEERING AND SCIENCE
LOUISIANA TECH UNIVERSITY

May, 2003

ProQuest Information and Learning Company
300 North Zeeb Road
P.O. Box 1346
Ann Arbor, MI 48106-1346

LOUISIANA TECH UNIVERSITY

THE GRADUATE SCHOOL

05/12/2003
Date

We hereby recommend that the dissertation prepared under our supervision by Wei Zhao

entitled Finite Element Analysis and Statistical Modeling of Pipeline Rehabilitation Liners with Material Imperfections

be accepted in partial fulfillment of the requirements for the Degree of Doctor of Philosophy

Supervisor of Dissertation Research

Head of Department

Department

Recommendation concurred in:

Advisory Committee

Approved:
Director of Graduate Studies

Approved:
Dean of the Graduate School

Dean of the College

GS Form 13
(5/03)

ABSTRACT

Thin-walled plastic liners are routinely used to rehabilitate structurally sound host pipes that have lost their hydraulic integrity. The liner/host pipe structure is treated as a ring encased in a rigid wall. Significant research work dealing with liner stability has been completed in North America and Europe. These research works include laboratory experiments, numerical analysis, and statistical modeling. The objective of this dissertation is to achieve a better understanding of liner buckling phenomenon using the finite element method and statistical analysis.

Short-term liner buckling models have been applied by several researchers to study the influence of liner geometric imperfections on the buckling pressure. Two-dimensional, plane-strain models were predominantly used in these studies. In this research, a three-dimensional liner buckling model was constructed using ABAQUS. This model was applied in studying the influence of liner thickness variations and local circular defects on the buckling pressure.

At first, the thickness variation of the liner wall was modeled in the longitudinal and circumferential directions separately. Next, liners with thickness variations in both directions were simulated. Two factors, the frequency and the magnitude of thickness variation, were studied quantitatively. A comparison between the buckling pattern and

thickness variation pattern was conducted to investigate the relationship between the buckling and thickness.

Local circular defects of reduced thickness and reduced flexural modulus were also modeled using the three-dimensional model. Three aspects, the frequency, the size, and the magnitude of defects were studied with respect to their influence on buckling pressure.

Long-term buckling experiments of liners have shown a large amount of scatter when the buckling time is plotted against the applied pressure. The presence of this scatter and other uncertainties are typically accounted for in liner design by applying a factor of safety. Moreover, an additional "factor of safety" is sometimes implied since the design equation in ASTM F1216 is generally considered to be conservative. The scatter observed in recent long-term, liner buckling experiments conducted at the Trenchless Technology Center was studied to associate reliability factors with selected confidence levels. This work resulted in a set of reliability factors that can be directly applied to the ASTM design equation for the partially deteriorated case. The reliability factors allow a designer to quantitatively estimate the influence of observed scatter on liner design and provide the designer with confidence that their design does not fall within the region of scatter observed in liner buckling experiments. Two separate statistical methods were applied to same set of experimental data, and the results were compared.

APPROVAL FOR SCHOLARLY DISSEMINATION

The author grants to the Prescott Memorial Library of Louisiana Tech University the right to reproduce, by appropriate methods, upon request, any or all portions of this Thesis/Dissertation. It is understood that "proper request" consists of the agreement, on the part of the requesting party, that said reproduction is for his personal use and that subsequent reproduction will not occur without written approval of the author of this Thesis/Dissertation. Further, any portions of the Thesis/Dissertation used in books, papers, and other works must be appropriately referenced to this Thesis/Dissertation.

Finally, the author of this Thesis/Dissertation reserves the right to publish freely, in the literature, at any time, any or all portions of this Thesis/Dissertation.

Author 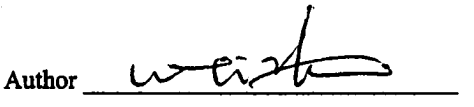

Date 05/14/2003

GS Form 14
(4/03)

TABLE OF CONTENTS

LIST OF TABLES

LIST OF FIGURES

ACKNOWLEDGMENTS

I would like to express my sincere gratitude and appreciation to those who provided me guidance and assistance in the preparation of this dissertation. My heartfelt thanks go to Dr. David Hall for his guidance in every step in this research, for his encouragements every time I was facing difficulties, and for his kindness to be a good friend. Much gratitude is extended to Dr. Raymond Sterling for his long-term support and understanding in all the years I am at Louisiana Tech University. I would like to thank to Dr. Raja Nassar for his time and guidance in finding the statistical truth. Also, I would like to show my appreciation to Dr. William Jordan and Dr. Jay Wang for their support, encouragement, and service on my advisory committee. Sincere acknowledgement is also extended to Dr. Hisham Hegab for his kindness of serving as advisory committee member.

I wish to express my gratitude to the professors and staff at the Trenchless Technology Center and the College of Engineering and Science. This research work would not have been finished without their help.

I also want to say thank you to all my friends and fellow students. Your help made this work easier and more enjoyable. Finally, I would like to thank my parents and brothers in China, your love is with me everyday.

CHAPTER ONE

INTRODUCTION

Piping systems constructed of concrete, clay and cast iron have been in use around the world for more than a century. Many of these systems have deteriorated significantly and are in need of repair. Rehabilitation of existing sewer-pipe system in the United States using "trenchless" methods has become popular over the past 20 years. Trenchless methods, which replace or repair existing pipelines with little or no soil excavation, can reduce damage to existing services and structures, disruption of environmental quality, traffic delays and damage to other facility. Trenchless methods are especially attractive for pipelines located in congested areas.

One method of trenchless repair involves insertion of a tight fitting, polymeric liner into the deteriorated host pipe. Insertion of this liner stops the infiltration of groundwater into the sewer system and stabilizes the soil around the host pipe. Cured in place pipe (CIPP) is the most widely-used method of pipeline rehabilitation, which was introduced into the United States about 20 years ago. With the increasing application of the CIPP lining method, there are also concerns about the long-term performance of the liners that sometimes impede their acceptance. These concerns include the lack of accurate structural design equations, the geometric and material imperfections of the

liners, and the significant scatter observed in liner laboratory tests. These concerns have invoked attention of those both in industry and academia to produce safe and economical liner designs.

1.1 Background and Research Need

The structural deterioration of an underground pipeline typically consists of two situations. The damaged pipe is either partially deteriorated (structurally safe) and can carry the soil and surcharge loads for a considerable time, or it is fully deteriorated and unable to support the soil load above it. Most of time, the damaged pipelines are structurally safe, but with passing time the soil pressure and/or removal of soil around the pipe by infiltration into the pipe can lead to pipe collapse. This research is focused on partially deteriorated host pipes.

The loads which a buried pipe is subjected to are mainly the soil, traffic and external groundwater pressure. The soil and traffic loads act on the pipe through the interaction with the soil. When a rigid sewer pipe is subjected to excessive vertical force caused by the soil and traffic loads, it is likely to crack. If the deterioration of the rigid pipe exceeds 10% of its vertical diameter, it is customary to replace the pipe. For deformation less than 10%, rehabilitation is an attractive option. For rehabilitation applications, the only load subjected to the pipe liner is the groundwater pressure caused by the infiltration through the cracks of the host pipe.

It is well-known that the thin-walled structural elements are susceptible to instability (or buckling) when they are exposed to in-plane compressive stresses. Since the external groundwater pressure induces a compressive hoop stresses in the wall of the

liner, a liner that bas been incorrectly sized (is too thin) may buckle within the host pipe before the expected service life is exhausted. Geometric and material property imperfections of the liner, which may be introduced in the liner curing process, are other significant factors lead to the instability of the liner.

For long-term liner design applications, the liner must be able to withstand the groundwater pressure for the desired design life. The liner may not collapse right after it is installed, and the ground water pressure may cause the polymeric material to slowly deform over time. If the accumulated deformation becomes too great, the liner will collapse. Thus, the time-dependent creep deformation of the liner should be accounted for during the design process.

The current design equations (ASTM F1216-95) used for the buckling pressure of partially deteriorated liners are based on Timoshenko's model for short-term buckling of an unconstrained pipe (Timoshenko and Gere, 1961). The unconstrained ring model has been modified by a factor (termed the "enhancement factor") to account for the deviation between experimental results of constrained liners and theoretical predictions of unconstrained rings. The effect of creep deformation is accounted for using a long-term elastic modulus in place of the short-term elastic modulus. The long-term elastic modulus is typically taken as one-half of the measured short-term flexural elastic modulus. One geometric reduction factor, due to flattening or ovaling of the host pipe, is introduced into the design equation.

In this study, the short-term buckling pressure is studied while investigating the effects of geometric and material imperfections. The long-term liner buckling experimental data is used in the statistical modeling.

During the past 10 years, the Trenchless Technology Center (TTC) at Louisiana Tech University (LTU) has been actively involved in the liner buckling research. The TTC has carried out a variety of experimental, computational and statistical studies to provide utility owners and designers useful information to help them in designing and specifying polymeric liner products. Both long-term and short-term two-dimensional (2D) finite element (FE) simulations have been completed by researchers at TTC. In this study, a three-dimensional (3D) model is constructed and applied to study both geometric and material property imperfections in liners. The statistical modeling is based on the recent long-term liner buckling experiments performed at the TTC.

1.2 Objective and Scope

The objective of this research is to better understand the buckling phenomenon of underground rehabilitation liners and to provide improved guidelines for liner design. A 3D FE model is constructed to study the effects of liner thickness variations and localized circular defects on the liner. Statistical modeling of liner experimental data is used to introduce a reliability factor into liner design.

To fulfill this objective, this research program is comprised the following activities:

- Conduct a literature review of the design models and finite element models used for rehabilitation liner applications.
- Construct a 3D finite element liner buckling model. This three-dimensional model will be verified through a simpler 2D model.

- Investigate the influence of variations in liner thickness on the liner performance. These variations are referred to here as global distributed variations because the liner thickness varies both along the length and circumference of the liner as observed in field specimens. Furthermore, the variation is not limited to a certain section or area of the liner, but is spread all over the liner.
- Investigate the influence of a localized area of material weakness and thickness reduction on liner buckling. This local defect represents a location of incomplete curing or a region of thinning of the liner wall. Both the magnitude of the elastic modulus reduction or thickness and the size of the defect will be parametrically studied.
- Account for the scatter observed in liner buckling experiments by introducing reliability factors into liner design models. The reliability factors will allow a designer to quantitatively estimate the influence of observed scatter on liner design.

CHAPTER TWO

LITERATURE REVIEW

Lining is a trenchless technology used for rehabilitation of sewers and other pipelines. The CIPP technique for pipeline rehabilitation was developed in the United Kingdom in the early 1970s and was transferred to the United States in the late 1970s.

Design of linings has to deal with both safety and usability issues. Loads considered in normal liner design include traffic, soil and water pressure. Depending on the states of host pipe, three normally defined cases are given by Falter (2001).

1. Host pipe is structurally sound with no cracks, but it leaks.
2. Host pipe-soil system is stable, four longitudinal cracks are visible, and deformations are less than 5% of the diameter.
3. Host pipe-soil system not stable for long-term conditions, four longitudinal cracks are visible, and deformations are larger than 5% of the diameter.

The first case where the liner is only designed to sustain the ground water pressure has received much attention in the past decade. It is also the basic assumption of this research. Research on the soil/host pipe/liner interaction system can be seen in Omara's (1997) thesis.

2.1 Theoretical Liner Buckling Model

In general, liner buckling can be seen as the problem of buckling of elastic ring inside a rigid boundary. Based on the Timoshenko's (1960) work on buckling of circular rings under uniform external pressure, a number of research efforts (Soong et al., 1985; Moore, 1988; Omara et al., 2000) have worked to develop improved equations governing the liner buckling process. The following are some of the theoretical models.

2.1.1 ASTM Model

The current CIPP design equation for partially deteriorated pipes is taken from ASTM Designation F1216-95 Appendix XI (ASTM, 1995) as shown in Eq. 2.1. This equation is only valid for buckling with ovality of the host pipe of up to 10 percent. When the host pipe is more than 10 percent out-of-round, special considerations are required (Guice et al., 1994(1)).

$$P_{cr} = \frac{2 \cdot K \cdot E_L}{1-\nu^2} \times \frac{1}{(SDR-1)^3} \times \frac{C}{N} \qquad (2.1)$$

where

$$C = \text{ovality reduction factor} = \left[\frac{(1-\frac{q}{100})}{(1+\frac{q}{100})^2} \right]^3$$

P_{cr} = groundwater load, psi (Mpa)

K = enhancement factor of the soil and existing pipe adjacent to the new pipe (a minimum value of seven is recommended where there is full support of the existing pipe)

ν = Poisson's ration (0.3 average)

SDR= standard dimension ration of CIPP = D/t = outside liner diameter / average liner thickness

q = percent ovality of original pipe

$$= \frac{[MaximumInsideDiameter - MeanInsideDiameter] \times 100}{MeanInsideDiameter}$$

N = factor of safety

E_L = long-term (time corrected) modulus of elasticity for CIPP, psi (Mpa)

2.1.2 Glock's Model

The ASTM F1216 model is based on the buckling theory of free rings, while, in reality, the liners are encased in a rigid host pipe. Consequently, the ASTM model is too conservative because of the inappropriate mathematical model.

Glock (1977) analyzed the stability problem of a circular thin ring encased in rigid boundaries under the effect of external hydrostatic pressure as well as thermal load. Glock's model assumes that there is no friction between the ring and the rigid cavity, and used the nonlinear-deformation theory to develop his model. Glock's model is given as

$$P_{cr} = (\frac{1}{SDR-1})^{2.2} \frac{E}{1-\nu^2} \qquad (2.2)$$

where P_{cr} = critical buckling pressure

E = flexural modulus of elasticity

SDR = Standard Dimension Ratio

= outside diameter / mean pipe wall thickness

t = mean liner thickness

ν = Poisson's ration (0.3 average)

2.1.3 Omara's Model

Omara (1997) developed a modified Glock's model which includes an ovality reduction factor C. Omara's model is given as

$$P_{cr} = \frac{CE}{1-\nu^2}\left(\frac{1}{SDR-1}\right)^{2.2} \tag{2.3}$$

Omara also conducted a series of tests to verify his model. See detailed information about his tests in the Appendix titled Liner Buckling Data. The test results were compared with his mathematical model and the current design practice (ASTM F1216-95). The analysis showed that ASTM F1216-95 underestimated the buckling pressure for all degrees of ovality under study. His mathematical model showed good agreement with the experimental results but still overestimated the critical pressure for all degrees of ovality.

2.1.4 Lu's Model

Lu studied on Omara's model and concluded that Omara's model was incomplete because it neglected the reduction effect of gap on the prediction of critical buckling pressure. Furthermore, he noted that Omara's model neglected the gap effect on the determination of S0/L0 ratio (Lu, 1999). Based on his study, he constructed a modified model given as

$$P_{cr} = C_{oval} \cdot C_{gap} \cdot \left(\frac{1}{SDR-1}\right)^{2.2} \cdot \frac{E}{1-\nu^2} \tag{2.4}$$

where C_{oval} = ovality reduction factor

C_{gap} = gap reduction factor

The ovality and gap reduction factor are defined as

$$C_{gap} = \frac{1}{1 + (1.3 \cdot SDR - 7.7) \cdot R_g} \tag{2.5}$$

where R_g = gap ratio = $\frac{W_g}{R_0}$

= maximum gap size between liner and host pipe / mean radius of inside pipe

$$C_{oval} = e^{\frac{-q}{20}} \tag{2.6}$$

Lu also verified his model using the testing data obtained from short-term buckling tests conducted in Louisiana Tech University (Seemann, 2000) as shown in Table 2.1. The comparison showed that the critical pressures calculated from the proposed equation were close but higher than the actual critical pressures. The reason for this phenomenon is the CIPP local imperfection reduction effect is not considered (Lu, 1999). Lu's model closely resembled the approached used earlier by ElSawy and Moore (1998).

Table 2.1 Comparison of CIPP Critical Buckling Pressure between LTU(1998) Tests and Lu's (1999) Model

Name	SDR	Ovality (100%)	Wg/R0 (Gap ratio 100%)	Actual Critical Pressure(psi)	Critical Pressure from Eq.2.7 (psi)
0% ovality					
1	38.48	0	0.48	134.0	146.98
2	40.45	0	0.44	116.7	131.94
3	40.73	0	0.40	124.7	131.72
4	N/A	N/A	N/A	130.7	N/A
5	39.41	0	0.44	108.7	140.63
2% ovality					
1	40.29	1.9	0.47	105.0	119.81
2	40.83	1.8	0.45	105.0	117.41
3	38.20	1.6	0.48	90.0	138.14
4	38.96	1.6	0.43	98.7	134.00
5	42.47	1.8	0.46	98.0	106.19
5% ovality					
1	39.39	4.1	0.36	75	118.16
2	40.67	4.7	0.46	80.7	102.12
3	41.21	5.4	0.53	67.3	93.04
4	40.70	4.9	0.47	74	100.58
5	39.45	4.5	0.42	78	112.84

2.2 Liner Buckling Experiments

Early large-scale liner buckling tests were performed in Europe in the 1980s. Aggarwal and Cooper (1984) reported a series of test results for encased liners. Their results are still useful because of the large number of samples (49), the large range of standard dimensional ratio (29.9 to 90.2), and the variety of material properties (Young's Modulus varies from 9.6×10^5 to 27.5×10^5 KPa). Their test results are in the Appendix titled Liner Buckling Data.

Liner buckling tests were conducted in North America beginning in the early 1990s. Significant testing programs have been completed at the TTC at LTU. Guice et al. (1994) conducted a serious of tests on commercially available CIPP liners. Both short term and long term (10,000 hrs) tests were performed in this project. The diameter to thickness ratio ranged from 30 to 70 for the samples. The load ratio, which is the ratio of the long term sustained pressure to the critical pressure observed in the short term test, was in the range of 40% to 90%. Results of linear regression analyses, which correlated the external pressure to the buckling time, suggested that the ratio of long-term (50-years) to instantaneous critical pressure would be in the range of 34% percent to 46% percent. This result was smaller than the value of 50% suggested by ASTM specification. These test results are shown in the Appendix titled Liner Buckling Data.

Tests of 15 samples with different ovalities were reported by Omara (1997) in his thesis. Sample geometric factors and test results are shown in the Appendix. After comparing the test results, an ovality reduction factor was introduced into Glock's design equation to take account of the influence of the ovality of the liner.

In the BORSF (Board of Regents Support Fund) tests performed by Straughan and Hall et al. (1999), 180 specimens of the Insituform Enhanced polyester resin were subjected to long-and short-term tests. DR ranged from 40 to 70 for these tests. Six series of tests were conducted, including tests on 8-inch diameter 4.5mm thick liners, 8-inch diameter 5.0mm thick liners, 8-inch diameter 5.5 thick liner, 12-inch diameter 5.5 thick liners, 12-inch diameter 6.5mm thick liner, and 12-inch diameter 7.5mm thick liners. While the liners were allowed to carry the external pressure for maximum of 10,000 hours, most of the liners buckled long before the 10,000 hour limit was reached. Tests results are shown in the Appendix.

Tests of oval liners were also reported by Seeman (2000) in her thesis. Short-term tests were performed on two sets of oval liners with ovalities of 3% and 5%, which were much smaller than the ovality in Orama's tests (5%, 10% and 20%). A liner displacement system, which employed three linear variable differential transformers (LVDTs), successfully monitored the evolving deflections prior to buckling. These test results are shown in the Appendix.

All the tests described above are conducted under room temperature. A series of tests were completed at the TTC that included temperature as a test variable to better predict the long-term liner behavior with feasible lab experiments.

In the past decade, liner buckling tests were conducted in the Civil Engineering Department at Tulane University in New Orleans, Louisiana. Short-term tests on six deforming-reforming liners samples were reported by Chunduru et al. (1996). Three of the samples have an SDR of 32.5 while the other three have an SDR of 26. Air pressure was applied instead water pressure. The test results are shown in the Appendix. From

their tests and theoretical analyses, the authors concluded that host-pipe resistance, ovality, and stress concentrations were factors that have significant influence on the liner critical buckling pressure.

About 200 samples were tested in Tulane according to Bakeer et al. (1999). Tests were established to help determine the influencing parameters including the length to diameter ratio, short/medium/long term test durations, and imperfect field conditions such as ovality, joint offset and structural deterioration leading to lack of liner confinement. Part of their test results are shown in the Appendix. The following conclusions are made by the authors

1. Stresses due to manufacturing and installation of the lining system should be considered when estimating the ultimate buckling resistance in addition to the pipe thickness, diameter, and ovality.

2. The end effects from the testing chamber were effectively eliminated when the length to diameter ratio exceeded 10.

3. The average short-term critical pressures of liners processed in oval casing chambers was between 46% and 55% of similar liners with the same diameter and SDR, but processed in circular chambers.

4. Most liners bulked inward at three different regions: near the two ends and at the center of the setup. None of the collapsed liners, however, returned back to a full U-shape after collapse. In most cases, bulking at the center was on the opposite side of the bulges near the ends of the chamber.

Long term buckling experiments were also conducted to test the creep behavior of HDPE liners in Tulane (Bakeer, 2001). According to their analyses, a creep curve is

generally broken into three specific regions: initial or primary creep, secondary creep, and tertiary creep. A water displacement creep measurement system was used to monitor the creep process. Two groups of tests were performed. Nineteen of twenty liners in Group A failed within 2,328 hours, which the loading pressure is about 50% of critical buckling pressure measured in short term tests. In group B, all twenty (20) liners survived more than 10,000 hours under the loading pressure of 25% to 33% percent of critical pressure. The authors, therefore, recommended one-fourth of short term buckling pressure as the maximum long-term buckling pressure. As for the average creep duration stage, they observed that the primary creep stage was 1.16 hours while the secondary creep stage was 1,733 hours. Part of their tests results are shown in the Appendix.

2.3 FE Modeling

The finite element (FE) method has been used successfully analyze many problems in various fields. It is well known for its flexibility in dealing with complicated geometry and boundary conditions. The FE method has been applied in modeling the liner buckling process by a number of researchers (Zhao, 1999, Lu, 1999, Zhu, 2000, El-Sawy et al., 1998, Falter, 2001). FE modeling plays a powerful role in parameters study, stress/strain visualization, and boundary condition analyses. Most of these researchers verified their modeling with their own tests and other available test data, and satisfactory matching between the modeling and tests were found. The assumptions, parameter definitions, and conclusions used in these studies are summarized below.

2.3.1 Assumptions

1. It is assumed that the liner and the host pipe are long compared with the liner diameter, and that the geometrical, material, and loading conditions do not vary along the liner longitudinal axis. It is thus valid to simplify the problem to two-dimensional a plane strain problem.
2. Friction between the host pipe and the liner is neglected.
3. The host pipe, though deteriorated, is assumed rigid because its stiffness is typically much higher than that of a liner. The interaction between the host pipe and liner strongly influences the behavior of the encased liner.
4. The only loads acting on the liner are the external groundwater pressure and the contact force from the host pipe. It is also assumed that the ground-water pressure increases constantly and is distributed uniformly around the liner (soil force was considered in Falter's modeling).

2.3.2 Parameter Definitions

Standard Dimension Ratio (SDR) is defined as the outer liner diameter D (the average of the mean major and minor diameters for oval liners) to the thickness of a liner as

$$SDR = \frac{D}{t} \tag{2.7}$$

Notice that in some studies, the dimensional ratio (DR) was used to represent the dimension ratio, i.e. DR = SDR-1. DR is an essential factor in CIPP buckling analysis, which has dramatic effects on the critical pressure.

Table 2.2 and 2.3 shows the DR effect on the buckling pressure in the tests and FE modeling, respectively. It is obvious that the parameters related to DR should be measured with extreme care to avoid errors.

It is suggested in LTU test procedures that the thickness of each liner is measured by averaging measurements taken at three locations along the circumference of each end of the liner.

Table 2.2 Short-term Buckling Test Summary with Different DRs (BORSF*)

Mean Diameter(in)	Liner Thickness (in)	DR	Buckling Pressure (psi)
7.8261	0.1495	52.35	82.4
7.6373	0.1611	47.41	106.8
7.7961	0.1770	44.05	117.8

*Board of Regents Support Fund

Table 2.3 FEM Summary with Different DRs (Zhu, 2000)

DR	Ovality	Gap	Buckling Pressure (psi)
30	3%	0.4%	234
45	3%	0.4%	99
60	3%	0.4%	51.4

Annular Gap between Liner and Host Pipe During the cooling phase of the CIPP inversion process, a small radial gap usually develops between the liner and the host pipe. We can define the gap either in even distributed mode or uneven distributed mode. In the even distributed case, the gap is defined as

$$g = \frac{\Delta}{2} \tag{2.8}$$

where Δ is the difference of the inner diameter of the host pipe and the outer diameter of the liner. Fig. 2.1 illustrates this gap.

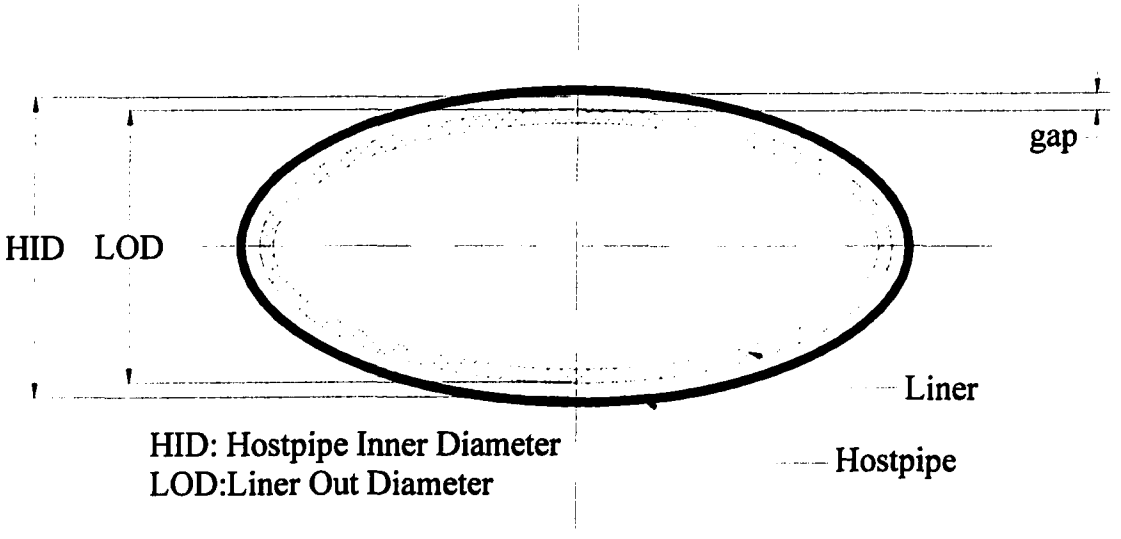

Fig. 2.1 Gap between the Host Pipe and Liner

The relative or dimensionless gap is defined as

$$G\% = \frac{g}{D} \cdot 100 \tag{2.9}$$

The evenly distributed gap is adopted in the two-lobe buckling models as shown in Fig. 2.2.

In the unevenly distributed case, the gap is assumed to have the maximum magnitude Δ at one side and no gap at the opposite side. One-lobe buckling modeling employs the uneven distributed gap assumption as shown in Fig. 2.3.

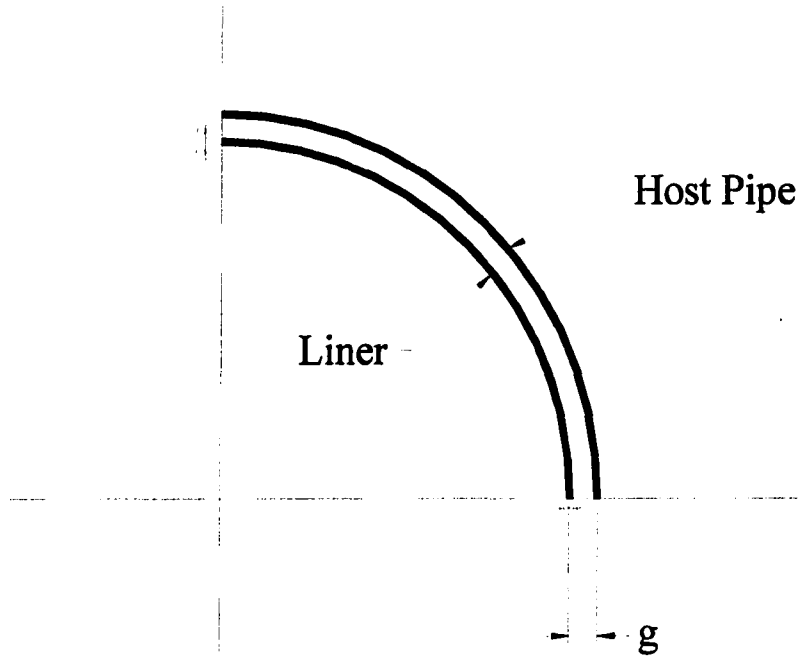

Fig. 2.2 Schematic of the Two-lobe Model with Even Gap

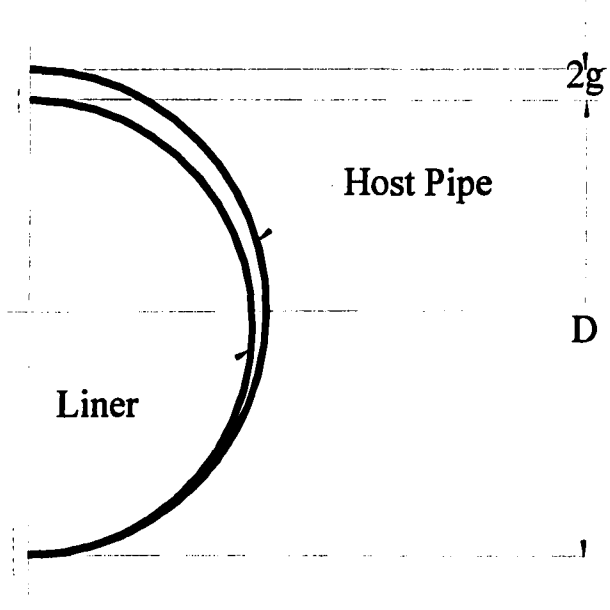

Fig. 2.3 Schematic of the One-lobe Model with Uneven Gap

Seeman (2000) described two methods to measure the gap between the liner and host pipe: the volumetric method and deflection method. She also compared the results of

these gap calculations in her tests and concluded that volume-based gap measurements adequately predict the average gap for liner buckling experiments.

In the volumetric method, the gap was measured by collecting the water drained from the test specimen before pressure was applied. The gap is assumed to be uniform. Volume measurements are equal to

$$Vol = \frac{\pi d_0^{\,2}}{4} \times L - \frac{\pi d_L^{\,2}}{4} \times L \tag{2.10}$$

so that

$$g = \frac{d_0 - d_L}{2} = \frac{d_0 - \sqrt{d_0^{\,2} - \frac{4}{\pi L}(Vol)}}{2} \tag{2.11}$$

where

Vol = gap water volume measurement taken in the experiments (cube inches)

d_0 = inside diameter of the host pipe (inches)

d_L = outside diameter of the liner (inches)

L = length of the host pipe (inches)

g = uniform gap measurement (inches)

Ovality In the present study, the initial ovality of the liner is always assumed to be the same as that of its host pipe. For the steel host pipes, most deteriorated pipes have various degree of ovality (they are not perfectly circular). Another fairly common host pipe shape for concrete pipes is the egg shape. Theoretical analyses, modeling, and test set-up of egg shaped liners is discussed to some extent in the following papers: Thepot (2001), Boot et al. (2001), and Falter (2001).

In the parameter study, the ovality is defined as in the following equation.

$$V\% = \frac{D_{max} - D_{min}}{D_{max} + D\min} \times 100\% \tag{2.12}$$

where

V = ovality of the liner

D_{max} = major outer diameter of the liner

D_{min} = minor outer diameter of the liner

Li et al. (1995) studied on the ovality reduction factor for rigid encased thin rings. The value of the ovality reduction factor C is determined by the following equation.

$$C = \frac{1}{(1+q/100)^{8/5}(1-q/100)^{1/5}} \cdot \tag{2.13}$$

Under the assumption of small deflection of the radius Δr, q is the percentage ovality defined as follows:

$$q = 100 \times \frac{\Delta r}{r_0} \tag{2.14}$$

Compared with the reduction factor given by the ASTM as provided in Eq. 2.1, ASTM reduction factor is a very conservative value. The main reasons are that its derivation only considers the effect of the maximum radius of curvature when a circular ring is changed to an ellipse, and it was derived on basis of an unconstrained ring model.

Zhu (2000) studied the reduction factor in buckling pressures due to ovality, and her FE model results are shown in Table 2.4.

Table 2.4 Reduction Factor in Buckling Pressures Due to Ovality (Zhu, 2000)

		Oval 0%	Oval 3%	Oval 6%
DR=40 Gap=0.25%	P_{cr}	152	132	114
	Reduction Factor	0	0.868	0.75
DR=40 Free Pipe	P_{cr}	17.2	15.6	14.1
	Reduction Factor	0	0.907	0.82

In his thesis Omara (1997) described the process of pressing the host pipes to the desired ovality. Using a 400 ton press, the pipes were pressed into an oval shape. Special jigs were fabricated to ensure that the pipes did not simply flatten out where the press contacted the pipes. To achieve the proposed degree of ovality, each pipe was pressed twice. The first press was provided to bring the pipe's cross-section within the range of the required dimensions. Load was then removed, and the pipe was relinquished to spring up freely. The second press was applied to bring the pipe's cross-section to the required dimensions. The actual magnitude of major diameter and minor diameter can be measured using an LVDT.

Local Intrusion Another geometric parameter studied is a wavelike longitudinal intrusion. As shown in Fig. 2.4, it can be defined by the relative local denting LI and the wavelength ratio S as

$$LI\% = \frac{H}{D} \cdot 100\% \tag{2.15}$$

$$S = \frac{L}{\pi \cdot R} \tag{2.16}$$

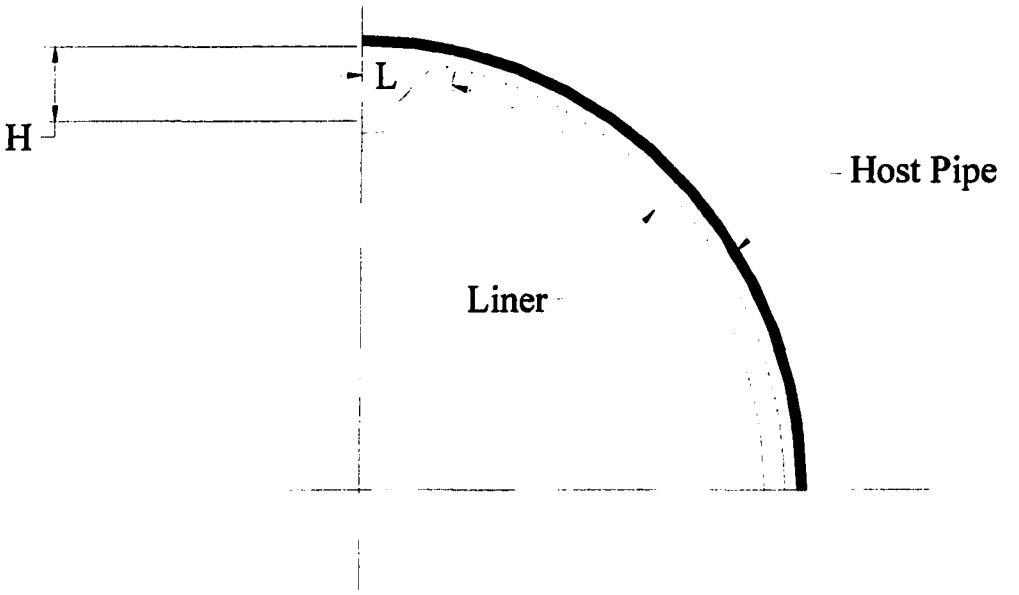

Fig. 2.4 Schematic of Longitudinal Imperfection

Zhu (2000) studied the influence of both the length ratio S and the depth ratio LI on the critical pressure. She found that the length ratio has little effect, while the depth ratio has a significant effect. Her FE modeling is shown in Table 2.5.

Table 2.5 Comparison of the Influence of Length Ratio versus Depth Ratio on the Critical Buckling Pressure (Zhu, 2000)

Type	P_{cr} (psi)	Relative Change
S=0.1 **LI=2.25%**	54	0.0%
S=0.05 **LI=2.25%**	54.2	0.4%
S=0.1 **LI=4.5%**	45.5	15.7%

She also studied the influence of local imperfections combined with other geometric parameters (such as DR, ovality and gap). Her modeling results for an ovality of 0%, a gap of 0.1% and different DRs are shown in Table 2.6.

Table 2.6 FEA Predictions of Critical Buckling Pressures with Different DRs and LI (ovality = 0% and gap=0.1%)

Pipe type	LI=0.0%	LI=2.25%	LI=4.5%
DR=30	266	222	187
DR=45	104	81.8	65.3
DR=60	53.6	40.7	31.2

2.4 Conclusions

In the past two decades, significant pipe liner research has been completed in Europe and North America. The previous three sections gave a brief review on this research. A number of conclusions have been drawn by various researchers and have been accepted both in the academic and engineering field, as listed below.

1. The ASTM F1216-95 model as given in Eq. 2.1 is conservative.

2. Geometric parameters, including DR, ovality, gap, and longitudinal intrusion, have a significant influence on liner behavior. Overlooking the effects of these parameters may result in a system lifetime much shorter than predicted and may produce scatter in buckling tests.

3. The interaction between the liner and the rigid host pipe strongly influences the behavior of the encased liner. Based on the FE modeling and experimental observations, larger contact areas and forces associated with thinner liners leads to

shorter span for the lobe, decreasing deflections and stresses, and increasing critical buckling pressure. Thus, thinner liners have higher enhancement factors.

4. Liner deformation starts from a two-lobe pattern and then transforms to a one-lobe pattern either before or during collapse. In FE modeling, one-lobe and two-lobe buckling models provide the lower and upper limit of buckling pressure, respectively. One-lobe buckling models (which give lower collapse pressures) are recommended for design applications.

5. Several researchers have recommended that future research should include three-dimensional modeling to allow for further parameter variation, including the consideration of variations in wall thickness and material discontinuity.

CHAPTER THREE

3D LINER BUCKLING MODEL SETUP

Several researchers (Zhao 1999, Lu 2000, Zhu 2001) applied 2D FE models to study the effects of geometrical imperfections on liner buckling pressures. In their models, the 3D physical phenomenon was simplified to a 2D FE model based on the plane strain assumption, which is valid because the length of the liner is much longer than its diameter. Although presented in different formats, the geometrical imperfections in their studies can be generalized into three categories: ovality, gap, and longitudinal intrusion. These imperfections can be easily included into 2D FE models.

In this study, the focus is on the effect of imperfections which cannot be modeled using 2D models. One of the most common imperfections is the variation in thickness of a liner, which is observed both along the longitudinal and circumferential directions of the liner. Other defects, such as a circular defect, will be studied using the 3D models as well. In the following sections, some issues concerning the 3D model setup are discussed.

3.1 Model Setup

3.1.1 Basic Liner Geometrical Parameters

The critical buckling pressure of a liner is largely determined by its own geometrical parameters, which include dimensional ratio (DR), annular gap between the liner and host pipe (gap), ovality, and longitudinal intrusion. Early in the development of the 3D model, typical values of these parameters were selected based on tests at the TTC, as summarized in Table 3.1.

Table 3.1 Geometric Parameters for the 3D Models

Geometrical Parameter	Value
DR	45 (1)
Ovality	3% (1)
Gap	0.0176
Longitudinal Intrusion	NA (2)

(1) These two parameters were calculated by the equations in Chapter 2 with the following measured parameters:
Major Liner Outside Diameter = 8.24 in.
Minor Liner Outside Diameter = 7.76 in.
Liner Thickness = 0.178 in.

(2) Longitudinal intrusion is not applied to the 3D model at this stage.

The elastic modulus was set at 459,000 psi, and Possion's ratio was set to 0.3.

3.1.2 Element Selection

In the ABAQUS FE package, shell elements are used to model 3D thin shell structures. As discussed in ABAQUS (2001), shell element S9R5 is preferred for modeling doubly curved shells and for contact analyses, which is the case of the liner buckling model. Furthermore, since this study focuses on the thickness variation of the

liner, the thickness is defined at it nodes. Clearly, more nodes in an element will increase the flexibility of the thickness variation modeling. Thus, S9R5 elements are selected in our modeling.

According to ABAQUS (2001), the S9R5 element uses five degrees of freedom (three displacement components and two in-surface rotation components) where possible to achieve more economical computation.

In ABAQUS 6.2 and the previous versions 6.1 and 5.8, element S9R5 performed well in the models with thickness variation and local defects, as discussed in chapters 4 and 5. However, in ABAQUS 6.3, which was released in October, 2002, some negative eigenvalues and over-constraint errors were generated during the standard processing. One of the possible reasons was that the ABAQUS code modified how contact analyses are handled, resulting in differences between different versions of the software. The following is quoted from the ABAQUS new release notes of version 6.3: "Overconstraints that cannot be resolved automatically, such as overconstraints in contact analyses or overconstrained closed-loop mechanisms, are detected by ABAQUS/Standard during preprocessing or during the analysis."
(http://www.abaqus.com/support/ts_v63/books/rnb/default.htm)

To adjust to ABAQUS 6.3, element S9R5 was replaced by element S4R5, 4-node doubly curved thin shell, reduced integration with hourglass control, using five degrees of freedom per node. All the models were rerun, and very similar results were observed.

3.1.3 Reference Surface

The reference surface, which is the surface containing the element nodes, is typically coincident with the mid-surface of the shell. In the liner modeling, it is more

convenient to define the reference surface as the outer surface of liner. This is the surface that contacts the inner surface of the host-pipe. This is preferred to setting the reference surface as the mid-surface for the following reasons. First of all, it is convenient to define a more precise surface geometry, which is critical in modeling the contact between the liner and host-pipe. Second, it is observed that the outer surface of the liner is smooth while the inner surface is relatively rough of the liner. Third, the gap between the liner and host pipe can be precisely defined. The optional command OFFSET = 0.5 is used in *SHELL SECTION to set the reference surface to the outer surface.

3.1.4 Boundary Conditions

Based on the symmetrical two-lobe buckling assumption, one quarter of the liner circumference is modeled with the boundary conditions as shown in Table 3.1. The x-axis is horizontal, the y-axis is vertical and the z-axis is along the length of the liner.

Table 3. 2 Boundary Condition of Two-lobe Buckling Model

	U_x*	U_y*	U_z*	ϕ_x**	ϕ_y**	ϕ_z**
Crown	Fix	Free	Free	Free	Fix	Fix
Mid	Free	Fix	Free	Fix	Free	Fix
Top	Free	Free	Fix	Fix	Fix	Free
Bottom	Free	Free	Fix	Fix	Fix	Free

* U_x, U_y, U_z is the displacement along x, y, and z axis respectively

** ϕ_x, ϕ_y, ϕ_z is the rotation about x, y and z axis respectively

The boundary conditions are shown in Fig. 3.1.

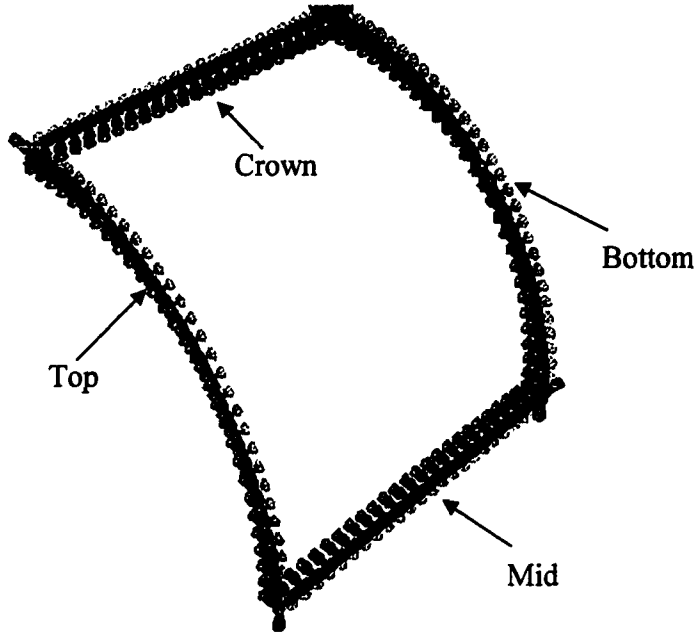

Fig. 3.1 Model Boundary Condition

3.1.5 Loading

As described in Chapter 2, the loads applied to the liner are the ground water pressure and the constraint load from the host pipe. The ground water pressure is modeled using the element-based distributed load with the ABAQUS *DLOAD command.

The constraint force from the host pipe is simulated by the contact and interaction between the host pipe and liner. The inner surface of the host and the outer surface of the liner are defined as the contact surfaces. The host pipe inner surface is defined as the master surface, while the liner outer surface is set as the slave surface. The nodes of the slave surface are constrained not to penetrate into the master surface. In the boundary condition definition, all the degrees of freedom of the host pipe are constrained such that

it remains rigid. The surface definition and contact condition is modeled using the ABAQUS commands *SURFACE DEFINITON and *CONTACT PAIR.

3.1.6 Solution Procedure

Short term buckling is modeled assuming elastic material behavior with a pressure that increases monotonically from zero to the buckling pressure. ABAQUS provides two approaches for non-linear static analyses. One for cases where the loading variations over the step must follow a prescribed history such as a prescribed displacement, and the other for cases where the loading is proportional (the loading over the complete structure can be scaled with a single parameter). In the later approach, load magnitude is considered to be part of the solution because buckling or collapse may occur. The solution is found by specifying the loading as a function of time and incrementing time to obtain the non-linear response. The latter case was chosen in the current FE model. For this method, ABAQUS breaks the simulation into a number of time increments and finds the approximate equilibrium configuration at the end of each time increment. The solution is sought to a proportional loading case, including the possibility of unstable behavior. The loading increments were written into the results (.fil) file by the command *EL FILE for the use with the x-y plotting facility in ABAQUS/Post.

3.2 Model Verification

3.2.1 Length Effects

As described in last section, one of the basic assumptions of the 3D model is the plane strain assumption. Based on this assumption, the length of the model is assumed to have no effect on the results, i.e. the critical buckling pressures are not expected to change if the liner length is changed. Four models with the lengths of 10, 20, 40 and 60

inches were run to test the length effects. In all of the four models the aspect ratio of the elements is kept at 1.0 and all the other characteristics of the models are identical. The critical buckling pressure of 120 psi is observed in all of these four models as excepted. The 10 inch pipe is adopted and is used in the mesh refinement study to verify the model.

3.2.2 Mesh Refinement

In the finite element model, choosing an appropriate number of elements is one of the key issues influencing the computational accuracy and cost. A mesh that is too coarse will lead to iteration divergence. However, a too fine mesh will unnecessarily increase computer time.

One of the requirements in mesh refinements is to keep the aspect ratio in all of the models approximately one when possible. With this constraint and all the other conditions keep identical, the mesh refinements are conducted as shown in Table 3.2.

Table 3.3 Mesh Refinement for the 10-inch Long Model

Mesh Discretization *(circumferential * longitudinal number of elements)*	**Buckling Pressure (psi)**
10*16	123.6
15*24	113.6
20*32	111.2
26*42	109.4
30*48	108.8
40*64	107.8
60*96	107
100*160	106.6

With the consideration of both accuracy and computation cost, the 30*48 mesh is selected, which means 30 elements on the circumferential direction and 48 element on the longitudinal direction.

3.2.3 Verification with Glock's Model

Glock's analytical model was used to evaluate the accuracy of the finite element models for perfectly circular pipes. The two-lobe buckling model is shown in Eq. 3.1.

$$P_{cr} = 1.323(\frac{t}{D})^{2.2} \frac{E}{1-\nu^2} \tag{3.1}$$

Setting the standard dimensional ratio $SDR = \frac{D}{t} = 45$, the elastic modulus E = 459,000 psi, and Possion's ratio $\nu = 0.3$, the calculated critical buckling pressure P_{cr} is

154 psi, while the critical buckling pressure from the finite element model with no ovality and gap is 149 psi. The relative error is 3%. Another point to consider is that a very small ovality is imposed to avoid the undesirable effects of that an initial disturbing force would have on the stress evolution. The ovality of 0.17% is referred to 0% in this study. This small ovality would help explain why the computational results were slightly lower than the analytical results.

3.2.4 Verification of the 3D Model with a 2D Model

To verify the 3D model, the 2D model used by Zhu (2000) is implemented using identical geometrical parameters. The resulting buckling pressure from a highly refined 2D model is 113 psi, while the corresponding pressure from the 30*48 3D model is 108.8 psi. The 2D model is somewhat stiffer than the 3D model, but the results lie within 4% of one another and are assumed to be acceptable.

3.3 Conclusions

1. A 3D liner buckling model was developed based on the geometric parameters shown in Table 3.1.

2. The S4R5 shell element was chosen to represent the wall of the liner.

3. The mid-surface was set as the outer surface of the liner to facilitate the definition of the contact surface.

4. Periodic boundary conditions were set as defined in Table 3.2.

5. The liner is uniformly loaded by external pressure (to simulate ground water pressure) and is constrained by the host-pipe.

6. Loading is applied in increments, going from zero to the buckling pressure. The increments are chosen by ABAQUS in a way so that the convergence criteria are not violated. The loading increments (or time steps) decrease as buckling is approached due to the "large" deflections that are caused by "small" pressure increments.

7. The length of the 3D model has no influence on the resulting buckling pressures.

8. The 3D model is verified by Glock's analytical model and by comparison with a 2D FE model.

CHAPTER FOUR

INFLUENCE OF THICKNESS VARIATION ON LINER BUCKLING

The variation of liner thickness has been observed both in laboratory specimens and in the field. In laboratory tests, the thickness of a pipe liner is usually calculated by taking the average of the thicknesses at different locations along liner circumference. Since thickness is a crucial factor in determining the performance of the liner, the effects of thickness variation has invoked the interests of the researchers for a long time.

Furthermore, thickness has been observed to vary both in the circumferential and longitudinal directions. It is impossible to cover variations in both directions using a 2D model. In this chapter, a study of the influence of liner thickness variation on critical buckling pressure using a 3D FE model is presented

4.1 Thickness Variation along Longitudinal Direction

4.1.1 Sinusoidal Thickness Variations

Careful examination of liner specimens reveals that thickness variations are randomly distributed along the inner surface of the liner (assuming a smooth host pipe) and/or along the outer surface of the liner for rough host pipes. There are no papers in the literature that discuss the distribution and magnitude of thickness imperfections for CIPP products. Using qualitative observations of experimental specimens tested at the TTC, the variations are continuous instead of abrupt. Here, it is assumed that the variations have a sinusoidal pattern. The sinusoid variation assumption makes modeling and analysis of thickness imperfections tractable, as periodic boundary conditions would apply for a non-uniform distribution of thicknesses.

In ABAQUS, the thickness of a shell element is controlled by the thickness at the nodes. The thickness between adjacent nodes varies linearly. The thickness of a node is given as

$$t = t_A + \Delta t \cdot \sin(\frac{n}{N} 2\pi) \tag{4.1}$$

where t = liner thickness at specific node

t_A = average thickness of the liner

Δt = the maximum thickness variation of the liner

N = number of nodes in a period

n = nodal index

The magnitude and frequency of variation is controlled by Δt and N, respectively.

4.1.2 Length of the Model

The sinusoidal wave pattern was employed in simulating the thickness variation along the length of the liner. The periodic boundary conditions shown earlier in Table 3.1 are enforced. Taking advantage of the symmetry property of the sinusoidal wave and the periodic boundary condition, only one half of the period of a sinusoid is modeled to simulate the infinite length of the liner. This significantly reduces the computational cost. To make sure that only one half of a wave is sufficient to model the behavior of thickness imperfections along the length, a test case involving a whole period of a sinusoidal wave was simulated, and the results were the same as for the half wave.

In all of the models, the dimension ratio of the elements was kept approximately at one. This restriction determines the relationship between the number of elements in each direction. Also, a minimum number of nodes along the length is required to simulate the sinusoidal wave pattern of thickness variations. Too few elements will lead to the inaccurate simulation of the sinusoidal wave pattern because the thickness between adjacent nodes changes linearly. However, too many elements result in a large computational cost.

The length of the element along the longitudinal direction (L_e) is determined by the length of the model (L) and the number of elements in the longitudinal direction (N_L), i.e. $L_e = L / N_L$. Similarly, if we define the element number in the circumferential direction as N_c, then the length of the element is $L_e = \frac{\pi d}{4N_c}$ since one fourth of the liner is modeled. Notice that the lengths in both directions are approximately the same because the aspect ratio is one. By combining the above two equations together, the length of the

model is given as, $L=\frac{\pi d}{4}\frac{N_L}{N_C}$. While the diameter of the liner is eight inches, the length has to be carefully selected to offset the computational cost and simulation accuracy. A very short length will result in an excessive number of elements around the circumferences. In the next section, one fifth of the simulated one quarter circumference is selected for the length as

$$L = \pi d \cdot \frac{1}{4} \cdot \frac{1}{5} \tag{4.2}$$

Here, if d is 8 inches, then the length of the model becomes 1.256 inches. A model with a length of 1.256 inches is used for mesh refinement.

4.1.3 Mesh Refinement

With the ratio of elements in the circumferential to longitudinal direction set at 5, mesh refinement is conducted by choosing the maximum thickness variation as 20% of the average thickness. That is, the average thickness of 0.178 inches corresponds to a Δt of 0.0356 inches. The results are shown in Table 4.1. The mesh described as 120*24 corresponds to 120 elements in the circumferential direction and 24 elements in the longitudinal direction. Notice that 120 divided by 24 is 5.0. This discretization is chosen for the simulation discussed below.

Table 4.1 Mesh Refinement for Longitudinal Thickness Variation

Mesh	Buckling Pressure (psi)
100*20	121.6
120*24	111.4
150*30	111.4
170*34	111.2
200*40	111.2

4.1.4 Effects of Frequency on Buckling Pressure

The frequency of thickness variation in the longitudinal direction of the model is determined by the length of the model. As discussed in section 4.1.2, the length of the model is one half of the wavelength of the sinusoidal wave. Thus, shorter model length corresponds to higher thickness variation frequency, and longer length corresponds to lower variation frequency. Models with different lengths were run to test the influence of variation frequency on the buckling pressure as shown in Table 4.2 and Fig. 4.1. The maximum thickness variation, Δt, is one half of the average thickness, 0.089 inches.

Table 4.2 Variation of Buckling Pressure with Frequency in the Longitudinal Direction

Model Length (inches)	$\frac{Model\ Circumfernece}{Model\ Length}$	**Buckling Pressure (P_{cri})(psi)**	P_{cri}/P_{cri}'
3.14	2	129.8	121.54%
2.09	3	131.2	122.85%
1.57	4	134.8	126.22%
1.256	5	136.6	127.90%
1.047	6	138.6	129.78%
0.897	7	139.8	130.90%
0.785	8	141.6	132.58%
0.7	9	142.2	133.15%
0.68	10	143.4	134.27%

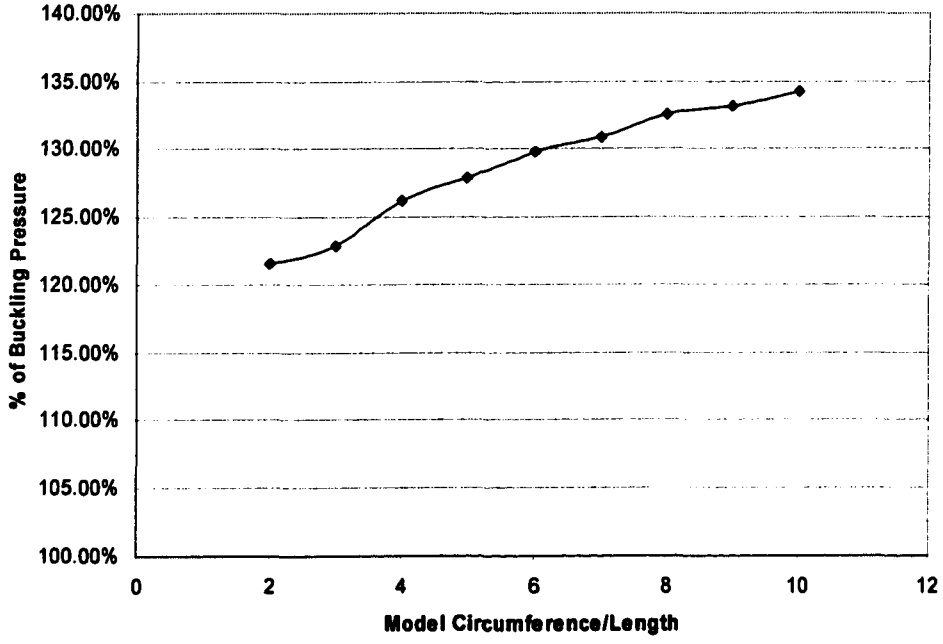

Fig. 4. 1 Variation of Buckling Pressure with Frequency in the Longitudinal Direction

Table 4.2 and Fig. 4.1 clearly show that the buckling pressure increases with the increasing of thickness variation frequency in the longitudinal direction. In the simulation, the shortest half-wavelength (highest frequency) was 0.68 inches. Shorter wavelengths were not simulated because wavelengths that are too short lead to abrupt changes in thickness.

4.1.5 Effect of Thickness Variation on Buckling Pressure

This section explores the influence of thickness variations on buckling pressure, where the thickness variations, Δt, are distributed according to Eq. 4.1. The average thickness of liner, t_A in Eq. 4.1, is 0.178 inch. Here, the thickness is allowed to vary from 0% to 50% of 0.178 inches for a liner with a circumference to length ratio of 5. For 0% variation, the thickness is uniform and the resulting buckling pressure, P_{cri}', is 106.8 psi. For a 50% variation, the thickness varies between 0.089 inches (0.178-0.178*0.50 = 0.089) and 0.267 inches (0.178+0.178*0.50=.267). The results for variations ranging from 0% to 50% in increments of 5% are shown in Table 4.2 and in Fig. 4.1.

Table 4.3 Variation of Buckling Pressure with the Magnitude of the Thickness Variation along the Length of the Liner for a Circumference to Length Ratio of 5

% of Δt	Magnitude of Δt	P_{cri}	P_{cri} / P_{cri}'
0%	0	106.8	100%
5%	0.0089	107	100.20%
10%	0.0178	107.8	100.90%
15%	0.0267	109.2	102.20%
20%	0.0356	111.4	104.30%
25%	0.0445	114.4	107.10%
30%	0.0534	117.2	109.70%
35%	0.0623	121.2	113.50%
40%	0.0712	125.8	117.80%
45%	0.0801	131	122.70%
50%	0.089	136.8	128.10%

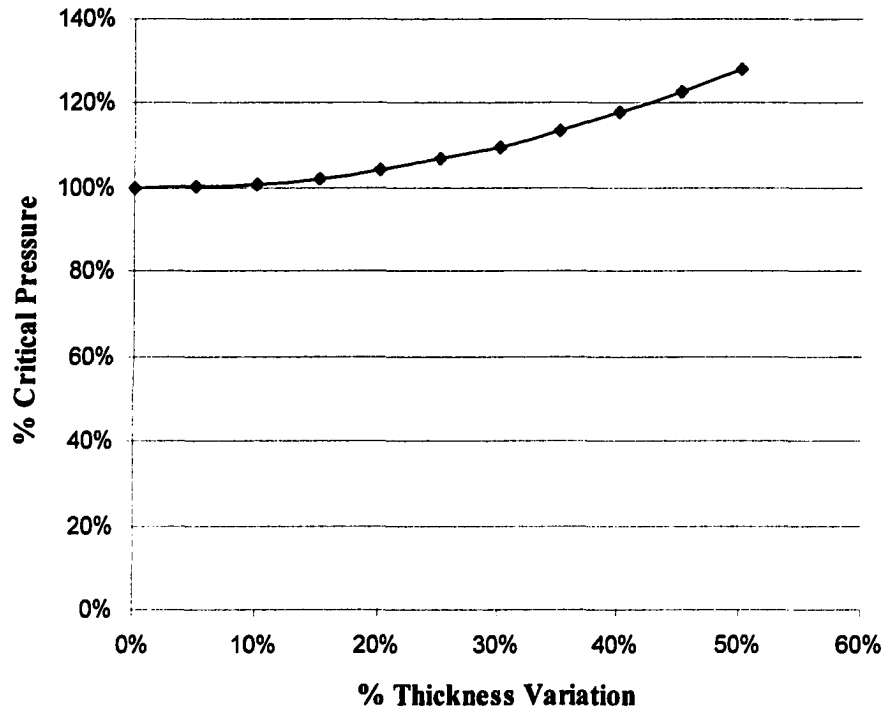

Fig. 4.2 Variation of Buckling Pressure with the Magnitude of the Thickness Variation along the Length of the Liner for a Circumference to Length Ratio of 5

4.2 Thickness Variation along the Circumferential Direction

4.2.1 Influence of the Thickness at the Crown on Buckling Pressure

As discussed in Chapter 3, the 3D model used in this study is a 2-lobe buckling model such that only one quarter of the liner circumference is modeled. Because the minor axis of the ovalized pipe model lies in the vertical direction and passes through the crown, buckling will always occur at the crown. However, in field applications and laboratory experiments, it is believed that buckling occurs at a relatively thin or weak part of the liner (or where several weak areas work together to reduce the overall buckling

resistance). This implies that, in the model, the thickness of the liner close to the crown plays an important role in determining the buckling pressure.

To verify this, two liner buckling cases were run which involved only one half period of a sinusoidal wave. The only difference between these two cases is that the liner is thinnest at the crown in case 1 and is thickest at the crown in case 2. In the first case, the buckling pressure is 81.2 psi, while it is 125.8 psi in case 2. The buckling pressure is 1.55 times larger when the liner is thickest close to the crown. Thus, the distribution of thickness around the circumference, and not just the magnitude of the thickness variation, plays an important role in the buckling resistance of a liner. Since the buckling pressure is lowest when the thinnest region lies at the crown, all of the simulations given here will be based on the assumption that the liners are thinnest at the crown where buckling occurs.

4.2.2 Frequency of Thickness Variation

The frequency of the thickness variations will govern how many sinusoidal waves make up the quarter model of the liner circumference. It is assumed that both the frequency and magnitude of thickness variations influence the buckling pressure. To simplify the analysis, the influence of frequency is studied for a fixed magnitude, and then the magnitude is varied for a fixed frequency.

One of the corner stones in studying frequency variations of liner thickness is that the variation is usually random and unpredictable. No available document describes the thickness or material property variations that are common in CIPP liners. Observing the experimental specimens, it is found that frequency of thickness variation is generally high. One idea is that increasing the frequency of the thickness variations (using more waves) will result in less and less influence on the buckling pressure. This is the view promoted

by several researchers. Notice that a frequency that is too high will result in abrupt thickness changes, which is not desirable. Also, when modeling high frequency variations, finer meshes are required to avoid abrupt changes in thickness.

In the ABAQUS model the thickness varies linearly between adjacent nodes. As shown in Table 3.1, there is no significant difference in the buckling pressure between meshes with 120*24 and 200*40 elements when the frequency variation is low. When modeling higher frequencies, the 200*40 mesh is chosen even though it will lead to much higher computational costs.

Table 4.3 and Fig. 4.2 show the variation in buckling pressure as a function of frequency for a variation magnitude that is 20% of the average thickness. It is observed that the buckling pressure varies significantly for low frequencies (less than 5 periods). Notice that the minimum is 75.8 psi with one period, while the maximum is 98.5 with 5 periods. When the frequency is getting higher, the buckling pressure converges as the periods increasing as expected. Also notice that the buckling pressure for three periods is less than the buckling pressure for two periods. This dip in the curve shown in Figure 4.2 is due to the grouping of thin areas both at the crown and at the location of maximum tensile stress on the outer diameter of the liner (a point between the crown and the first point of contact of the liner with the host pipe).

Table 4.4 Variation of Buckling Pressure with Frequency

Number of Periods	Buckling Pressure (psi)
1	75.8
2	84
3	80
4	88.2
5	98.5
6	95.6
7	94.8
8	96.6
9	95.4
10	96.2

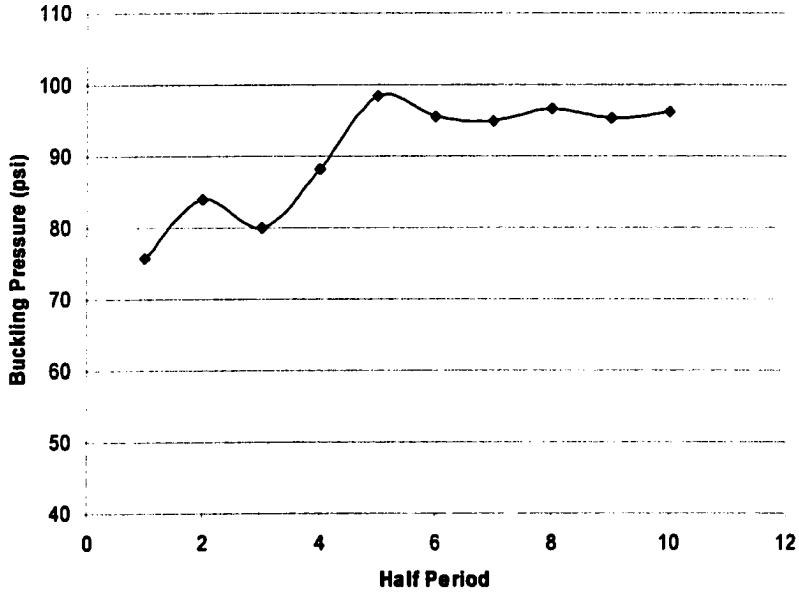

Fig. 4.3 Variation of Buckling Pressure with Frequency

Based on the conservative design rule, the minimum buckling pressure case, i.e., the frequency is the lowest, should be chosen for further study. However, based on the observation that the thickness variation frequency is normally high, the high frequency case is chosen to study. It is difficult to determine which frequency is the best among the high frequencies because there is no available guideline. Fortunately, there are very small differences between the high frequency results. The 10-period case is chosen for further study. This means that 10 periods will be modeled in the circumferential direction and 2 periods will be modeled in the longitudinal direction. Recall from Eq. 4.2 that the length is one fifth of the circumference in the model.

4.2.3 Magnitude of Thickness Variations

As indicated in Fig. 4.1 for the case where the thickness varies along the longitudinal direction of the liner, the buckling pressure increases while the variation magnitude increases. Here, the same method was applied in studying the effects of the magnitude of thickness variation along the circumferential direction of the liner. Using a fixed frequency of 10 periods for a quarter model, the buckling pressure is recorded for different magnitudes of thickness variation as shown in Table 4.4 and Fig. 4.3.

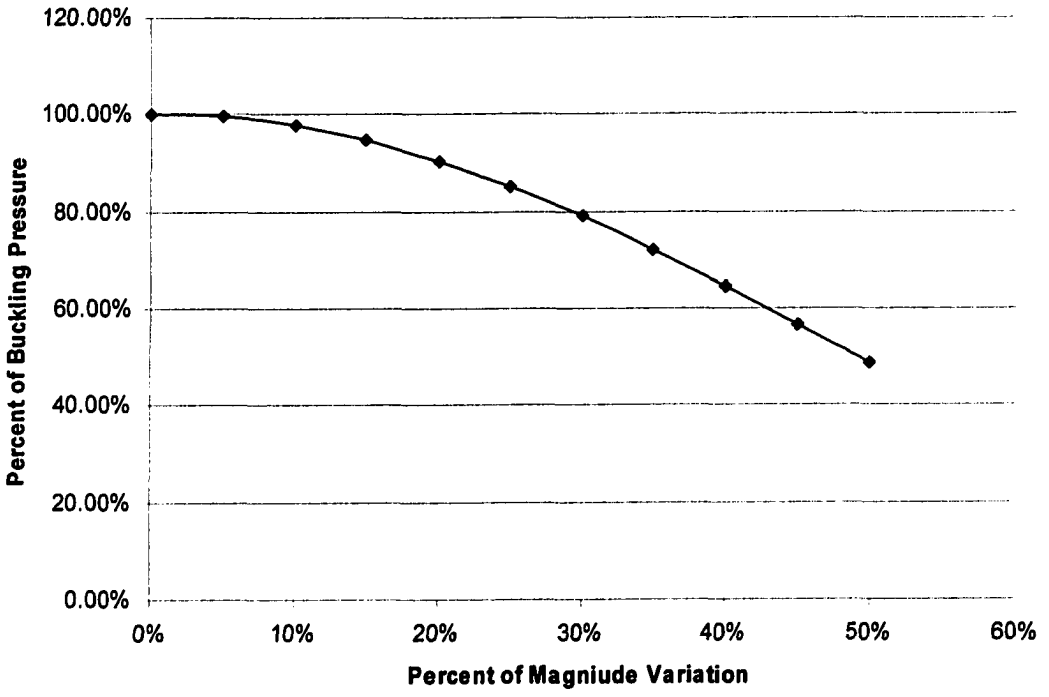

Fig. 4.4 Buckling Pressure Variation with Magnitude of Thickness Variation along the Circumference of Liner

Table 4.5 Buckling Pressure as a Function of Different Thickness Variation Magnitudes

Magnitude of Δt (inch)	**% of Δt**	P_{cri}	$P_{cri} / P_{cri}^{'}$
0	0%	106.4	100.00%
0.0089	5%	106	99.62%
0.0178	10%	104	97.74%
0.0267	15%	100.8	94.74%
0.0356	20%	96.2	90.41%
0.0445	25%	90.6	85.15%
0.0534	30%	84	78.95%
0.0623	35%	76.6	71.99%
0.0712	40%	68.6	64.47%
0.0801	45%	60.4	56.77%
0.089	50%	51.8	48.68%

It is obvious that the critical buckling pressure decreases while the magnitude of thickness variation along the circumferential direction increases.

4.3 Thickness Variation along both Circumferential and Longitudinal Directions

As shown in Figs. 4.1 and 4.3, it is interesting to notice that buckling pressure increases with the magnitude of thickness variation along the longitudinal direction, while it decreases with the magnitude of the thickness variation along the circumferential

direction. From observations of the test specimens, the thickness of liners varies in both the longitudinal and circumferential directions simultaneously. This makes investigation of thickness variations in both directions necessary.

4.3.1 Variation Pattern

The sinusoidal wave pattern was employed in modeling thickness variation along the circumferential and longitudinal direction separately. The advantages of using the sinusoidal wave, as mentioned above, is that the variation is continuous and gradual, and the magnitude and frequencies of the variation can be easily controlled by modifying related parameters in the sinusoidal equation.

When modeling the thickness variations in both directions, the same properties provided by the sinusoidal wave pattern in the previous two sections are still relevant. Eq. 4.3 is used in calculating the nodal thickness in this case.

$$t = (t_A + \Delta t \cdot \sin(\frac{n_C}{N_C} \cdot P_C \cdot 2\pi + \frac{n_L}{N_L} \cdot P_L \cdot 2\pi)) \cdot W_f \qquad (4.3)$$

where t = the thickness at a specific node

t_A = the average thickness of the liner

Δt = the maximum thickness variation of the liner

N_c = the number of nodes along the circumferential direction

n_c = the node index along the circumferential direction

P_c = the number of periods along the circumferential direction

N_L = the number of nodes along the longitudinal direction

n_L = the node index along the longitudinal direction

P_L = the number of periods along the longitudinal direction

W_f = the weight factor

Another consideration in modeling the thickness variation is the average thickness along the longitudinal direction. Notice that a weight factor is applied to Eq. 4.3 to set the average thickness of each longitudinal line of nodes to be same (0.178 inches). Since the same weight factor is applied for each specific line, the thickness variation retains a sinusoidal wave pattern.

In Eq. 4.3, the thickness variation magnitude is controlled by Δt. Frequencies of variation are controlled by P_c and P_L along the circumferential and longitudinal direction, respectively. Fig. 4.5 shows the 3D configuration of the inner surface of the liner modeled using Eq. 4.3.

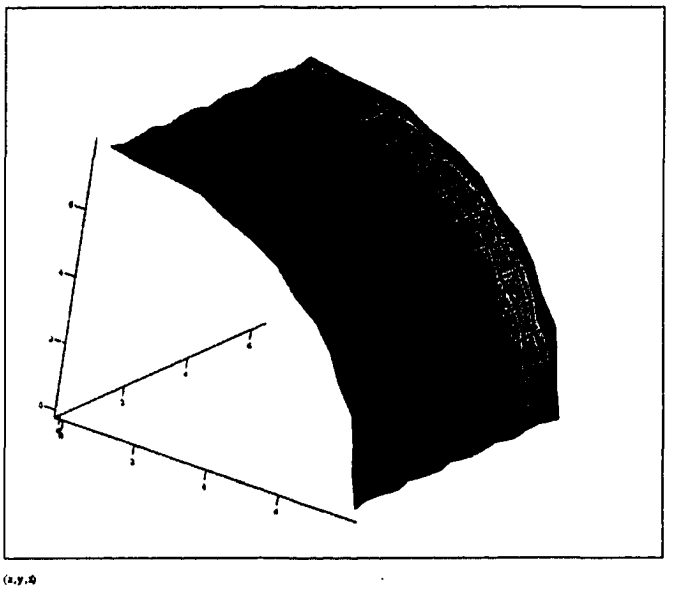

Fig. 4.5 3D Configuration of the Inner Surface of a Liner with Thickness Variations along Both Directions

4.3.2 Verification of Periodic Boundary Conditions

Periodic boundary conditions are applied on both ends of the model, which is specified as shown in Table 3.2. It was verified in Chapter 3 that the length of the liner

model has no effect on the buckling pressure when the liner has uniform thickness. Also, when studying how the thickness varies along the longitudinal direction (as in Section 4.1), the model length was verified to have no effect on the buckling pressure.

When studying the thickness variation in both directions, Eq. 4.3 is applied in modeling the variation pattern. One half of the wave-length is used in the model to simulate the infinite length of the liner based on the symmetry of sinusoidal wave and the periodic boundary conditions on the both ends of the model along the length. To test the validity of the boundary conditions, models with a length of one half of a wavelength (0.628 inches), one wavelength (1.256 inches), and two wavelengths (2.512 inches) were run. The same buckling pressure, 94.8 psi, was obtained in all of the three cases. The maximum thickness variation was one half of the average thickness for these three runs. Fig. 4.6 shows stress distribution of model with one half of wavelength and one wavelength. This figure clearly shows that stress distribution is completely symmetric with respect to the center line in longitudinal direction in the one wavelength model. It is also observed that the stress distribution of the half wavelength model was essentially identical to the right half of the full wavelength model. This validates the periodic boundary conditions on both ends of the liner model and indicates that one half wave-length, 0.628 inches, is appropriate for simulating a liner with infinite length.

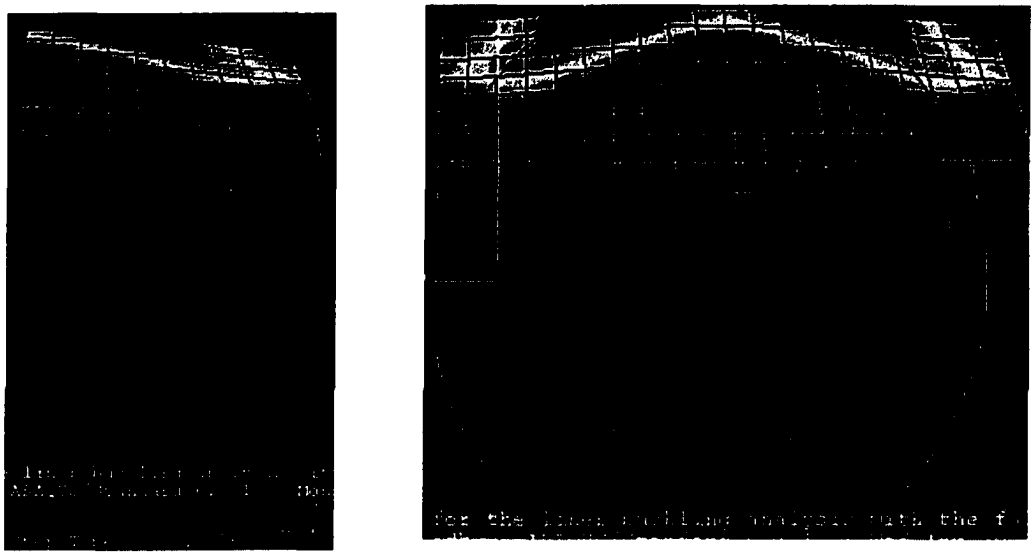

Fig. 4.6. Stress Distribution in Models with One Half (Left) and One (Right) Wavelength in the Longitudinal Direction

4.3.3 Variation of Frequency in Both Directions

One of the assumptions in the modeling is that the thickness variation follows the same pattern (the same magnitude and frequency) along both the circumferential and longitudinal directions. In Eq. 4.3, only one Δt is applied, which implies that the magnitudes of thickness variations are identical in both directions. The same frequency is simulated using the same sinusoidal wavelength in both directions. As discussed in the previous section, the length of the model has no effects on the buckling pressure and one half of the wavelength is adequate to simulate a liner with infinite length. The length of the model is determined by the wavelength of the thickness variation along the circumference of the model. For example, the longitudinal length should be one eighth of the circumferential length of the model if four periods of thickness variation are simulated in the circumferential direction ($\frac{1}{2} \cdot \frac{circumference}{4 \cdot 4}$). The additional 4 in the denominator here is due to the fact that we are modeling only ¼ of the circumference.

4.3.4 Effect of Frequency Variation on Buckling Pressure

As discussed in section 4.2, the frequency of thickness variation is determined by the number of sinusoidal periods along the circumference of the model. A higher number of periods corresponds to a higher frequency. The length of the model is one half of the wavelength in the circumferential direction. Table 4.6 shows the buckling pressure variation with different frequencies of thickness variation.

In column 4 of Table 4.6, the ratio of the buckling pressure for a specified thickness variation frequency to the buckling pressure with no thickness variation (106.8 psi) is given. The percentages of buckling pressure and periods are plotted in Fig. 4.7.

This figure shows that the buckling pressure decreases with the increasing of the frequency of thickness variation. It is also shows that the buckling pressure decreases in lower rate when the frequency of thickness variation is high.

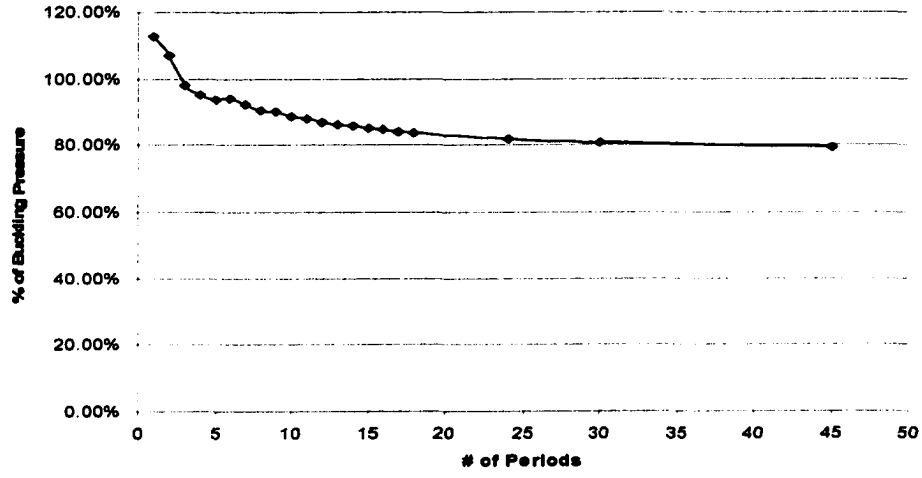

Fig. 4.7 Influence of the Frequency of Thickness Variation on Buckling Pressure

Table 4.6 Influence of the Frequency of Thickness Variation on Buckling Pressure

# Periods along Model Circumference	Model Length (inches)	P_{cr} (psi)	% P_{cr}
1	3.14	120.6	112.92%
2	1.57	114.4	107.12%
3	1.047	104.8	98.13%
4	0.785	101.6	95.13%
5	0.628	100.2	93.82%
6	0.523	100.4	94.01%
7	0.449	98.6	92.32%
8	0.393	96.8	90.64%
9	0.349	96.2	90.07%
10	0.314	94.6	88.58%
11	0.285	94	88.01%
12	0.262	93	87.08%
13	0.242	92.2	86.33%
14	0.449	91.6	85.77%
15	0.209	90.8	85.02%
16	0.196	90.4	84.64%
17	0.185	89.6	83.90%
18	0.174	89.4	83.71%
24	0.131	87.4	81.84%
30	0.105	86.2	80.71%
45	0.070	84.8	79.40%

4.3.6 Influence of the Magnitude of Thickness Variation on the Buckling Pressure

In the study above, the magnitude of the thickness variation was set to the a severe level where Δt was one half of the average thickness, t_A. The effects of thickness

variation magnitude are studied in this section. Table 4.7 shows the buckling pressure variation with changing values of the thickness variation magnitude. In all of the models in Table 4.7, the length of the model is 0.628 inches, which is one tenth of the model circumference. This implies that there are 5 sinusoidal wave periods along the circumferential direction and only one half along the longitudinal direction.

Table 4.7 Buckling Pressure with Different Thickness Variation Magnitude

% of Δt	Δt (inch)	P_{cr} (psi)	% P_{cr}
0%	0	106.8	100.00%
5%	0.0089	106.8	100.00%
10%	0.0178	106.8	100.00%
15%	0.0267	106.8	100.00%
20%	0.0356	106.8	100.00%
25%	0.0445	106	99.25%
30%	0.0534	105.6	98.88%
35%	0.0623	104.8	98.13%
40%	0.0712	103.6	97.00%
45%	0.0801	102.2	95.69%
50%	0.089	100.2	93.82%

The percentage of thickness variation and percentage of buckling pressure are plotted in Fig. 4.8. This figure shows that buckling pressure doesn't change when the thickness variation is small (lower than 20%). When thickness variation is larger than 20%, buckling pressure decreases with the increasing of thickness variation. Recall that the mean thickness is the same in all of the cases, so although the thinner areas may reduce the stiffness, the thicker areas may work together offset this reduction in stiffness.

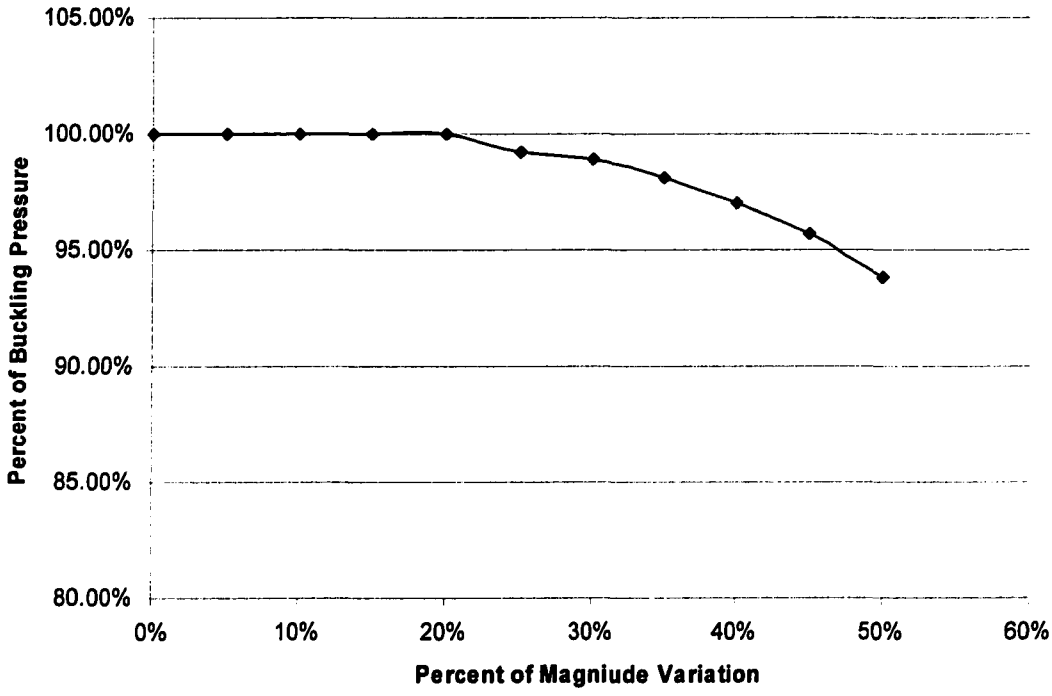

Fig. 4.8 Critical Buckling Pressure Variation with the Magnitude of Thickness Variation

4.5 Liner Buckling and Thickness Distribution

4.5.1 Buckling Location and Thickness Variation

It is believed that the ovality is a key factor that influences both buckling pressure and where buckling occurs. Higher ovality leads to lower buckling pressure. Liners buckle along the minor axis of the elliptical cross section, which for our case is the crown of the model. Fig. 4.9 shows contour plots of effective stress and displacement for a liner with 3% ovality and uniform thickness. Notice that both stress and displacement reach the maximum value at the crown.

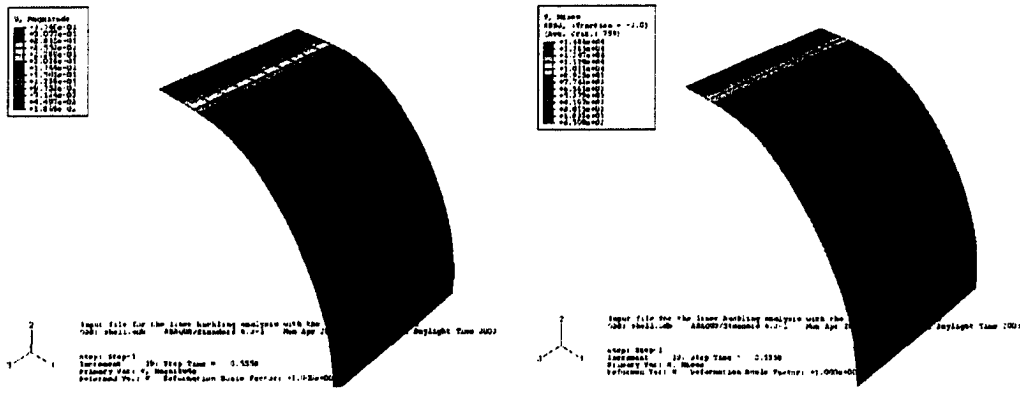

Fig. 4. 9 Contours of Displacement (Left) and Stress (Right) for a Model with 3% Ovality and Uniform Thickness

When the liner thickness is not uniform, the thickness variation will influence the buckling pressure, as discussed earlier. At the same time, the thickness variation influences where the buckling occurs. Fig. 4.10 shows contours of thickness variation and FE displacements for a buckling model with both ovality and thickness variation.

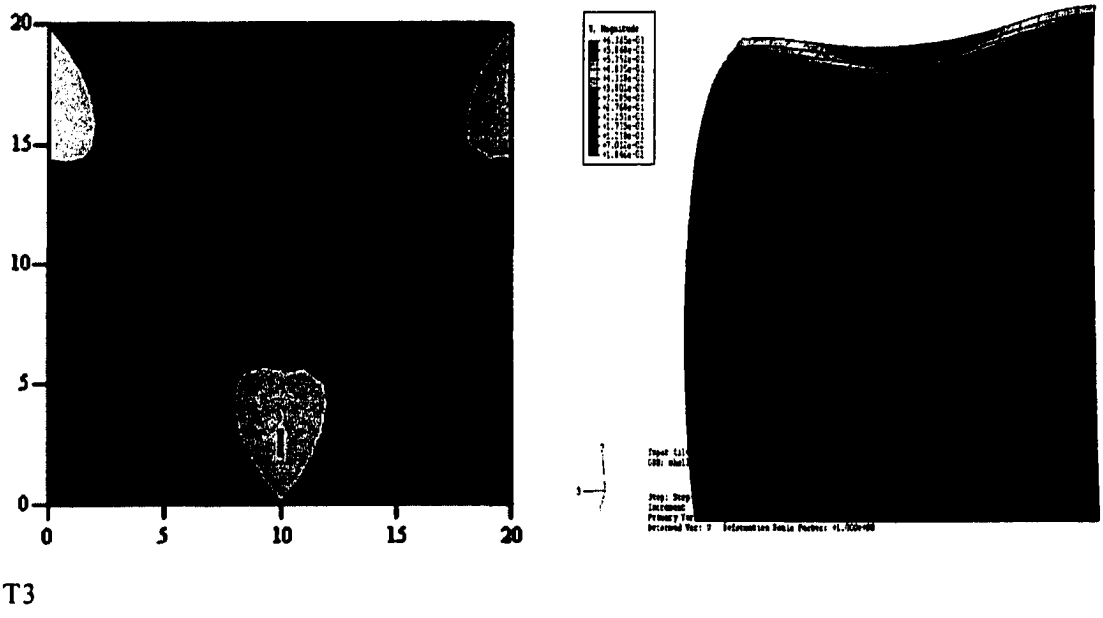

Fig. 4. 10 Contours of Thickness (Left) and Displacement (Right) for a Model with 3% Ovality and Thickness Variation

From Fig. 4.10, it is clearly that buckling occurs at the crown of the liner. However, due to the thickness variation of the liner, the displacements are not uniformly distributed in longitudinal direction. Larger displacements occur at the area of thinner thickness near liner crown. To demonstrate this observation, a displacement contour for a liner with the same ovality but different thickness distribution was plotted in Fig. 4.11

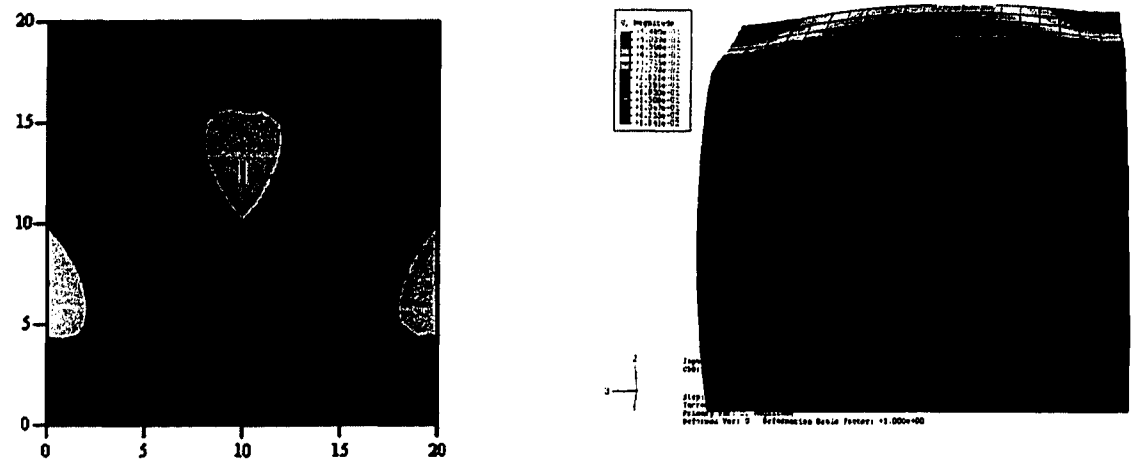

Fig. 4. 11 Contours of Thickness (Left) and Displacement (Right) for a Model with 3% Ovality and Thickness Variation (thinner thickness at the ends of the liner)

In Fig. 4.10 and Fig. 4.11, both models have the same variation frequency, which is one period of the sinusoidal wave on the circumference of the model. Low frequency results in large continuous thinner and thicker areas. With the increase of thickness variation frequency, the size of the continuous thinner and thicker areas decreases. Fig. 4.12 shows the thickness contours of models with 1 and 6 period(s) in circumferential direction.

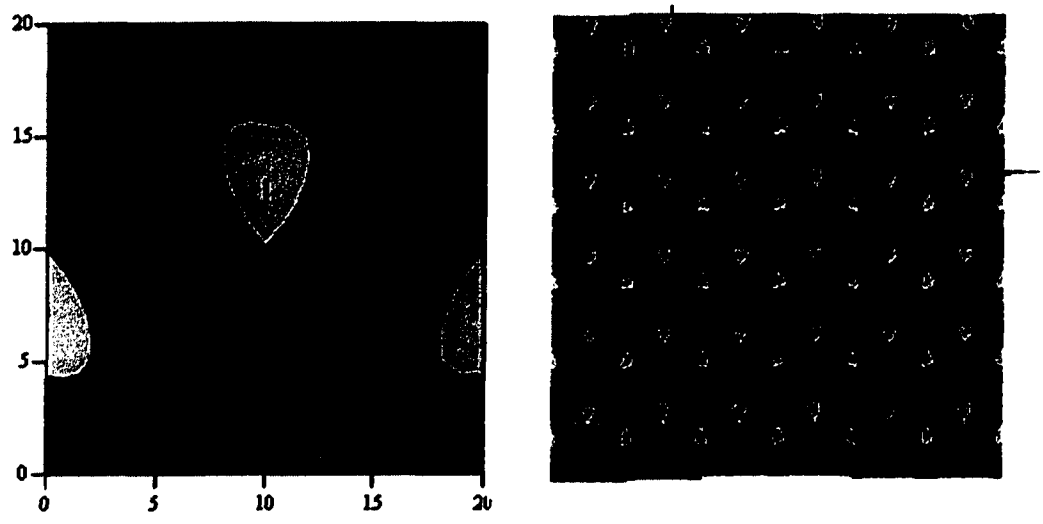

Fig. 4.12 Thickness Contour of Model with One Period (Left) and 6 Periods (Right) in Circumferential Direction

With smaller and smaller continuous thinner and thicker areas, it is expected that the influence of the thickness variation on the buckling location will decrease. Fig. 4.13 shows model with the thickness, displacement, and stress contours for a model with six periods of thickness variation in the circumferential direction.

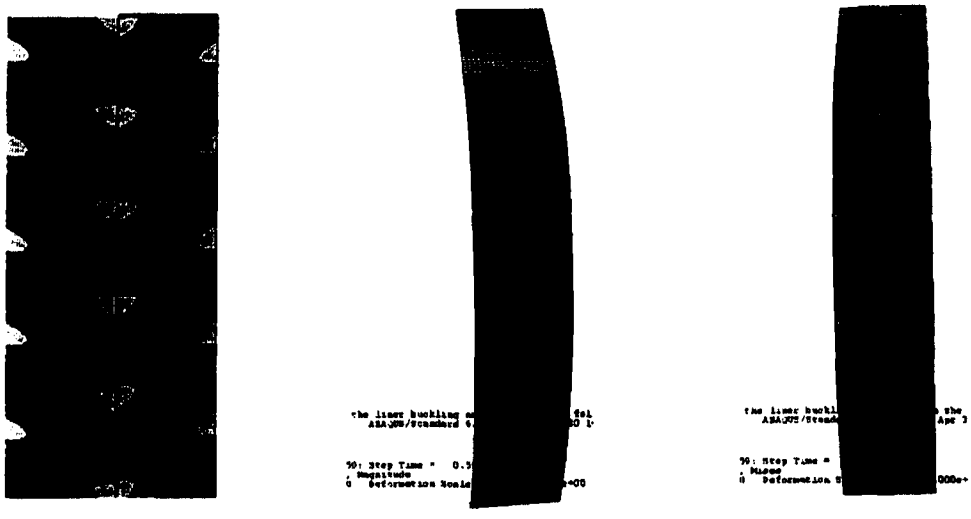

Fig. 4.13 Contours of Thickness (Left), Displacement (Middle), and Stress (Right) for the Model with Six Periods of Thickness Variation in the Circumferential Direction

From the displacement contour, it is clear that the displacement is not following the thickness distribution because the areas of small thickness are very close to the crown. It is more like the displacement contour for the case of uniform thickness. The stress contour shows that the peak stresses follow the thickness distribution pattern. The influence of thickness variation on the buckling location decreases with increasing defect frequency.

4.5.2 Buckling Pressure and Thickness Variation

Fig. 4.14 shows buckling pressure with different frequencies of thickness imperfections. In all of the models, the thickness variation magnitude is one half of the average thickness of the liner. The thickness varies from 120.6 psi for 1 period along the circumference (1 wave) to 100.2 for 5 waves. Table 4.6 summarizes buckling versus frequency results for frequencies up to 45 periods. As the frequency increases, the area of small thicknesses (the dark blue area) moves closer to the crown causing the area of reduced thickness to act more and more like a longitudinal defect near the crown. On the other hand, when the frequency is low, much of the thin area is away from the highly stressed crown region. As frequency continues to increase, the defect gets closer and closer to the crown, thus resulting in lower buckling pressures.

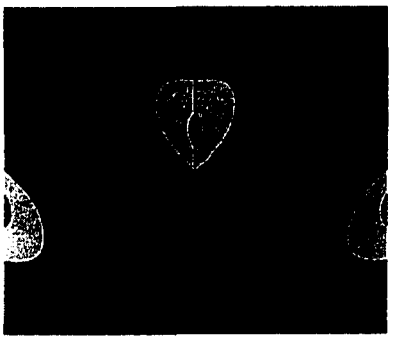

P = 120.6psi (1 waves)

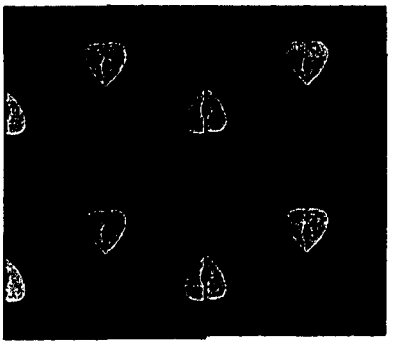

P = 114.4psi (2 waves)

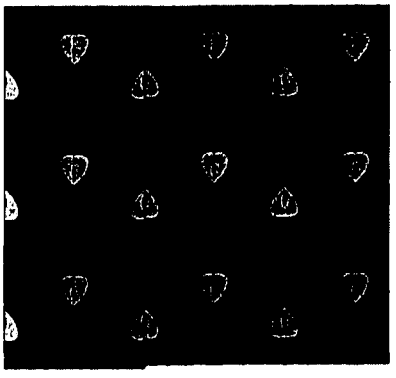

P = 104.8 psi (3 waves)

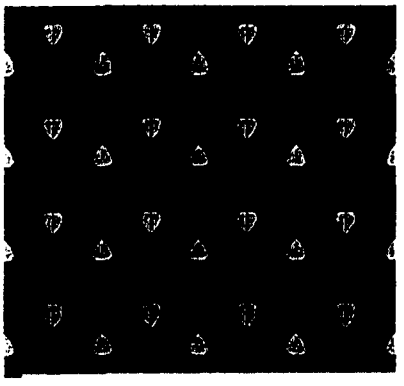

P = 101.6psi (4 waves)

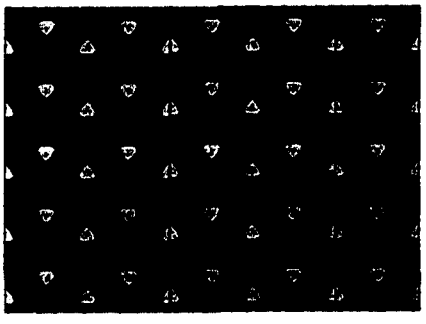

P = 100.2psi (5 waves)

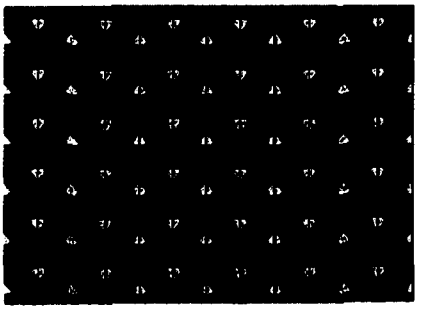

P = 100.4 psi (6 waves)

Fig. 4.14 Buckling Pressure with Different Thickness Distribution Pattern

4.6 Conclusions

1. A three dimensional (3D) 2-lobe liner buckling model was used to model the thickness variations. A sinusoidal wave pattern was employed in modeling the thickness variation both in the circumferential and longitudinal directions.

2. Thickness variations in the circumferential and longitudinal direction were studied independently at first. When the thickness varies exclusively in the longitudinal direction, the buckling pressure increases as the magnitude of the thickness variation increases. The opposite behavior was observed when studying the thickness variation in the circumferential direction. For this case, the buckling pressure decreases when the magnitude of thickness variation increases.

3. The following are some high-lights of the set-up of the model for the thickness variations in both directions simultaneously:

- periodic boundary conditions are applied to both longitudinal ends;
- Eq. 4.5 provides the nodal thickness of the sinusoidal wave;
- one half of the wavelength of the sinusoidal wave in the circumferential direction is the length of the model;
- thickness variations in both individual directions have the same magnitude and frequency;
- the average thickness along each longitudinal nodal line is the same.

4. For thickness variation in both directions, the buckling pressure decreases with the increasing of the frequency of thickness variation. The buckling pressure decreases in lower rate when the frequency of thickness variation is high. Under high frequency variation, the buckling pressure doesn't change while the thickness variation is

less than 20%. The buckling pressure decreases with increasing thickness variations when the magnitude is larger than 20%.

5. The distribution of displacement and stress of a liner with thickness variation follows the distribution of the thinner wall distribution. When the thickness variation frequency is low, it is clear that the large displacements follow the thinner band. When the frequency is high, the influence of thickness distribution on the buckling location is less obvious.

6. The liner buckling pressure is high wherever there is wide band of continuous thickness at the crown part of the liner.

CHAPTER FIVE

LOCAL DEFECTS

Point and area defects on the liner are a concern in liner design and application. For example, the technical specification for the Department of Public works in Indianapolis, Indiana addresses this issue in Section 1101 - Cured-in-Place Sewer Segment Lining (http://www.indygov.org/dcam/specs_manuals/pdf/rehab_tech_spec.pdf). The specification states that *"prior to the installation of a cured-in-place liner, the contractor shall thoroughly clean the sewer designated to receive the liner. Cleaning shall constitute removal of all debris, solids, roots and other deposits in the sewer line. The contractor shall be responsible for clearing the designated sewer line of obstructions such as dropped joints, protruding lateral connections, and broken pipe/crushed pipe which reduces the cross-sectional area by more than 40% and/or which will prevent the insertion of the liner. The finished cured-in-place pipe shall be continuous over the entire length of the insertion run and be free from significant defects including dry spots, lifts, and delaminations. Any defects which will affect the integrity or strength of cured-in-place pipe shall be removed and replaced at Contractor's expense."*

In this chapter, the effects of circular local defects on the buckling pressure are studied using 3D liner buckling model. The local defects are simulated by reducing the thickness and modulus of elasticity in certain areas on the liner. Three aspects of local defects are of interest: (1) the frequency of defects, (2) the magnitude of the defects (maximum thickness variation or reduction of flexural modulus), and (3) the size of the defects. The effects are studied numerically by simulating the critical buckling pressure for different cases.

5.1 Continuous Thickness Variation

5.1.1 Defect Frequency Along the Length of the Liner

In the previous two chapters, only one quarter of a liner was simulated in the 3D models due to symmetry along the circumferential direction of the liner. The results were assumed to be independent of the length of the model due to the periodic boundary conditions. However, in the case of local defects, the length of the model determines the longitudinal distance between adjacent defects. This is the longitudinal occurrence frequency of the local defects. The length of the model is studied to determine the minimum distance between adjacent local defects which ensures the adjacent defects have no interaction with each other.

Local Defect Location and Pattern. When studying the influence of defect frequency, the worst case for defect separation is simulated so that the results will be conservative for all cases.

The local defects are assumed to be approximately circular in shape. Similar to the thickness variation discussed in Chapter 4, the thickness at the local defect changes

gradually instead of abruptly. A sinusoidal wave is employed to model the thickness at a given node according to Eq. 5.1.

$$t = t_A + \Delta t \cdot \sin[(-\frac{\pi}{2}) \cdot (1 - \frac{d}{R_{wp}})] \tag{5.1}$$

where t = the thickness at specific node

t_A = average thickness of the liner

Δt = the maximum thickness variation of the liner

d = the distance between the specific node and the center of the local defect

R_{wp} = the radius of the local defect

Using Eq. 5.1, the thickness at nodes in the local defect area changes gradually, and all thicknesses are smaller than the average thickness of the liner. In the model, the local defect is located at the upper right corner of the model and the thickness in the center of the circle is set as the minimum. The worst case in this study assumes that the minimum thickness at the center of the defect is one half of the liner average thickness and that the radius of the local defect is one half of the mean inner diameter of the host pipe.

Mesh Refinement. The local defect is simulated using $\Delta t = t_A/2 = 0.178/2 = 0.089$ inches with a defect radius of R = 8/2 = 4 inches. The mesh refinement is performed as shown in Table 5.1. Notice that the mesh discretization is given as the number of elements along the circumferential direction times the number of elements in the longitudinal direction.

Table 5.1 Mesh Refinement for a 10 inch Long Model

Mesh	buckling Pressure
10*16	65.8
12*20	64.2
15*24	62.4
30*48	60.6
40*64	60.2
45*72	60.2

The mesh refinement study shows that a mesh with 30 elements in the circumferential direction is sufficient when considering computational accuracy and cost. Note that for this modeling, the objective is to find out the minimum length of the model such that two adjacent defects do not interact with one another. The number of elements in the longitudinal direction depends on the length of the model. Consequently, the mesh refinement study given in Table 5.1 (which applies to a 10-inch long model) only determines the required number of elements in the circumferential direction. The number of elements in longitudinal direction for different length models is determined by the requirement that the aspect ratio of the element is one.

Length Effects. Simulations are run for models with lengths of 0.5d, 0.625d, 0.875d, 1.25d, 1.875d, and 2.5d, where d is the mean inside diameter of the host pipe (8 inches). The results of these six simulations are shown in Table 5.2.

Table 5.2 Influence of Model Length for a Worst Case Local Defect

Model Length (inches)	Length/Diameter	Mesh	Buckling Pressure (psi)
4	0.5	30*20	49.4
5	0.625	30*24	57.8
7	0.875	30*34	60.2
10	1.25	30*48	60.6
15	1.875	30*72	60.6
20	2.5	30*96	60.6

From Table 5.2, it is clear that for models with length to diameter ratios greater than 1.25, the buckling pressure no longer depends on the length of the model. Notice that the local defect is located at the right upper corner of the model and the model is symmetric along the longitudinal direction, which implies that distance between the centers of two local defects is two times of the length of the model. Thus, when the distance between the centers of two adjacent local defects is 2.5 times the mean inner diameter of the host pipe (20 inches for the 8 inch pipe), adjacent local defects don't interact with each other. Thus, a 10-inch model is chosen in the studying of the magnitude and area of local defects.

5.1.2 Local Defect Area and Magnitude

Variation Magnitude. Table 5.3 and Fig. 5.1 show the effects of the maximum thickness variation on the buckling pressure for a defect with a radius of 4 inches and a spacing between defects of 20 inches. The plot and table clearly show that the buckling pressure decreases as the thickness at the center of the defect decreases.

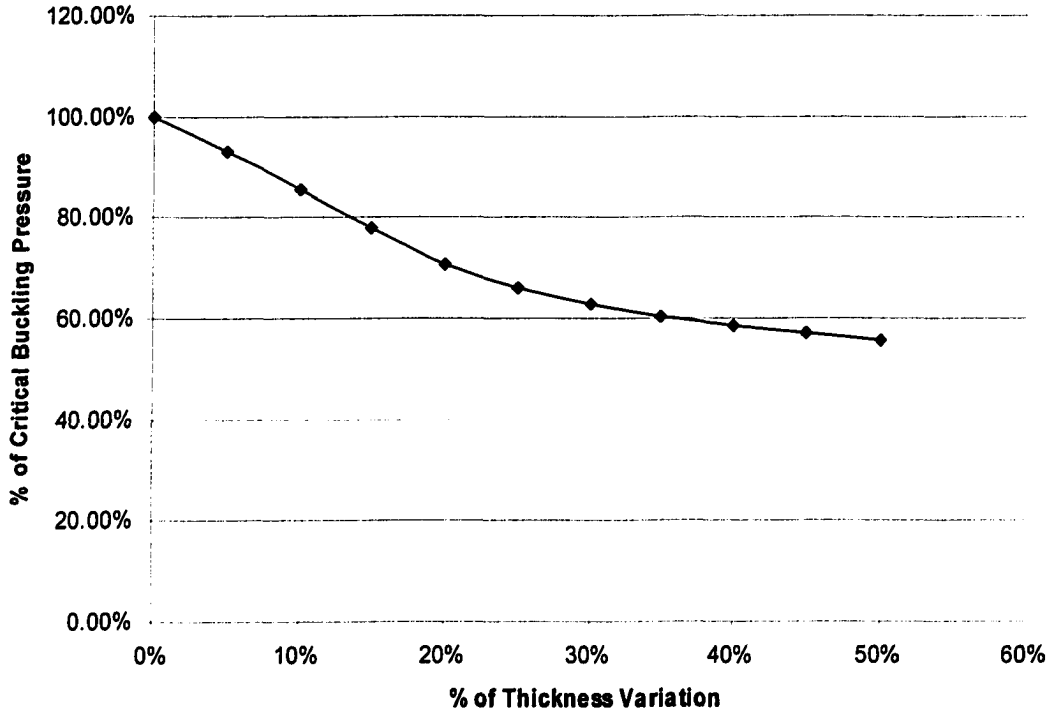

Fig. 5.1 Variation of Buckling Pressure with the Magnitude of the Thickness Variation for a Local Defect with a Radius of Four Inches

Table 5.3 Variation of Buckling Pressure with the Magnitude of the Thickness Variation for a Local Defect with a Radius of Four Inches

% of Δt	Magnitude of Δt (inches)	P_{cri} (psi)	P_{cri} / P_{cri}'
0%	0	108.8	100.00%
5.00%	0.0089	101.4	93.20%
10.00%	0.0178	93	85.48%
15.00%	0.0267	84.8	77.94%
20.00%	0.0356	77.2	70.96%
25.00%	0.0445	71.8	65.99%
30.00%	0.0534	68.4	62.87%
35.00%	0.0623	65.8	60.48%
40.00%	0.0712	63.8	58.64%
45.00%	0.0801	62	56.99%
50.00%	0.089	60.6	55.70%

Local Defect Diameter. The diameter of the local defect also influences the buckling pressure. Table 5.4 and Fig. 5.2 show that increasing of the area of the local defect causes the buckling pressure to decrease. In all of the models, the maximum magnitude of the thickness variation, which is the thickness of the center of the local defect, is one half of the average thickness.

Table 5.4 Critical Buckling Pressure Variation with the Diameter of the Local Defect

$D_{weak-point} / D_m$	$D_{weak-point}$ **(inches)**	P_{cri} **(psi)**	P_{cri} / P_{cri}'
0.00%	0	108.8	100.00%
10.00%	0.8	106.4	97.79%
20.00%	1.6	101	92.83%
30.00%	2.4	95.4	87.68%
40.00%	3.2	89.8	82.54%
50.00%	4	84.6	77.76%
60.00%	4.8	79.2	72.79%
70.00%	5.6	73.8	67.83%
80.00%	6.4	69	63.42%
90.00%	7.2	64.6	59.38%
100.00%	8	60.6	55.70%

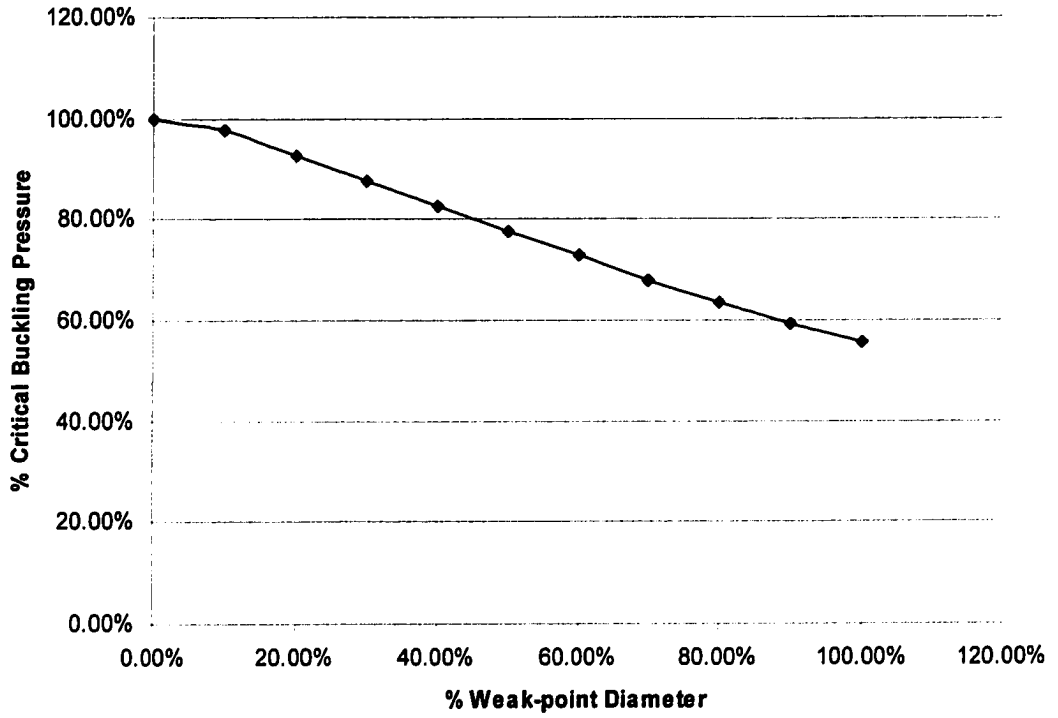

Fig. 5.2 Buckling Pressure Variation with the Diameter of the Local Defect

Compound Effects of Magnitude and Area. Table 5.4 and Fig. 5.3 show the compound effects of the defect area and the magnitude of the thickness change on the buckling pressure. Notice that the buckling pressure of model with no local defect is 108.8 psi.

Table 5.5 Percent of Buckling Pressure for a Pipe with No Defect (108.8 psi) as a Function of the Thickness Variation Magnitude and the Area of the Local Defect

$\frac{Defect\_Diameter}{Host\_Pipe\_Diameter}\cdot 100\%$	**Thickness at the Center of the Defect**				
	$0.9t_{avg}$	**$0.8\ t_{avg}$**	**$0.7\ t_{avg}$**	**$0.6\ t_{avg}$**	**$0.5\ t_{avg}$**
10%	99.63%	99.08%	98.71%	98.35%	97.79%
20%	98.53%	96.69%	95.04%	93.75%	92.83%
30%	96.88%	93.57%	90.99%	89.15%	87.68%
40%	95.04%	90.26%	86.95%	84.56%	82.54%
50%	93.38%	87.13%	82.90%	79.96%	77.76%
60%	91.36%	83.64%	78.49%	75.37%	72.79%
70%	89.52%	79.96%	74.26%	70.59%	67.83%
80%	88.05%	76.65%	70.04%	66.18%	63.42%
90%	86.58%	73.53%	66.36%	62.32%	59.38%
100%	85.48%	70.96%	62.87%	58.64%	55.70%

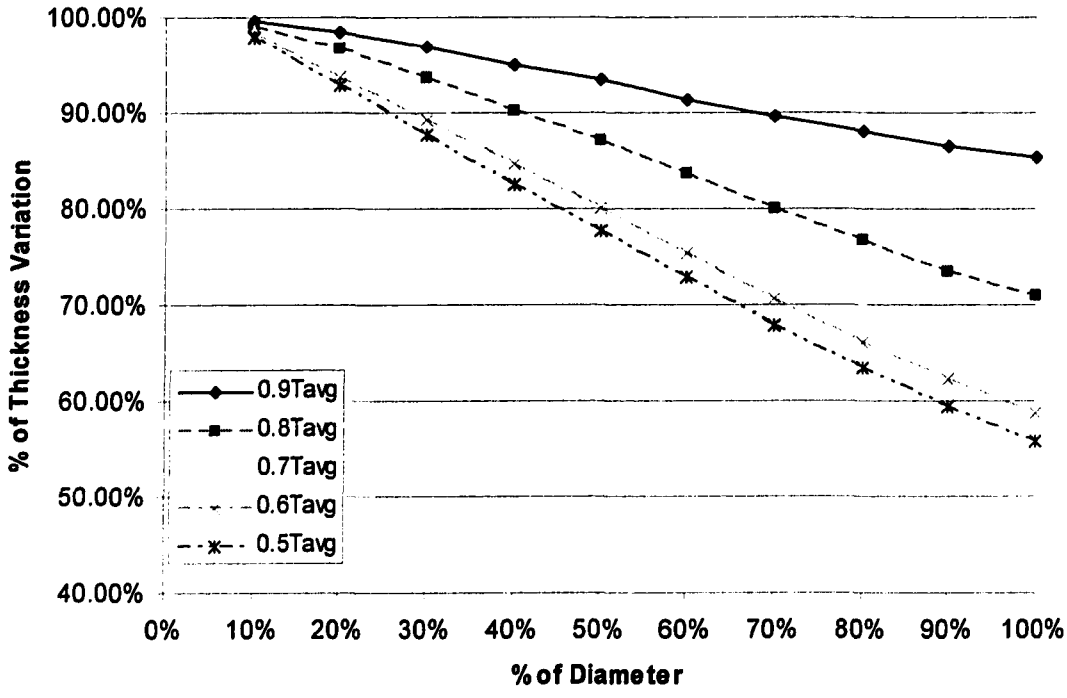

Fig. 5.3 Percent of Buckling Pressure for a Pipe with No Defect (108.8 psi) as a Function of the Thickness Variation Magnitude and the Area of the Local Defect

5.2 Local Defects with Weaker Material Properties

Due to the inappropriate operations in liner curing process or cleaning of the host pipe, the resin may not be properly cured as expected in some areas of the pipe. This can cause the flexural modulus (E) at a given location to be lower than the average modulus of the pipe liner.

In this section, a liner with a local defect consisting of a reduced elastic modulus is modeled to investigate the effects on the critical buckling pressure. In all of the models in this section, the flexural modulus of the entire weak point is the same (there is no variation of flexural modulus across the weak point as was the case for the thickness

imperfection). This implies that the material property at the edge of the defect changes abruptly.

5.2.1 Frequency

The shape of the local defect with weaker material properties was simulated as a circle. As described in the previous chapters, only one quarter of the liner circumference was simulated in the 3D model, as shown in Fig 5.4. Consequently, one quarter of the local defect was simulated in the model as well due to the periodic boundary conditions. The occurrence frequency is again studied to determine the minimum distance between two local defects which ensures no interaction between adjacent local defects. Note that the spacing determined earlier for a thickness defect does not necessarily apply to the defect modeled here.

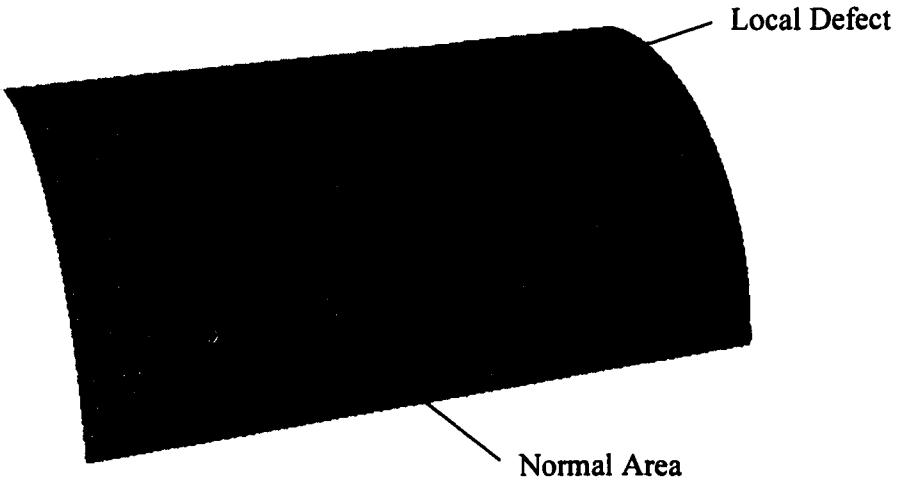

Fig. 5.4 Model with a Local Defect

5.2.2 Mesh Refinement

The mesh refinement of the model with a local reduction in the flexural modulus is summarized in Table 5.5. Notice that the diameter of the defect in the models in this

mesh refinement study is the same as the liner mean diameter and that the flexural modulus of elasticity at the local defect area, E_d, is one half of the average modulus E, i.e., $E_d = \frac{1}{2}$E. The length of the models is 5 inches. The value mesh discretization column is interpreted as the number of element along the circumferential direction * the number of element along the longitudinal direction.

Table 5. 6 Mesh Refinement for the Model with Local Material Property Reduction

Mesh	Buckling Pressure (psi)
15*12	66.4
20*16	62.2
30*24	60.8
60*48	59.8
90*72	59.6

The mesh of 30*24, which means 30 elements along circumferential direction, is selected for the following models to balance computational accuracy and cost. Notice that only the mesh discretization along the circumferential direction is of interest because the model length varies (as was the case for the thickness imperfections). The number of elements in the longitudinal direction is set to keep the aspect ratio of the elements approximately one.

5.2.3 Model Length Effects

In Table 5.6, the buckling pressures of models with different lengths and different local defect diameters are listed. The purpose here is to find the minimum distance between adjacent local defects which ensures the adjacent defects have no interaction

with each other. Notice in the table that the first row stands for the model length and the first column stands for the ratio between the diameters of the local defects with the host-pipe inner diameter. The intersection of this row and column is the buckling pressure corresponding to a specific model length and local defect diameter. One of the rules in the model construction is that the length of the model is larger than the radius of the local defect, otherwise the model is not applicable (NA). Otherwise, the defects would overlap.

Table 5.7 Buckling Pressures (psi) for Models with Different Lengths and Local Defect Diameters

Defect Size / Pipe ID	One-Half of the Distance Between Defects (inches)							
	1 in.	**2 in.**	**3 in.**	**4 in.**	**5 in.**	**7 in.**	**8 in.**	**10 in.**
0.1	100.6	106.4	106.4	106.8	107.8	107.8	107.8	107.8
0.2	87.8	97.4	101.6	102.2	103	103.2	103.2	103.2
0.3	NA	85.3	97.4	98.2	98.6	98.6	98.6	98.6
0.4	NA	82	90.2	91.8	92.2	92.6	92.6	92.6
0.5	NA	NA	81.8	84.8	85.4	86	86	86
0.6	NA	NA	73.2	77.8	78.2	79	79.6	79.6
0.7	NA	NA	66.4	70.8	72.2	72.8	73.4	73.4
0.8	NA	NA	NA	64.4	64.4	64.4	64.4	64.4
0.9	NA	NA	NA	62.2	62.2	62.2	62.2	62.2
1	NA	NA	NA	60.8	60.8	60.8	60.8	60.8

In Table 5.6 for models where the diameter of the local defects are larger than seven-tenths of the liner mean diameter (the bottom three rows of the table), the length of the model doesn't affect the buckling pressure. This occurs because the influence of the

local defects in the circumferential direction dominates the buckling pressure and overrides the effects from the longitudinal direction.

In studying other local defects with a diameter less or equal than seven-tenths of the liner mean diameter, the buckling pressure increases as the model length increases. This indicates that the interaction between adjacent local defects is decreasing as the distance between them increases. For all of the defects given in the table, there is no difference in the buckling results for the 8-inch length and 10-inch length models. It is concluded that as long as the distance between the centers of adjacent defects is larger than 16 inches (which is 2 times the mean diameter of the liner), the adjacent defects have no interaction with each other. Consequently, the eight inch model is used in the following modeling.

5.2.4 Local Defects with Different Areas and Material Properties

It is expected that the area and material properties of a given local defects will influence liner performance. In Table 5.7, a reduced flexural modulus of 0.5E, 0.6E, 0.7E, 0.8E, and 0.9E, are modeled. For each of these cases, ten different defect diameters are simulated, with the diameter ranging from 0.1d to 1d, where d is the mean diameter of the liner.

Table 5.8 Buckling Pressure Reduction (from 108.8 psi) for Models with Local Defects of Varying Size and Flexural Modulus

$\frac{Defect\_Diameter}{Host\_Pipe\_Diameter}\cdot 100\%$	**Fraction of the Flexural Modulus E**				
	0.9E	**0.8E**	**0.7E**	**0.6E**	**0.5E**
10%	99.82%	99.63%	99.26%	98.90%	97.43%
20%	99.26%	98.35%	97.06%	95.77%	94.67%
30%	98.71%	97.06%	95.04%	92.83%	90.26%
40%	96.69%	95.59%	88.97%	86.03%	84.74%
50%	96.14%	92.37%	84.93%	82.54%	78.49%
60%	95.40%	89.52%	82.90%	77.21%	71.88%
70%	94.49%	87.87%	79.78%	72.06%	66.36%
80%	93.75%	86.67%	77.57%	68.57%	59.19%
90%	93.20%	84.93%	76.10%	66.91%	57.17%
100%	92.65%	84.01%	75.00%	65.63%	55.88%

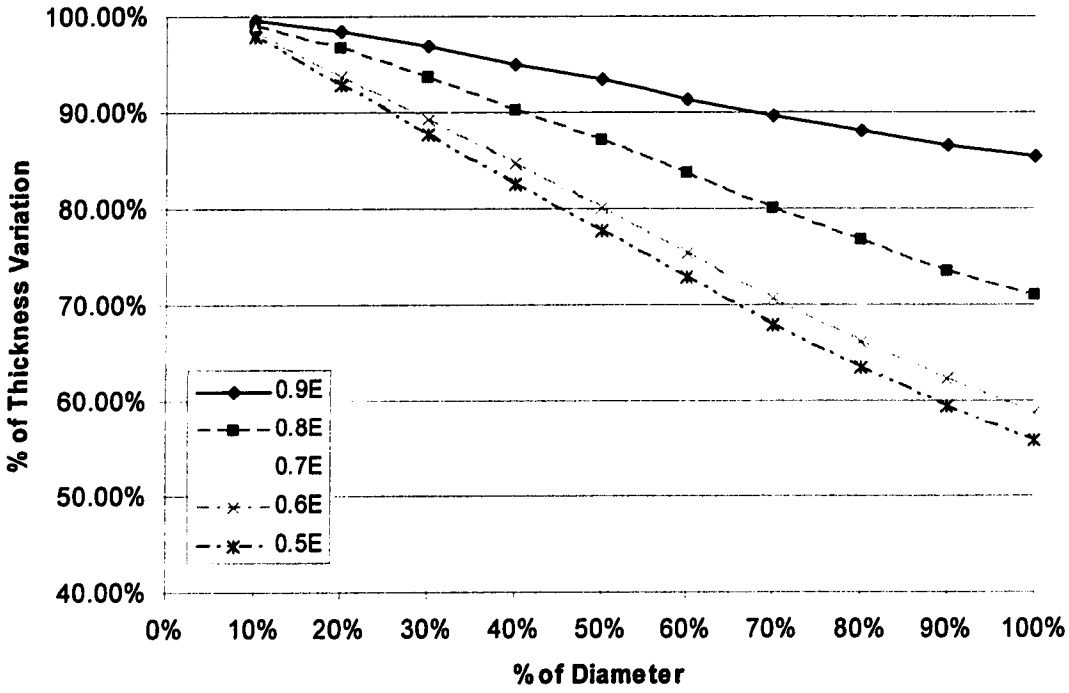

Fig. 5.5 Buckling Pressure Reduction (from 108.8 psi) for Models with Local Defects of Varying Size and Flexural Modulus.

5.3 Conclusions

1. Circular local defects with a thickness that varies continuously in a sinusoidal manner as in Eq. 5.1 were modeled using a 3D FE model. Defect frequency, magnitude, and size were investigated. The following conclusions are drawn:

- When the distance between the centers of two adjacent defects is larger than 2.5 times of the outer diameter of the liner, the adjacent defects do not interact with each other.
- The critical buckling pressure decreases as the size and the magnitude of thickness variation increase.

- The compound effects of magnitude and size of the local defects on buckling pressure is shown in Fig. 5.3.

2. Circular local defects with a reduced flexural modulus were modeled using a 3D FE model. The flexural elastic modulus of the local defect changes abruptly to the reduced value at the edge of the defect. Defect frequency, magnitude, and size are investigated with the following conclusions:

- When the diameter of the local defect is larger than seven-tenths of the mean diameter of the liner, the defect is so large that the longitudinal spacing no longer influences the buckling resistance. That is, the critical buckling pressure does not change with the model length for models where the diameter of the defect is greater than 0.7 times the outer diameter of the liner.
- In the case that the local defect diameter is smaller than seven-tenths of the mean diameter of the liner, the adjacent local defects do not interact with each other when the distance between them is larger than 2.0 times the liner diameter.
- The critical buckling pressure decreases with a decrease in the flexural modulus of the defect and an increase in the size of the defect.
- The compound effect of the magnitude of the modulus reduction and the size of the local defects on buckling pressure was shown in Fig. 5.5.

CHAPTER SIX

INCORPORATING RELIABILITY INTO THE DESIGN OF PIPELINE REHABILITATION LINERS

Laboratory liner buckling experiments are an essential step in developing an understanding of liner buckling processes, and researchers attempt to predict the long-term behavior of liners using such experimental data. In the last two decades, a large number of laboratory tests have been performed by different groups (Aggarwal and Cooper (1984), Lo and Zhang (1994), Guice (1994), Boot and Javadi (1998), Bakeer (1999)). Significant scatter in the buckling time corresponding to a given applied pressure was observed for long-term buckling tests, causing concern when applying the conclusions from the experimental data to real design situations (Moore (1998), McAlpine (1996)). This study analyzes two sets of buckling tests recently performed at the Trenchless Technology Center (TTC), Louisiana Tech University (LTU) using statistical methods. Reliability factors are introduced into the ASTM design model, providing a method for designers to quantitatively estimate the influence of observed scatter on liner design.

6.1 Inverse Prediction of Liner Buckling Pressure

6.1.1 Time Corrected Elastic Modulus in ASTM 1216

According to ASTM F1216-98, the design equation for liners installed in partially deteriorated gravity pipes is shown in Eq. 2.1 in Chapter 2.

One of the key issues in applying this model, as well other existing models, is the determination of the long-term (time corrected) elastic modulus, E_L. Designers typically take E_L as one half of the short-term modulus of elasticity, E, for a design life of 50 years. Falter et al. (1996) derived an expression for the variation in the elastic modulus by assuming that the short-term modulus corresponds to a time of 0.1 hours and the long-term modulus corresponds to 50 years. Fitting an equation using these two modulus-time pairs on a Log(E) versus Log(time) plot results in

$$E(t) = \frac{E_{0.1h}}{(10 \cdot t)^{0.0453}} \tag{6.1}$$

This expression allows the modulus to vary smoothly between the short-term modulus at 0.1 hour and the long-term modulus, which is taken as ½ the short-term modulus at 50 years.

6.1.2 Experimental Data Used for Reliability Calculations

The objective of this paper is to examine the scatter in applied pressure versus buckling time plots so that reliability can be incorporated into liner design. The data gathered from two sets of liner buckling experiments on CIPP liners is used as the basis for examination of liner reliability. All of these experiments were completed at the TTC. The first test program was partially funded by the State of Louisiana Board of Regents Support Fund (BoRSF). The BoRSF data involves three sets of long-term buckling

experiments in 8 inch diameter pipes and three sets of experiments in 12 inch diameter pipes. Each set of BoRSF data involved 25 long-term liner buckling experiments. The average liner outer diameter to thickness ratios (DRs) of the liners installed in the 8 inch pipes were 54.6, 49.4, and 45.8 while the DR values for the 12 inch diameter pipes were 58.6, 48.9, and 43.8. The second test program was funded by the National Science Foundation and involved 13 long-term liner buckling experiments in 8 inch diameter host pipes. The average DR for these tests was 43.0.

6.1.3 Regression Analysis of Experimental Data

A log-log plot of time versus pressure for the BoRSF data set with a DR of 58.6 is seen in Fig. 6.1 along with a best fit line to the data. The data used to create this figure is given in Table 6.1, where only 21 of the original 25 test specimens resulted in usable data.

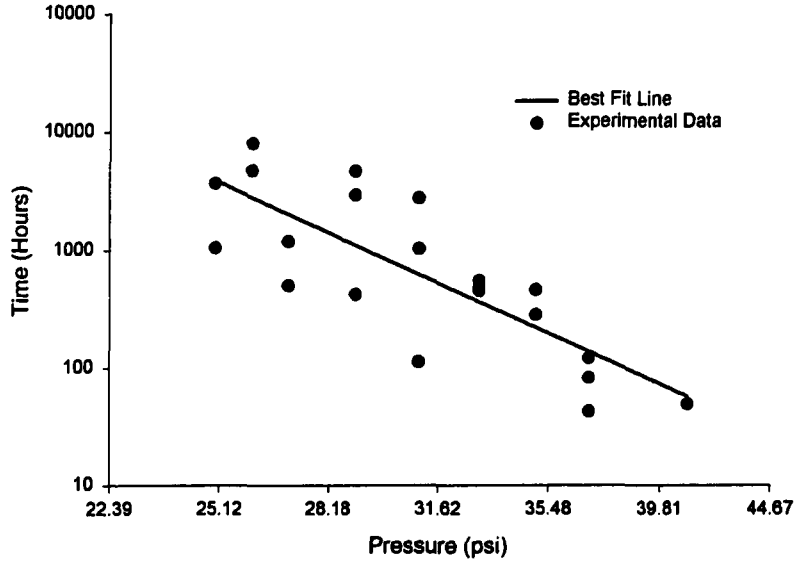

Fig. 6.1 Linear Regression for BoRSF Liners with a DR of 58.6

The least squares regression line for this data set is given by

$$\log(t) = \hat{\beta}_{0p} + \hat{\beta}_{1p} \cdot \log(p) = 15.55 - 8.55 \cdot \log(P) \tag{6.2}$$

where $\hat{\beta}_{0p}$ and $\hat{\beta}_{1p}$ are constants determined by linear regression, t is the buckling time, and P is the applied pressure.

Table 6.1 BoRSF Liner Buckling Data for a DR of 58.6

	without PE film			
Pipe No.	Thickness (in)	Dimension Ratio (DR) (D/t)	Ptest (psi)	Time (hours)
1	0.201	59.20	25	3701.5
2	0.213	55.86	25	1058.4
3	0.187	63.63	26	8070.3
4	0.197	60.40	26	4752.3
5	0.207	57.48	27	1198.3
6	0.196	60.71	27	503.7
7	0.209	56.93	29	423.3
8	0.196	60.71	29	4693.3
9	0.203	58.62	29	2950.7
10	0.197	60.40	31	1034.5
11	0.204	58.33	31	2786.5
12	0.195	61.02	31	112.8
13	0.223	53.36	33	453.3
14	0.208	57.21	33	481.2
15	0.214	55.60	33	554.5
16	0.202	58.91	35	462.0
17	0.211	56.39	35	285.0
18	0.205	58.04	37	121.2
19	0.198	60.10	37	42.6
20	0.198	60.10	37	82.1
21	0.204	58.3	41	49.2
Avg:	**0.203**	**58.6**		

Host Pipe Inside Diameter (in):	11.947
Uniform Gap for 12 inch Diameter 6.5 mm Liners (in):	0.024
Computed Liner OD (in):	11.899
Thickness of Polyethylene Coating (in):	0.015

6.1.4 Pressure Predictions

As plotted in Fig. 6.1, pressure (x-axis) is the independent variable in the experiments and buckling time (y-axis) is the dependent variable. The variables are plotted in this way because liner buckling experiments involve setting the pressure to a level below the critical pressure and recording the time required for failure. Thus, in laboratory tests, time depends on pressure. In field applications, we are interested in predicting the pressure that a liner can sustain for a given design life, which is usually taken as 50 years. In statistics, this problem of predicting x for a give value of y is called inverse prediction.

The prediction of x (or Log(pressure)) from Eq.6.2 for a given y (or Log(time)) is given by

$$x_p = \frac{y - \hat{\beta}_{0p}}{\hat{\beta}_{1p}} \tag{6.3}$$

where x_p is the estimate of x for a giving y, $\hat{\beta}_{0p}$ is the intersection of the best fit line with the y axis, and $\hat{\beta}_{1p}$ is the slope of the best fit line.

When designing for a given reliability level, it is customary to consider upper (x_{U_p}) and lower (x_{L_p}) confidence or prediction limits that lie on either side of the predicted value of x corresponding to the best-fit line. Fig. 6.2 shows how x_{U_p} and x_{L_p} are distributed around x_p for a given value of y.

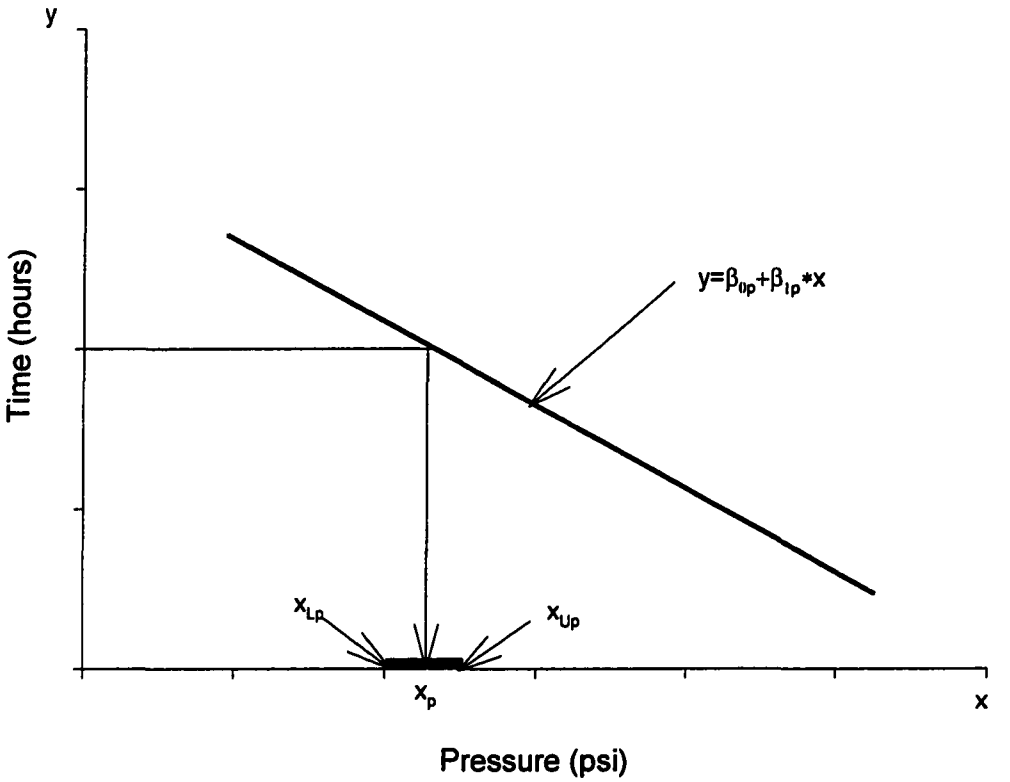

Fig. 6.2 Schematic of Inverse Prediction

For inverse prediction, these limits are given as (Ott, (1993))

$$x_{l/p} = \bar{x} + \frac{1}{1-c^2}[(x_p - \bar{x}) + d] \tag{6.4}$$

$$x_{l,p} = \bar{x} + \frac{1}{1-c^2}[(x_p - \bar{x}) - d] \tag{6.5}$$

where $\bar{x}$ is the mean value of the independent variable while c and d depend on the desired reliability level. Here, we specify the reliability level using α. When α is equal to 0.10, the reliability level is 1-α or 0.90 (90% reliability). If $t_{\alpha/2}$ is a constant obtained from the t-distribution table for the corresponding α, then c^2 and d are given as

$$d = \frac{t_{\alpha/2}\sqrt{\frac{SSE}{n-2}}}{\beta_{1p}}\sqrt{\frac{n+1}{n}(1-c^2)+\frac{(x_p-\bar{x})^2}{S_{XX}}} \tag{6.6}$$

$$c^2 = \frac{t_{\alpha/2}^{\,2}\,\frac{SSE}{n-2}}{\beta_{1p}^{\,2}\;S_{XX}} \tag{6.7}$$

where n is the number of data points in the experiment, SSE is the sum of squares error in the linear regression, and S_{XX} is the corrected sum of squares for the x_i's, which is calculated as $\sum_{1}^{n}(x_i-\bar{x})^2$. The regression analysis was accomplished by using the statistics software package SAS. The upper and lower bounds were calculated from Eqs. (6.4) and (6.5) using Microsoft Excel.

Two observations can be made from Eqs. (6.4) and (6.5). One is that the greater the strength of the linear relationship between x and y, the larger is the quantity $(1-c^2)$, making the width of the prediction interval narrower. In regression, the linear relationship is measured by the coefficient of determination, R^2, where $0 \le R^2 \le 1$. The larger R^2 is, the greater is the strength of the linear relationship between x and y. In our seven sets of experimental data, R^2 ranges from 0.4290 to 0.8026. The second observation is that one can obtain a more reliable prediction of x when y is closer to the center of the experimental region, as measured by $\bar{y}$. Using $\bar{y}$ in Eq. 6.3 gives an x_p which is equal to $\bar{x}$.

When applying Eqs. (6.4) and (6.5), the upper and lower bounds of pressure at different confidence levels can be obtained by using the corresponding α in the equations. In Fig. 6.3, the upper and lower pressure bounds of 90% and 98% confidence

are plotted for the experimental data given in Table 1. Notice that in the plot, time is taken as the x-axis while pressure is the y-axis. The upper and lower pressure bounds in the plot were obtained by using the inverse prediction method in Eqs. (6.4) and (6.5). The best fit line in the plot was obtained by using Eq. 6.3. Although both the lower and upper bounds of the pressure are plotted, what matters in the design is the lower bound, which leads to a conservative design. For example, for a given design life, a pressure level that lies below the experimental data would not cause the liner to buckle before the design life is achieved.

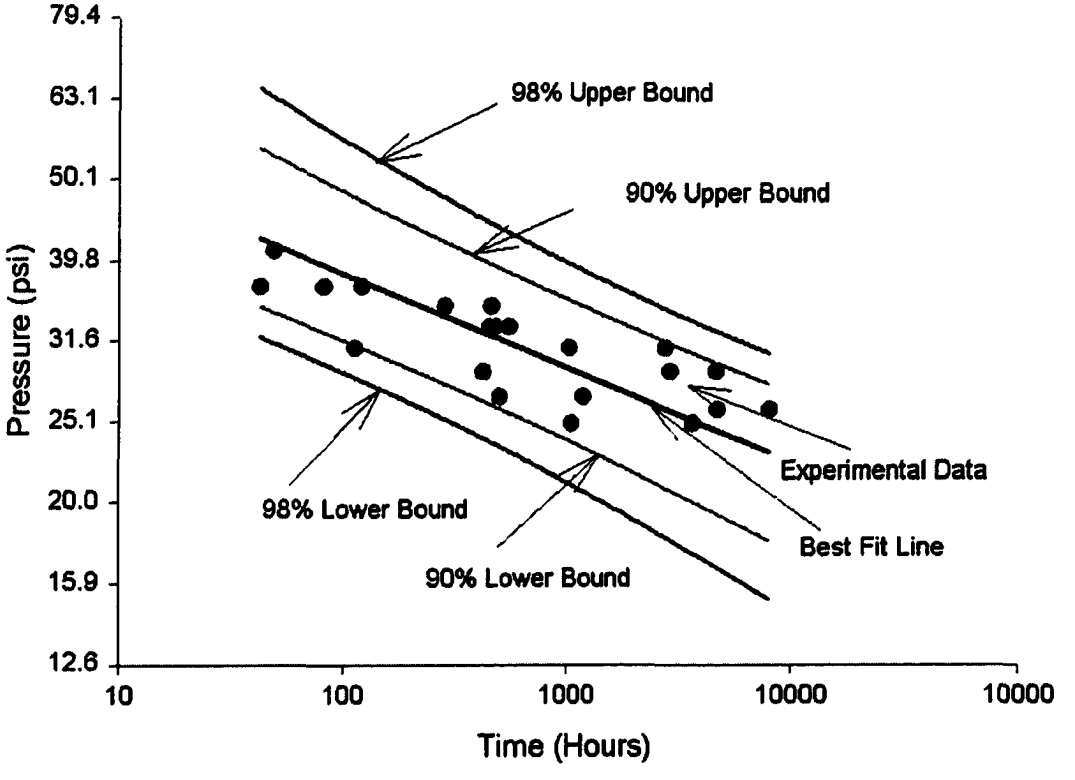

Fig. 6.3 70% and 90% Upper and Lower Pressure Bounds for BoRSF Liner with DR 58.6

6.2 Reliability Factor in Liner Design

6.2.1 ASTM Model Versus Experimental Data

One aim of the liner buckling experiments is to provide data that can be used to evaluate existing liner design models. The long-term liner buckling tests can be categorized as accelerated life tests (ALT), which means methods were devised to force the product to fail quicker than it would otherwise under normal operating conditions. The basic assumption is that the results of ALT can be used to approximate the long-term behavior of the product under normal operating conditions. For the experimental data given here, the test pressure was much higher than the expected ground water pressure, which caused all the test specimens to fail within 10,000 hours, while the design life of a gravity pipe liner is normally 50 years (438,000 hours).

Fig. 6.1 clearly showed that there is a large amount of scatter in the time required for buckling for a given applied pressure. In Fig. 6.4, for experimental data in Table 6.1, the best fit line, the lower 95% confidence level pressure line, and the ASTM model were plotted together for comparison purpose. Notice that the lower bound of the 90% pressure interval in Figure 6.3 is taken as the 95% lower bound of pressure, which means 95% percent of the predicted pressures are located above this line.

When comparing this test data to the prediction line from ASTM F1216 (obtained from Eqs. (2.1) and (6.1)), one observes that the ASTM model and the regression lines have different slopes. The obvious difference in slope may be caused by the inaccuracy of the design model and/or the large amount of scatter in the test data.

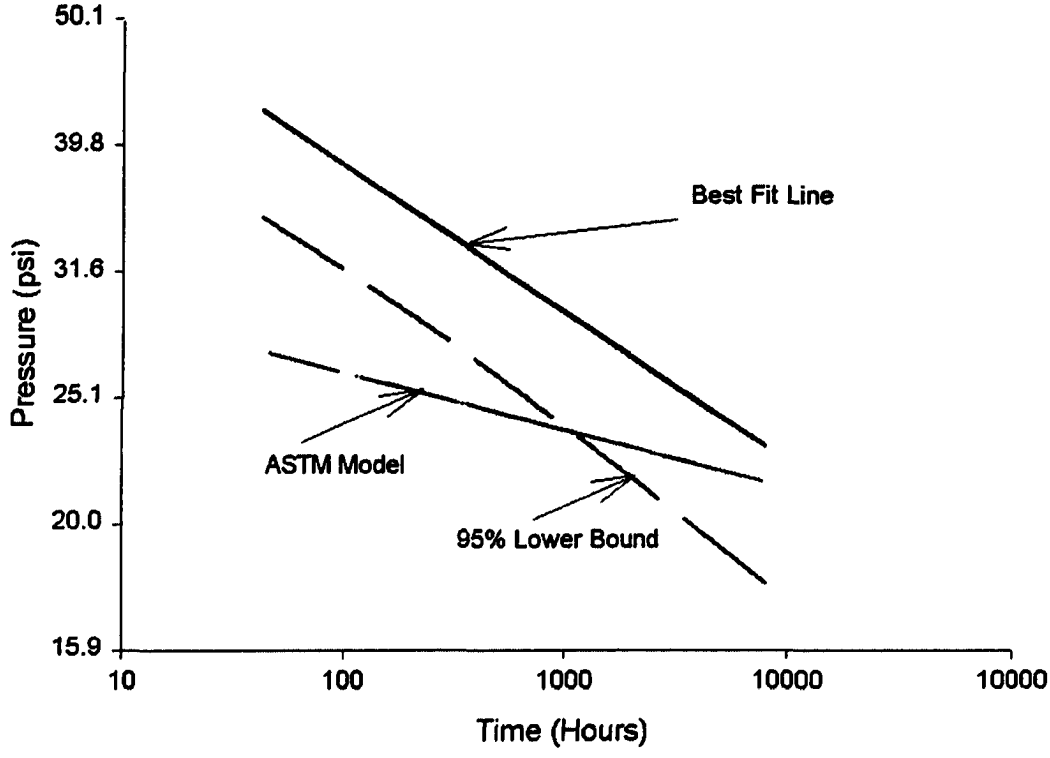

Fig. 6.4 ASTM Model Versus Linear Regression Lines with a DR of 58.6

It is important to note that the ASTM line shown in Fig. 6.4 is ***conservative*** over the 10,000 hour test period since it lies ***below*** the best fit line. That is, the experimental data reveals that the liner can withstand a pressure that is higher than the pressure computed from the design model given in Eqs.(2.1) and (6.1). However, the 95% pressure lower bound intersects with the ASTM model line. This indicates that the ASTM model is conservative for part of the experimental data and is non-conservative for the rest of the data. To compare the two models, we have chosen the predicted pressure corresponding to the mean value of the Log(time) data. This gave the most reliable prediction from the regression line.

6.2.2 Reliability Factors for the Experimental Data

The reliability factor (RF) is defined here as the ratio of the design pressure at a given confidence level (P_d) to the ASTM F1216 design pressure

$$RF = \frac{P_d}{P_{ASTM}} \tag{6.8},$$

where P_d is computed by using Eq. 6.5 with x_p estimated from Eq. 6.3 using $\bar{y}$ for the y value. The calculation results for all seven sets of data at confidence level 50%, 70%, 90%, 95%, 99% and 99.5% are shown in Table 6.2.

Table 6.2 Reliability Factors

Test ID	DR	Pastm	P50%	50% RF	70% RF	90% RF	95% RF	99% RF	99.50 % RF
BoRSF	54.50	31.79	48.99	1.54	1.43	1.27	1.17	0.92	0.76
BoRSF	49.10	42.22	61.84	1.46	1.40	1.31	1.26	1.17	1.12
BoRSF	45.80	53.12	70.96	1.34	1.28	1.20	1.16	1.07	1.03
BoRSF	58.70	24.48	31.37	1.28	1.21	1.10	1.05	0.94	0.89
BoRSF	48.90	43.37	52.81	1.22	1.14	1.02	0.96	0.84	0.78
BoRSF	43.80	57.96	70.59	1.22	1.15	1.06	1.02	0.93	0.89
NSF	43.00	62.58	104.34	1.67	1.55	1.35	1.20	NA*	NA*
			Ave.	1.39	1.31	1.19	1.12	0.98	0.91
			Max.	1.67	1.55	1.35	1.26	1.17	1.12
			Min.	1.22	1.14	1.02	0.96	0.84	0.76
			Stdev.	0.17	0.16	0.13	0.11	0.12	0.14

* NA indicates that the experimental data are not suitable for making the prediction at the corresponding confidence level

6.2.3 Analysis of Reliability Factors

To use the information presented in this paper for design purposes, the designer has to choose the reliability factors that are most reasonable for a given application. For a conservative design, a logical approach is to use the minimum reliability factor for the desired confidence level from Table 6.2.

These minimum reliability factors from Table 6.2, as summarized in Table 6.3, are plotted in Fig. 6.5. Notice that the values given in Table 6.3 are conservative for the other six test series.

Table 6.3 Recommended Reliability Factors for Design Purposes

Confidence Level	50%	70%	90%	95%	99%	99.95%
Reliability Factor	1.22	1.14	1.02	0.96	0.84	0.76

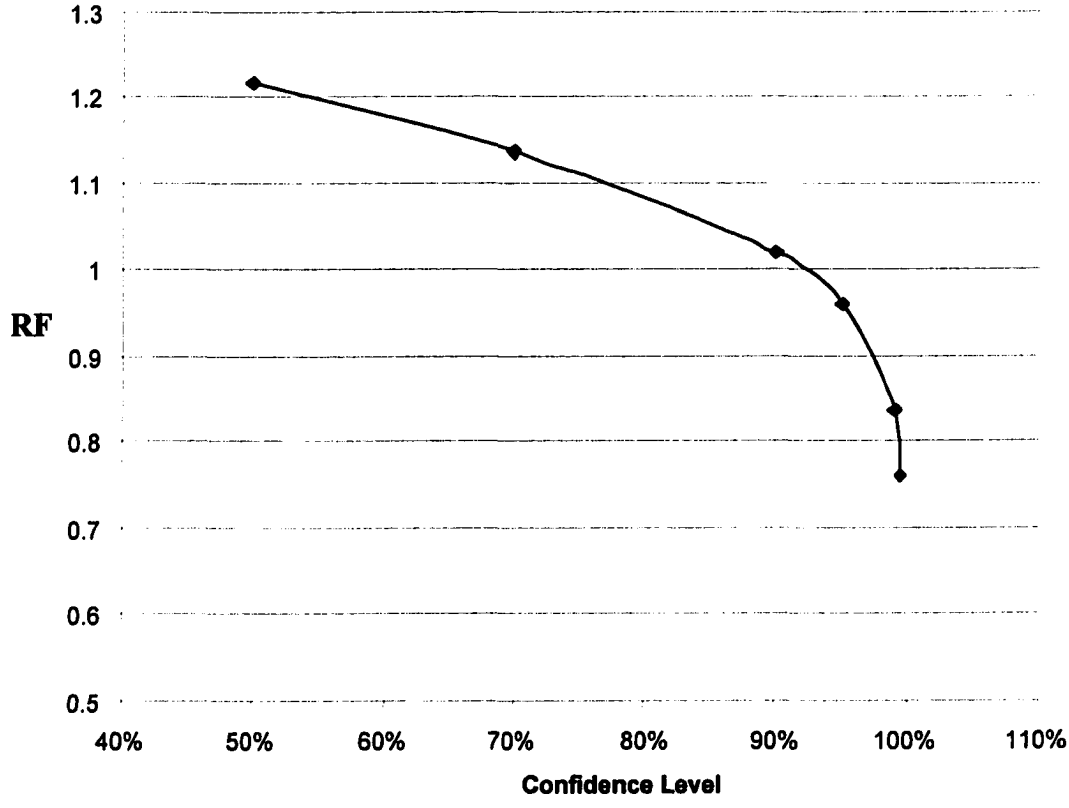

Fig. 6.5 Minimum Reliability Factors

6.2.4 Discussion of the Reliability Factors

The 8 inch diameter host pipes used in the experiments were 5 feet long and the 12 inch diameter pipes were 6 feet long. These pipes are clearly much shorter than a segment of liner pipe installed in the field. The longer lengths present in the field would

likely work to decrease the reliability factors somewhat below those shown in Table 6.3. However, many of the liner specimens whose buckling times were reported buckled near the ends due to the additional pressure exerted by the end clamps. This additional clamping pressure applied on top of the water pressure would tend to make the experimental results more conservative. Thus, this paper assumes that these two competing factors of liner length and end conditions offset one another so that the reliability factors remain unchanged.

Finally, it should be noted that the reliability factors given in this paper are dependent on the model used for liner design, as indicated by Eq. 6.6. If a model other than the design equation given in ASTM F1216 for the partially deteriorated case is used for liner design or if the long-term behavior is accounted for using an expression other than that given in Eq. 2.1, then the ASTM pressure in Eq. 6.5 should be replaced by the pressure computed by the model.

6.2.5 Reliability Factors Versus Factors of Safety

Factors of safety of 1.5 to 2.0 are typical in liner design. These factors of safety are applied to account for uncertainty in groundwater loading, host pipe condition, and imperfections in the liner / host pipe system. The ASTM design equation given earlier accounts for ovality (out of roundness) in the lining system using an ovality reduction factor C. Other types of possible imperfections include the gap between the liner and host pipe, local intrusions of the liner, variations of liner thickness, point-to-point variations in material properties, pipe offsets, and other types of imperfections due to host pipe deterioration. Of these defects, the liner specimens in the BoRSF and NSF experiments included gap and thickness imperfections and some material property variation. These

imperfections are therefore implicitly included in the analysis presented in this paper and would not need to be considered when choosing a factor of safety, assuming the levels present in the experimental specimens are similar to levels expected in the field.

A factor of safety may also be applied to account for potential soil or traffic loading that could be transferred to the liner. Many researchers believe that the host pipe and surrounding soil becomes stabilized when the pipe is lined (Gumbel, 2001) due to elimination of infiltration. Whether justified or not, applying a factor of safety gives the designer a certain level of comfort with regard to potential load transfer. Factors of safety also account for possible variations in curing for CIPP liners.

A reliability factor (RF) can be included in the ASTM design equation as

$$P_{cr} = \frac{2 \cdot K \cdot E_L \cdot C}{1 - \nu^2} \cdot \frac{1}{(SDR - 1)^3} \cdot \frac{RF}{N} \qquad (6.8).$$

For a given P_{cr} in Eq. 6.8, a reliability factor less than 1.0 will act to reduce the DR and increase the liner thickness for a given groundwater pressure. A factor of safety greater than 1.0 will also cause a decrease in DR and an increase in thickness. The designer has two choices for incorporating reliability into liner design:

(1) Design the liner using Eq. 2.1 assumes that the factor of safety is sufficient to account for two parts of uncertainties. One is the uncertainties that are present in the laboratory experiments but not accounted for in the design equation (reliability issues). The other uncertainties are those that may be present in field but are not represented in the test series at all. For example, annular gap between the liner and the host pipe was present in the laboratory tests but is not accounted for in the design equation. Likewise, longitudinal cracks of the host pipe were

not present in the experimental tests but may be present in the field and may act to reduce the buckling resistance of a liner. Assume that a liner is to be designed with 99% reliability corresponding to a reliability factor of 0.84 from Table 6.3. Separating the effective factor of safety into two parts, one that accounts for reliability and another that accounts for field conditions, leads to a factor of 1.19 (1/0.84=1.19) for reliability and 1.68 (2.0/1.19=1.68) for field conditions.

(2) Design the liner using Eq. 6.8 where the factor of safety and the reliability factor are applied separately. In this case, it would be advisable to reduce the factor of safety, since current liner design practices for partially deteriorated host pipes are generally considered to be conservative enough. If an overall factor of safety of 2.0 is desired along with a reliability of 99%, then the factor of safety that should be used in Eq. 6.8 would be 1.68. If the designer wishes to apply a factor of safety of 2.0 in addition to a reliability of 0.84, then the overall safety/reliability factor would be 2.38 (2 / 0.84 = 2.38).

6.2.6 Design Example

Consider a CIPP liner design as an example to illustrate the application of a reliability factor in ASTM1216-98. Assuming the mean inside diameter of the original host pipe is 12 inch with 5% ovality, the ovality reduction factor C is calculated to be 0.64. The ground water table is 20 feet above the invert of the pipe, which means P is $(20)\cdot(62.4)/144 = 8.67$ psi. Assuming that the short-term elastic modulus of the liner material, E, is 250,000 psi (the value of E for the CIPP material tested here was significantly higher at 447,650 psi). The 50-year corrected elastic modulus, E_l, is taken

as one half of E, which is 250,000/2 = 125,000 psi, and the Poisson's ratio is taken as 0.3. The enhanced factor, K, is 7 as recommended in ASTM1216-98.

The following shows the calculations and results by applying the two options discussed in the previous section.

Option 1

Applying a factor of safety of 2.0 in ASTM F1216-98, as given in Eq. 2.1 leads to

$$8.67 = \frac{2 \cdot 7 \cdot 125{,}000}{1 - 0.3^2} \cdot \frac{1}{(SDR - 1)^3} \cdot \frac{0.64}{2} \tag{6.9}$$

The resulting SDR is 42.4 which corresponds to a liner thickness of 0.283 inches (12/42.4). The factor of safety of 2.0 accounts for both reliability and uncertainties in field conditions. As mentioned earlier, a 99% reliability would correspond to a factor of 1.19 for reliability and 1.68 for uncertainties in field conditions.

Option 2

Using Eq. 6.8 with a reliability of 99% (reliability factor of 0.84 from Table 6.3) and a factor of safety of 1.5 results in

$$8.67 = \frac{2 \cdot 7 \cdot 125{,}000 \cdot 0.64}{1 - 0.3^2} \cdot \frac{1}{(SDR - 1)^3} \cdot \frac{0.84}{1.5} \tag{6.10}$$

The resulting SDR is 44.00 which corresponds to a thickness of 0.273 inches (12/44.00). Repeating the calculations in Eq. 6.10 for other reliability levels with a factor of safety of 1.5 results in Table 6.4.

Table 6.4 Calculated Liner Thickness for N=1.5 and Various Reliability Levels

Reliability Level	50%	70%	90%	95%	99%	99.99%
Liner Thickness for Design Example (inches)	0.241	0.247	0.256	0.262	0.273	0.282

The first approach is probably the most reasonable since using a safety factor of 1.5 or 2.0 in Eq.2.1 covers the reliability issue plus additional uncertainties even when 99.95% reliability is desired. That is, for 99.95% reliability, the reliability factor of 0.76 is equivalent to using a factor of safety of 1.32 (1 / 0.76 = 1.32) which is less than 1.5.

6.3 Conclusions

Reliability factors that can be used with the ASTM F1216 design equation for the partially deteriorated case have been developed as summarized in Table 6.3. These reliability factors are an attempt to incorporate the scatter that has been observed in liner buckling experiments into liner design. A designer can either use the reliability factors separately in the design formula, as suggested by Eq. 6.8, or the designer can use Eq. 2.1 and assume that the existing factor of safety applied accounts for all uncertainties in design, including reliability. Since the reliability factors are based on a limited amount of experimental data for a single CIPP configuration at greatly elevated pressures and sometimes using non-standard CIPP DRs, the more logical approach is to continue to use Eq. 2.1 with the understanding that the factor of safety accounts for

- scatter in the experimental data;
- parameters present in the experiments that are not accounted for in the design equation (like gap); and

- uncertainties that are expected in field applications.

The results of this paper should help to provide the designer with confidence that their design will plot below the region of scatter observed on pressure versus time plots.

CHAPTER SEVEN

FURTHER INVESTIGATION OF LINER DESIGN RELIABILITYUSING MULTIVARIATE REGRESSION

In Chapter 6, univariate linear regression was applied to the BoRSF and NSF experimental data. Buckling pressure was predicted using the inverse prediction method to introduce the reliability factor into liner design guideline. In this chapter, the BoRSF experimental data is analyzed using multivariate regression. The inverse prediction technique for the simple regression is extended and applied to the experimental data. Reliability factors obtained using multivariate regression is studied in comparison with those in chapter six using univariate regression.

7.1 Regression Analysis of Experimental Data

7.1.1 One-variable vs. Two-variable Analysis

In Chapter 6, BoRSF and NSF experimental data was analyzed using one independent variable in the linear regression. Pressure was taken as the independent variable, while time until buckling was the dependent variable. Inverse prediction was used in the prediction of pressure for an observed time until buckling and in the

calculation of confidence intervals. For this purpose of the analysis, experimental data were divided into 6 groups by DR value, where each group had from 14 to 22 data points. However, in linear regression, especially when a substantial scatter is observed, a large sample is desired. This was achieved in this study by pooling the data over DR and applying a multiple linear regression with DR and Log(pressure) as the independent variables and Log(time) as the dependent variable. The regression analysis was performed on 8-inch and 12-inch diameter host pipes separately. The inverse prediction technique for the simple regression was extended and applied to the multivariate case.

7.1.2 Experimental Data Used for Multivariate Regression

In these multivariate regression analyses, only the six groups of BoRSF experimental data were used as shown in Tables 7.1 and 7.2.

Table 7.1 Experimental Data for the 8-inch Diameter Pipes

Pipe No.	Ave. DR	Ptest (psi)	Time (hours)
1	54.52	39	2826.5
2	54.52	39	1051.1
3	54.52	43	304.7
4	54.52	45	476.4
5	54.52	45	419.2
6	54.52	48	672.3
7	54.52	48	314.1
8	54.52	52	209.3
9	54.52	55	333.2
10	54.52	55	74.8
11	54.52	58	3
12	54.52	58	253.3
13	54.52	58	8.3
14	49.11	51	2656.5
15	49.11	51	2875.5
16	49.11	51	1995.6
17	49.11	57	488.3
18	49.11	57	488.8
19	49.11	57	802.5

Table 7.1 (continued)

Pipe No.	Ave. DR	Ptest (psi)	Time (hours)
20	49.11	60	219.4
21	49.11	60	488.8
22	49.11	60	655.8
23	49.11	64	422
24	49.11	64	629
25	49.11	64	329.2
26	49.11	70	329.2
27	49.11	70	96
28	49.11	70	92.7
29	49.11	77	143.3
30	49.11	77	210.8
31	45.84	56	1938.8
32	45.84	58	942.6
33	45.84	60	804.6
34	45.84	60	540.2
35	45.84	60	963.3
36	45.84	67	184.8
37	45.84	67	727.4
38	45.84	73	211.8
39	45.84	73	515.5
40	45.84	73	353.9
41	45.84	80	244.7
42	45.84	80	144.3
43	45.84	80	140.3
44	45.84	87	46
45	45.84	87	141.4
46	45.84	87	35.5

Table 7.2 Experimental Data for the 12-inch Pipes

Pipe No.	Ave. DR	Ptest (psi)	Time (hours)
1	58.65	25	3701.5
2	58.65	25	1058.4
3	58.65	26	8070.3
4	58.65	26	4752.3
5	58.65	27	1198.3
6	58.65	27	503.7
7	58.65	29	423.3
8	58.65	29	4693.3
9	58.65	29	2950.7
10	58.65	31	1034.5
11	58.65	31	2786.5
12	58.65	31	112.8
13	58.65	33	453.3
14	58.65	33	481.2
15	58.65	33	554.5
16	58.65	35	462
17	58.65	35	285
18	58.65	37	121.2
19	58.65	37	42.6
20	58.65	37	82.1
21	58.65	41	1.9
22	58.65	41	49.2
23	48.85	41	2150.7
24	48.85	43	7088.7
25	48.85	43	782
26	48.85	45	668.3
27	48.85	47	692.2
28	48.85	47	241.5
29	48.85	47	1840.5
30	48.85	50	759.5
31	48.85	50	434.4
32	48.85	50	800.1
33	48.85	53	2528.8
34	48.85	53	794.1
35	48.85	57	145.8
36	48.85	57	117.6
37	48.85	57	107.7
38	48.85	61	379.8
39	48.85	61	31.8
40	48.85	61	44.8
41	48.85	66	23.2

Table 7.2 (continued)

Pipe No.	Ave. DR	Ptest (psi)	Time (hours)
42	48.85	66	45.8
43	48.85	66	368.8
44	43.78	56	7313.4
45	43.78	56	3301
46	43.78	58	5415.8
47	43.78	61	3697.2
48	43.78	61	1827.2
49	43.78	64	1438.1
50	43.78	64	2895.1
51	43.78	67	1588
52	43.78	67	522.4
53	43.78	67	2729.4
54	43.78	71	1619.4
55	43.78	71	1124.4
56	43.78	71	965.6
57	43.78	75	1188.1
58	43.78	75	1940
59	43.78	75	1821.1
60	43.78	80	41.8
61	43.78	80	255.8
62	43.78	80	932.8
63	43.78	90	185.7
64	43.78	90	99.3
65	43.78	90	123.8

7.1.3 Outlier Detection

Before performing a regression analysis, it is important to determine if there are any observations in the sample that do not seem to be consistent with the rest of data points. Identifying and deleting such observations (or outliers) may improve the fit of the regression model by increasing R^2, the proportion of the total variability that is due to regression.

The studentized deleted residuals were performed for detecting outliers. This was accomplished by deleting the i^{th} observation from the data and running the analysis on the

remaining data. If the studentized deleted residual was larger than 3.0, the i^{th} observation was identified as an outlier.

For the 8-inch diameter pipe, observations Nos. 11 and 13 were diagnosed as outliers. For the 12-inch diameter pipe, only observation No. 21 was diagnosed as an outlier. These outliers were removed and the regression analysis performed on the remaining data.

7.1.4 Two-variable Linear Regression of Experimental Data

The linear regression model for the 8-inch diameter pipe (with n=44) is given by

$$\hat{log}(t) = \hat{\beta}_{0p} + \hat{\beta}_{1p} \cdot \log(p) + \hat{\beta}_{2p} \cdot DR = 19.1986 - 6.2382 \cdot \log(P) - 0.1114 \cdot DR \quad (7.1)$$

Other regression estimates are listed in Table 7.3

Table 7.3 Regression Estimates for the 8-inch Diameter Pipe

Mean Square Error (S^2)	0.06081
C_{11} element of the $(x'x)$ matrix	6.4479
C_{22} element of the $(x'x)$ matrix	0.0047
C_{12} element of the $(x'x)$ matrix	0.1302

The linear regression model for the 12-inch diameter pipe (with n=64) is given by

$$\hat{\log}(t) = \hat{\beta}_{0p} + \hat{\beta}_{1p} \cdot \log(p) + \hat{\beta}_{2p} \cdot DR = 26.3488 - 7.9684 \cdot \log(P) - 0.2005 \cdot DR \quad (7.2)$$

Other regression estimates are listed in Table 7.4.

Table 7.4 Regression Estimates for the 12-inch Diameter Pipes

Mean Square Error (S^2)	0.1873
C_{11} element of the $(x'x)$ matrix	4.0038
C_{22} element of the $(x'x)$ matrix	0.0027
C_{12} element of the $(x'x)$ matrix	0.0961

7.2 Inverse Prediction of Pressure

In the above regression analysis, pressure is one of the independent variables in the experiments and buckling time (y-axis) is the dependent variable. The regression analysis is carried out in this way because liner buckling experiments involve setting the pressure to a level below the critical pressure and recording the time required for failure. Thus, in laboratory tests, time depends on pressure. In field applications, we are interested in predicting the pressure that a liner can sustain for a given design life, which is usually taken as 50 years. In statistics, this problem of predicting x for a give value of y is called inverse prediction.

7.2.1 Inverse Prediction of One of the Independent Variables

The regression model in Eq. 7.1 or 7.2 with two independent variables can be expressed as

$$Y = \beta_0 + \beta_1 x_1 + \beta_2 x_2 + \varepsilon . \tag{7.3}$$

The parameters β_0, β_1 and β_2 are estimated by the least squares method. The regression model with estimated parameters is given by

$$\hat{Y} = \hat{\beta}_0 + \hat{\beta}_1 x_1 + \hat{\beta}_2 x_2 \quad , \tag{7.4a}$$

where

$$\hat{\beta}_0 = \bar{Y} - \hat{\beta}_1 \bar{x}_1 - \hat{\beta}_2 \bar{x}_2 . \tag{7.4b}$$

From Eq. 7.4a, one may estimate Log(pressure) ($x_{1\bullet}$) for an observed Log(time) ($y_\bullet$) and a given RD ($x_{2\bullet}$). This is given by

$$x_{1\bullet} = \frac{y_\bullet - \hat{\beta}_0 - \hat{\beta}_2 x_{2\bullet}}{\hat{\beta}_1} . \tag{7.5}$$

Replacing $\hat{\beta}_0$ in Eq. 7.4a by its value from Eq. 7.4b gives

$$\hat{Y} = \bar{Y} + \hat{\beta}_1 (x_1 - \bar{x}_1) + \hat{\beta}_2 (x_2 - \bar{x}_2) . \tag{7.6}$$

For $x_1 = x_{1\bullet}$ and $x_2 = x_{2\bullet}$, the predicted Y value is given by

$$\hat{Y}_\bullet = \bar{Y} + \hat{\beta}_1 (x_{1\bullet} - \bar{x}_1) + \hat{\beta}_2 (x_{2\bullet} - \bar{x}_2) . \tag{7.7}$$

Since the errors have a normal distribution, ($Y_\bullet - \hat{Y}_\bullet$) is known to have a normal distribution with mean zero and variance $\sigma^2(1+\nu_\bullet)$, where

$$\nu_\bullet = \frac{1}{n} + c_{11}(x_1 - \bar{x}_1)^2 + c_{22}(x_{2\bullet} - \bar{x}_2)^2 + 2c_{12}(x_1 - \bar{x}_1)(x_{2\bullet} - \bar{x}_2) . \tag{7.8}$$

Hence,

$$Y_\bullet - \hat{Y}_\bullet = Y_\bullet - \bar{Y} - \hat{\beta}_1 (x_{1\bullet} - \bar{x}_1) - \hat{\beta}_2 (x_{2\bullet} - \bar{x}_2) \sim N(0, \sigma^2(1+\nu_\bullet)) , \tag{7.9a}$$

so that

$$T = \frac{Y_\bullet - \hat{Y}_\bullet}{S\sqrt{1+\nu_\bullet}} = \frac{Y_\bullet - \bar{Y} - \hat{\beta}_1 (x_{1\bullet} - \bar{x}_1) - \hat{\beta}_2 (x_{2\bullet} - \bar{x}_2)}{S\sqrt{1+\nu_\bullet}} , \tag{7.9b}$$

has a t distribution with (n-2) degrees of freedom.

From Eq. 7.9, it is seen that the set of all values of x_1 satisfying the inequality

$$[Y_* - \bar{Y} - \hat{\beta}_1(x_1 - \bar{x}_1) - \hat{\beta}_2(x_{2*} - \bar{x}_2)]^2 \le \lambda^2 S^2 (1 + v_*), \tag{7.10}$$

where

$$\lambda^2 = (t_{n-2,\alpha/2})^2,$$

provides a 100(1-α)% confidence region for the unknown x_{1*}, given $x_2 = x_{2*}$.

Letting $(x_1 - \bar{x}_1)$=d, Eq. 7.10 can be expressed as

$$\begin{aligned}&(\hat{\beta}_1^{\,2} - \lambda^2 S^2 c_{11})d^2 \\ &+[2\hat{\beta}_1\hat{\beta}_2(x_{2*} - \bar{x}_2) - 2(Y_* - \bar{Y})\hat{\beta}_1 - 2\lambda^2 S^2 c_{12}(x_{2*} - \bar{x}_2)]d \\ &+(Y_* - \bar{Y})^2 + (\hat{\beta}_2^{\,2} - \lambda^2 S^2 c_{22})(x_{2*} - \bar{x}_2)^2 - 2\hat{\beta}_2(Y_* - \bar{Y})(x_{2*} - \bar{x}_2) - \lambda^2 S^2 (1 + \frac{1}{n}) \le 0\end{aligned} \tag{7.11}$$

The inequality in Eq. 7.11 with $x_2 = x_{2*}$ provides a finite $(1-\alpha)$% confidence interval for the estimate $\hat{x}_{1*}$ and is given by $[d_1 + \bar{x}_1, d_2 + \bar{x}_1]$, where d_1, d_2 are the real roots of the quadratic expression in Eq. 7.11. For real roots to exist, $\hat{\beta}_1^{\,2}$ must exceed $\lambda^2 s^2 c_{11}$. This implies that β_1 is significantly different from zero and that there is an effect of pressure on buckling time.

7.2.2 Upper and Lower Bounds of Pressure

When applying Eq. 7.11, the upper and lower bounds of pressure at different confidence levels can be obtained by using the corresponding λ^2, which is the square of the t-distribution value at the required confidence level $(1-\alpha)$%. In Figs. 7.1 and 7.2, the upper and lower 95% pressure bounds are plotted for the experimental data of the 8-inch

diameter pipe with a DR of 54.52 and for the 12-inch diameter pipe with a DR of 43.78. Notice that in the plot, time is taken as the x-axis while pressure is the y-axis. The upper and lower pressure bounds in the plots were the antilog of the bounds for Log(pressure) obtained from the inverse prediction method in Eq. 7.11. The best fit line in the plots was obtained by using Eqs. 7.1 and 7.2. Although both lower and upper bounds of the pressure are plotted, what matters in the design is the lower bound, which leads to a conservative design. For example, for a given design life, a pressure level that lies below the lower bound of experimental data would not (with probability 0.5) cause the liner to buckle before the design life is achieved.

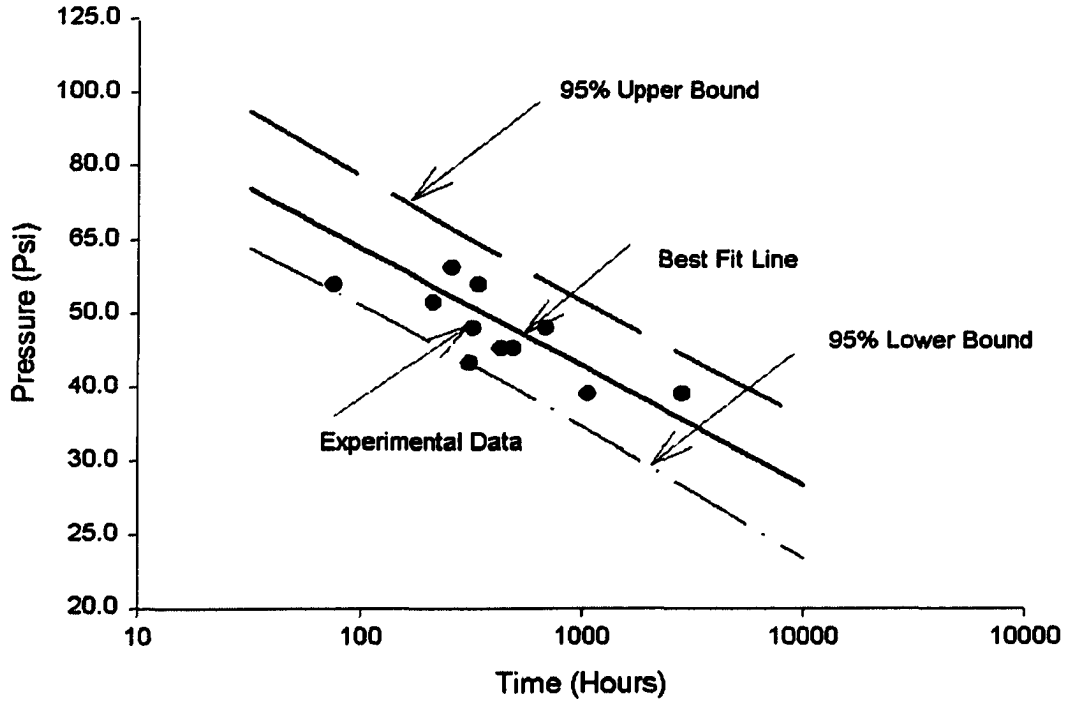

Fig. 7.1 95% Upper and Lower Pressure Bounds for the 8-inch Liner with DR = 54.52

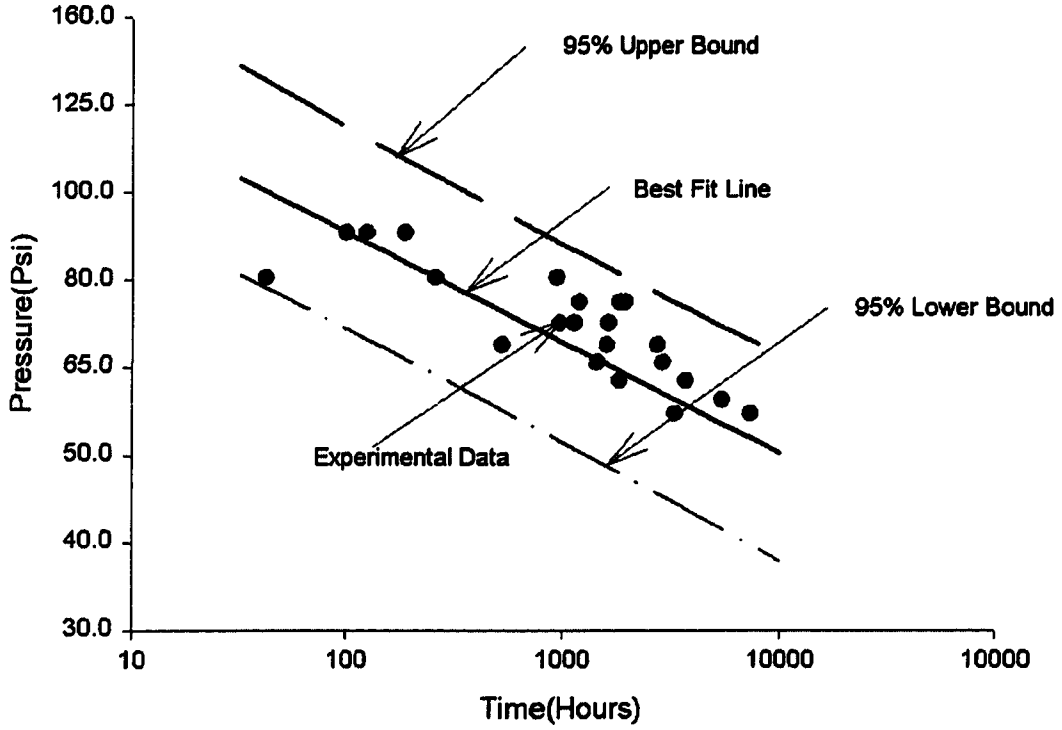

Fig. 7.2 95% Upper and Lower Pressure Bounds for the 12-inch Liner with DR = 43.78

7.2.3 ASTM Model Versus Experimental Data

Tables 7.1 and 7.2 clearly show that there is a large amount of scatter in the time required for buckling for a given applied pressure. Figs. 7.3 and 7.4 show the experimental data for the 8-inch (DR=54.52) and 12-inch (DR=43.78) liners, the best fit line, the lower 97.5% confidence level pressure line, and the ASTM model together for comparison purposes. Notice that the lower bound of the 95% pressure interval in Figure 7.3 is taken as the 97.5% lower bound of pressure. This means that 97.5% percent of the predicted pressures are located above this line.

When comparing the test data to the prediction line from ASTM F1216 (obtained from Eqs. 6.1 and 6.2), one observes that the ASTM model and the regression lines have

different slopes. The obvious difference in slope may be caused by the inaccuracy of the design model and/or the test data itself.

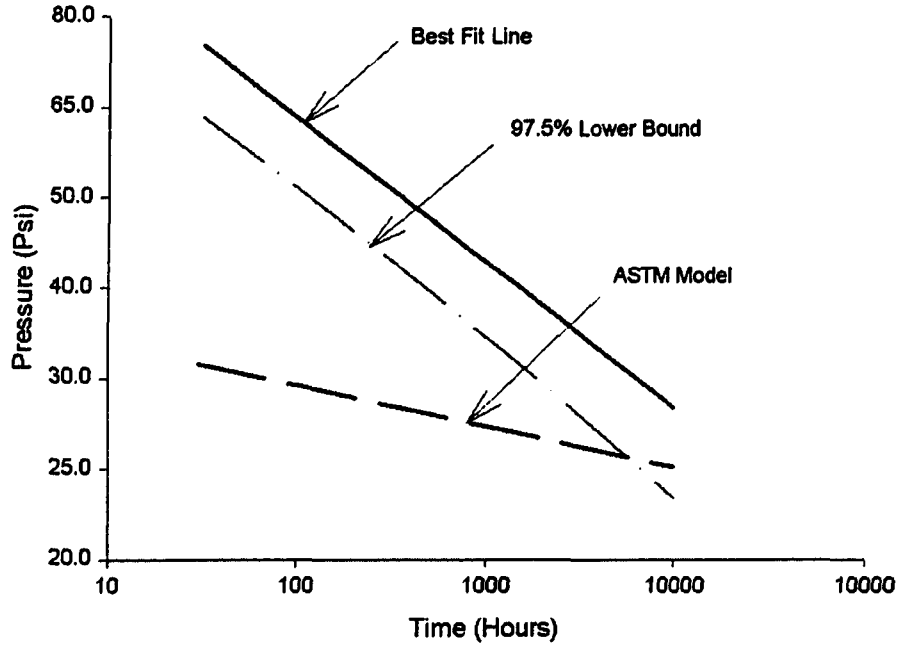

Fig. 7.3 ASTM Model Versus Regression Lines for the 8-inch Liners with DR = 54.52

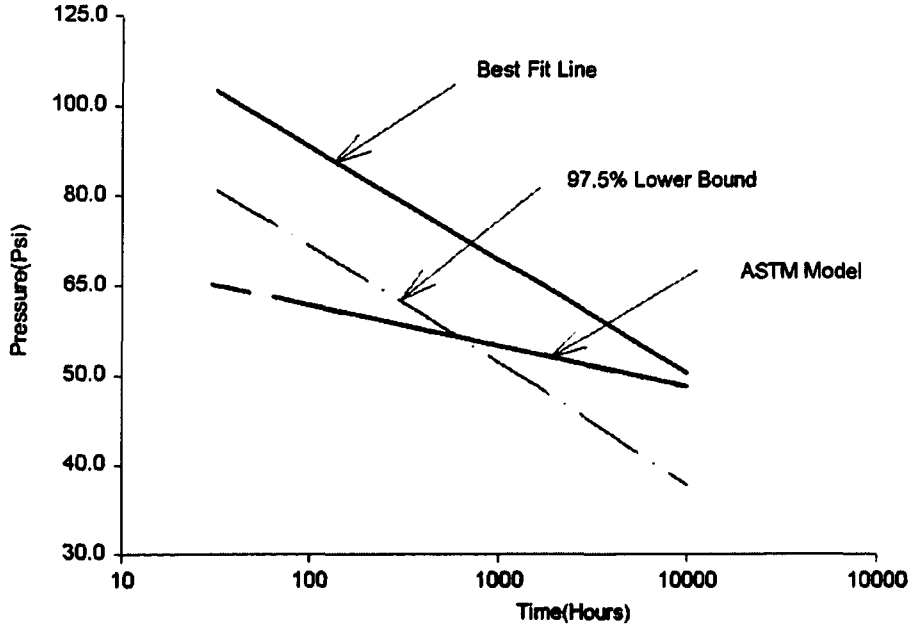

Fig. 7.4 ASTM Model Versus Regression Lines for the 12-inch Liners with DR = 43.78

It is important to note that the ASTM lines shown in Figs. 7.3 and 7.4 are ***conservative*** over the 10,000 hour test period since they lies ***below*** the best fit line. That is, the experimental data reveals that the liner can withstand a pressure that is higher than the pressure computed from the design model given in Eqs.6.1 and 6.2. However, the 97.5% pressure lower bound intersects with the ASTM model line. This indicates that the ASTM model is conservative for part of the experimental data and is non-conservative for the rest of the data when 97.5% confidence is required. To compare the two models, we have chosen the predicted pressure corresponding to the mean value of the Log(time) data. This gave the most reliable prediction from the regression line.

7.2.4 Reliability Factors for the Experimental Data

The reliability factor (RF) is defined here as the ratio of the design pressure at a given confidence level (P_d) to the ASTM F1216 design pressure:

$$RF = \frac{P_d}{P_{ASTM}} \quad , \tag{7.12}$$

where P_d is computed by using Eq. 7.11 with Y_* taken as the average of all measured Y values, $\bar{Y}$. The ASTM pressure is computed using Eqs. 6.1 and 6.2. The resulting reliability factors for all seven sets of data at confidence levels of 50%, 70%, 90%, 95%, 99% and 99.5% are shown in Table 7.5.

Table 7.5 Reliability Factors

DR	P_{ASTM}	P50%	50% RF	70% RF	90% RF	95% RF	99% RF	99.50 % RF
54.50	29.19	48.98	1.68	1.64	1.50	1.46	1.36	1.30
49.10	39.94	60.26	1.51	1.47	1.38	1.31	1.23	1.20
45.80	49.11	69.18	1.41	1.38	1.28	1.20	1.15	1.12
58.70	22.97	30.20	1.31	1.38	1.12	1.04	0.95	0.91
48.90	39.75	53.70	1.35	1.26	1.12	1.07	0.98	0.93
43.80	55.22	70.79	1.28	1.20	1.09	1.04	0.95	0.91
		Ave.	1.42	1.39	1.25	1.19	1.10	1.06
		Max.	1.68	1.64	1.50	1.46	1.36	1.30
		Min.	1.28	1.20	1.09	1.04	0.95	0.91
		Stdev.	0.15	0.16	0.16	0.17	0.17	0.17

7.2.5 Analysis of Reliability Factors

To use the information presented in this paper for design purposes, the designer has to choose the reliability factors that are most reasonable for a given application. For a conservative design, a logical approach is to use the minimum reliability factor for the desired confidence level from Table 7.5. These minimum reliability factors from Table 7.5, as summarized in Table7.6, are plotted in Fig. 7.5.

Table 7.6 Recommended Reliability Factors for Design Purposes

Confidence Level	50%	70%	90%	95%	99%	99.95%
Reliability Factor	1.28	1.20	1.09	1.04	0.95	0.91

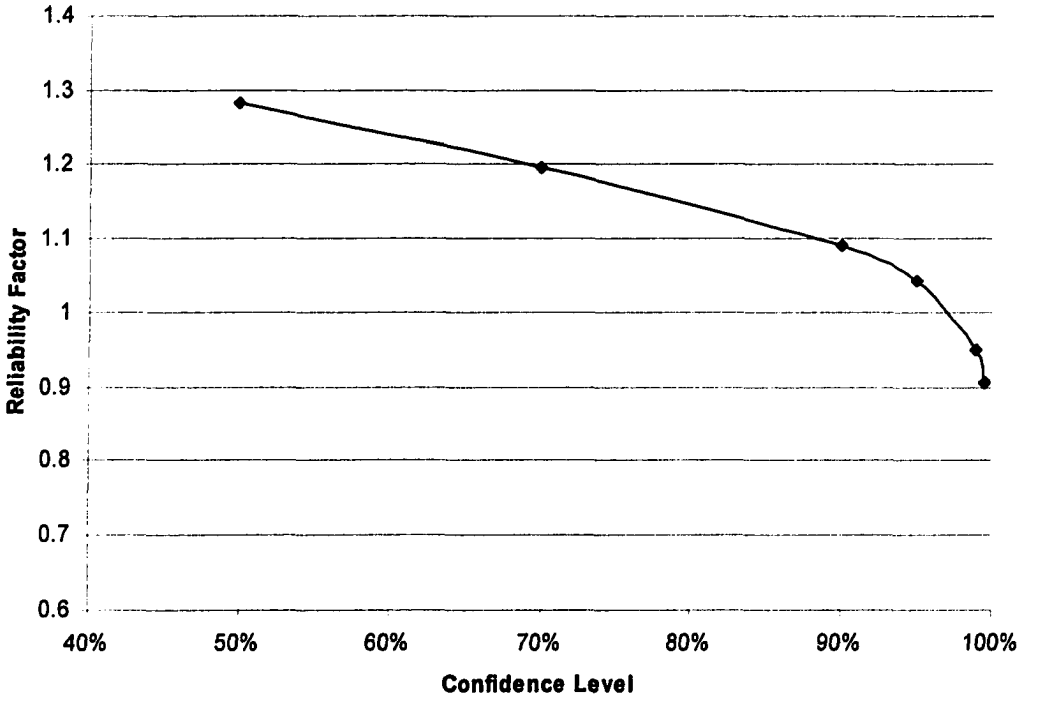

Fig. 7.5 Average Reliability Factors

7.2.6 Comparison with RF in Univariate Regression Analysis

For comparison purposes, the minimum reliability factors obtained using univariate regression analysis (Fig. 6.5) and multivariate regression analysis (Fig. 7.5) are drawn together in Fig. 7.6. It is clearly shows that the reliability factor obtained by multivariate regression analysis is higher than those of univariate regression analysis. The difference is caused by the better regression properties provided by the large sample in the multivariate regression model. Further research with more comprehensive experimental data in terms of material properties, sample size, and DR, is desired.

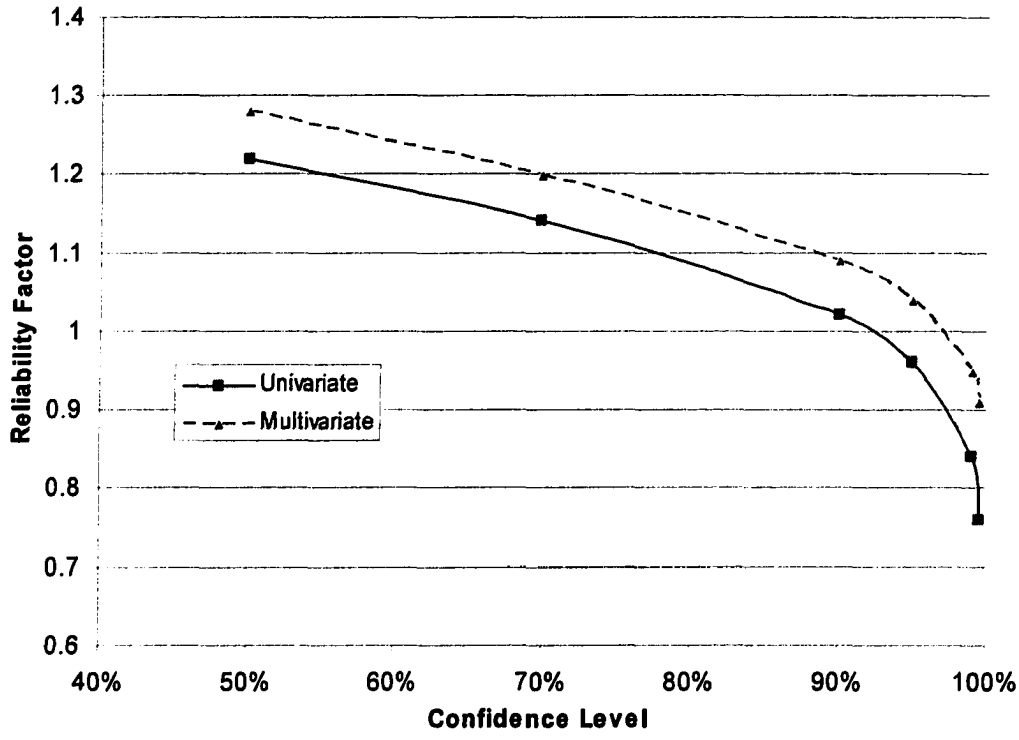

Fig. 7.6 Comparison of Average RF using Univariate and Multivariate Regression

7.3 Conclusions

1. The inverse prediction of one independent variable in the multivariate regression model, as shown in Eq. 7.11, is an extension of the single independent variable regression inverse prediction technique. It is shown to be valid in the inverse prediction of pressure in liner buckling experiments.

2. The reliability factors as shown in Table 7.6 are recommended for liner design. The recommended reliability factors give the designer confidence to use the ASTM F1216 to design the liner while considering the scatter observed in laboratory tests.

3. By comparing the reliability factors obtained in this chapter and those in Chapter 6, it is recommended that this research be extended as more experimental data becomes available.

CHAPTER EIGHT

CONCLUSIONS AND RECOMMENDATIONS

8.1 Conclusions

8.1.1 Conclusions of FE Analyses

In most previous liner buckling FE models, the liner buckling problem was simplified to a 2D model. In this study, a 3D liner buckling model was constructed using the ABAQUS FE software. In earlier studies, the influence of geometric factors, such as ovality, gap, and DR, was studied using 2D models. Here, the use of a 3D model makes the study of three dimensional imperfections possible. The variation of thickness in the circumferential, longitudinal, and combined longitudinal/circumferential directions were investigated along with a 3D circular defect. The details of these models and the conclusions resulting from these models are given below.

- A 3D liner buckling model was constructed with the following features:
    - The S4R5 shell element was chosen to represent the wall of the liner.
    - The reference surface of the flexible liner (where the nodes were actually defined) was set at the outer surface of the liner to facilitate the definition of the contact surface.
    - Periodic boundary conditions were employed so that an infinite length of the liner could be modeled with reasonable computational cost.

- The liner is uniformly loaded by external pressure (to simulate ground water pressure) and is constrained by the host-pipe.
- The length of the 3D model has no influence on the resulting buckling pressures.

- The 3D model is verified by Glock's analytical model and by comparison with a 2D FE model.
- Buckling pressure increases with both the frequency and magnitude of thickness variation in longitudinal direction. In this case, the thicker regions act as stiffening ribs.
- For thickness variation in circumferential direction, buckling pressure is stabilizes as the frequency of thickness variation increases, and buckling pressure decreases as the magnitude of thickness variations increase.
- For thickness variation in both directions, the buckling pressure decreases with the increasing of the frequency of thickness variation. The buckling pressure decreases in lower rate when the frequency of thickness variation is high. Under high frequency variation, the buckling pressure doesn't change while the thickness variation is less than 20%. The buckling pressure decreases with increasing thickness variations when the magnitude is larger than 20%.
- For thickness variation in both directions, the buckling pressure doesn't change while the thickness variation is lower than 20%. When the variation magnitude is larger than 20%, the buckling pressure decreases with the increasing of thickness variation magnitude.

- The distribution of displacement and stress of a liner with thickness variation follows the distribution of the thinner wall distribution. When the thickness variation frequency is low, it is clear that the large displacements follow the thinner band. When the frequency is high, the influence of thickness distribution on the buckling location is less obvious.
- The liner buckling pressure is high wherever there is wide band of continuous thickness at the crown part of the liner.
- For circular local defects with reduced thickness, adjacent defects don't interact with one another when the distance between the centers of two adjacent defects is larger than 2.5 times of the outer diameter of the liner. The critical buckling pressure decreases as the size and magnitude of the thickness variation increases as shown in Fig. 5.3.
- For circular local defects with a reduced flexural modulus, the critical buckling pressure doesn't change with the model length for models where the diameter of the defect is greater than 0.7 times the outer diameter of the liner. In the case that the local defect diameter is smaller than seven-tenths of the mean diameter of the liner, the adjacent local defects don't interact with each other when the distance between them is larger than 2.0 times the liner diameter. The critical buckling pressure decreases with a decrease in the flexural modulus of the defect and an increase in the size of the defect as shown in Fig. 5.5.

8.1.2 Conclusions of Statistical Modeling

Significant scatter in the buckling time corresponding to a given applied pressure has been observed for long-term buckling tests, causing concern when applying the conclusions from the experimental data to real design situations. This study analyzes two sets of buckling tests recently performed at the TTC at LTU using statistical methods. Reliability factors are introduced into the ASTM design model, providing a method for designers to quantitatively estimate the influence of observed scatter on liner design. Conclusions of the statistical analyses are given below.

- Liner buckling experiments involve setting the pressure to a level below the critical pressure and recording the time required for failure. Thus, in laboratory tests, time depends on pressure. In field applications, we are interested in predicting the pressure that a liner can sustain for a given design life, which is usually taken as 50 years. In statistics, this problem of predicting x for a give value of y is called inverse prediction.
- In Chapter 6, a regression analysis with one independent variable was conducted, where Log(time) was the independent variable and Log(pressure) was the dependent variable. In Chapter 7, a regression analysis with two independent variables was conducted, where Log(time) and DR were the independent variables and Log(pressure) was the dependent variable. The regression analysis with two independent variables achieved a larger sample size by pooling experimental data over three different DRs. This led to more reliable predictions.

- Upper and lower bound pressures for different design lives, with different confidence levels, were achieved using the inverse prediction method. The lower bound of pressure is of design interest.
- While comparing the plots of regression analysis results and the ASTM design model, an obvious difference in slope was observed. The obvious difference in slope may be caused by inaccuracy of the design model and/or the large amount of scatter in the test data.
- To achieve the most reliable prediction, the predicted pressure at the mean experimental life-time was applied in calculating the reliability factors.
- The minimum reliability factors of all data sets were chosen as the recommended reliability factors for conservative design purposes.
- Two alternatives were suggested to use the recommended reliability factors in liner design. The first alternative, as shown in Eq. 2.1 was to assume reliability factor is embedded in the safety factor. The second alternative was to add a reliability factor into liner design model as shown in Eq. 6.8. Since the reliability factors are based on a limited amount of experimental data for a single CIPP configuration at greatly elevated pressures and sometimes using non-standard CIPP DRs, the more logical approach is to continue to use Eq. 2.1 with the understanding that the factor of safety accounts for
  - scatter in the experimental data;
  - parameters present in the experiments that are not accounted for in the design equation (like gap); and
  - uncertainties that are expected in field applications.

- Eq. 7.11 can be used to predict the desired independent variable (pressure) for regression analyses with two-independent variables when the other independent variable (DR) is set.

8.2 Recommendations

- The 3D liner buckling model developed in this study can be directly used to study other 3D liner defects such as longitudinal intrusions.
- Simulating thickness variation of liners is a complex process which may require super computers to simulate realistic (or observed) thickness variation profiles. Other methods, such as stochastic finite element methods, may also be applied to simulate more realistic thickness variations.
- Incorporating reliability factors into liner design to cover the observed scatter may be further studied using more comprehensive experimental data or through a comprehensive computational analysis of pipe linings were observed imperfections are varied randomly.
- The equation of Falter (Eq. 6.1) assumes that the creep modulus at 50 years is ½ of the short-term flexural modulus of the material. This model was applied because it follows the ½ value for the 50 year modulus commonly used when applying ASTM F1216. However, other models of the variation of the creep modulus based on actual creep tests would likely provide a more accurate long-term design model with different reliability factors.

REFERENCES

1. Aggarwal, S. C. and Cooper, M.J. (1984). "External Pressure testing of Insituform Lining." Internal Rep., Coventry (Lanchester) Polytechnic, Coventry, U.K.

2. ASTM (1995). "Standard Practice for Rehabilitation of Existing Pipelines and Conduits by the Inversion and Curing of a Resin-Impregnated Tube." *ASTM Designation F1216-95*, Philadelphia, PA

3. Bakeer, M R., Barber, M. E., Pechon S. E., Taylor S. E., and Chunduru S. (1999). "Buckling of HDPE Liners Under External Uniform Pressure." Journal of Materials in Civil Engineering. Vol. 11, No. 4, PP 353-361

4. Bakeer, M R., Barber, M. E., Pechon S. E., and Taylor J. E. (2001). "Long-term Buckling Performance of HDPE Liners." Journal of Materials in Civil Engineering. Vol. 13, No. 3, PP176-184

5. Boot, J. C., Toropova, I. L., and Ashour, A.F. (2001). "The Structure Performance of Flexible Sewer Linings Subjected to External Pressure." Proceedings of the International Conference on Underground Infrastructure Research, Kitchener, Onrario, 11-13 June, 2001, PP39-47

6. Chunduru, S., Barber M. E., and Bakeer R. M. (1996). "Buckling Behavior of Polyethylene Liner System," Journal of Materials in Civil Engineering. Vol. 8, No. 4, PP201-206

7. EL-Sawy, K., and Moore I. D. (1998). "Stability of Loosely Fitted Liners used to Rehabilitate Rigid Pipes." Journal of Structural Engineering, Vol. 124, No. 11, PP1350-1357

8. Falter B. (2001). "Structural Design of Linings," Proceedings of the International Conference on Underground Infrastructure Research, Kitchener, Onrario, 11-13 June, 2001, PP49-56Glock, D. (1977). "Post-Critical Behavior of a Rigid Encased Circular Pipe Subject to External Water Pressure and Temperature Rise." Der Stahlbau, 46(7), PP212-217 (in German)

9. Guice, L.K., and Li, J.Y. (1994) (1). "Buckling Models and Influencing Factors for Pipe Rehabilitation Design." Proceedings of the North American NO-DIG '94, Dallas, Texas,April 1994, WS1:1-WS1:15

10. Guice, L. K., Straughan, W. T., Norris, C. R., and Bennett, R.D. (1994) (2). "Long-Term Structural Behavior of Pipeline Rehabilitation Systems." Technical Report No 302, Trenchless Technology Center, Louisiana Tech University, Ruston, La

11. Gumbel, J. (2001). "New Approach to Design of Circular Liner Pipe to Resist External Hydrostatic Pressure," Proceedings of the ASCE Conference Entitled "Advances in Pipeline Engineering & Construction, " July, San Diego, CA

12. Lin, H. (1995). "Creep Characterization of CIPP Material Under Tension, Compression, and Bending." MS Thesis. Department of Civil Engineering, Louisiana Tech University, Ruston, LA

13. Lo, K.H. and Zhang, J.Q. (1994). "Collapse Resistance Modeling of Encase Pipes," Buried Plastic Pipe Technology: 2nd volume, ASM STP 1222, Edited by Dave Eckstein, 97-110.

14. Lu, X. (1999), "Finite Element Analysis for CIPP encased in Oval Host Pipes." Master Dissertation, Louisiana Tech University, Ruston, LA

15. McAlpine, G.A. (1996). "TTC Report on Long-term Structural Behavior of Pipeline Rehabilitation Systems – A Discussion," No-Dig Engineering, Vol.3, No. 3. 21-24.

16. Moore, I. D. (1988). "Elastic Buckling of Buried Flexible Tubes – A Review of Theory and Experiment." Journal of Geo-technical Engineering, Vol. 115, No.3, PP340-357

17. Omara, A. M. (1997). "Analysis of Cured-In-Place Pipes(CIPP) Installed in Circular and Oval Host Pipes." Ph.D. Dissertation, Louisiana Tech University, Ruston, LA

18. Omara, A.A., Guice, L.K., Straughan, W.T., Akl, F.A. (2000). "Buckling Models of Thin Circular Pipes Encased in Rigid Cavity." *ASCE* Journal of Engineering Mechanics, PP214-220

19. Ott, R.L. (1993). "An Introduction to Statistical methods and Data Analysis," 4th Edition, Duxbury Press, Belmont, California, 533-535.

20. Seemann, R.K., Hall, D.E. and Straughan, W.T. (2000). "Buckling Experiments for CIPP Liners Installed in Ovalized Host Pipes." Trenchless Technology Center Internal Report, Louisiana Tech University, Ruston, LA

21. Soong, T.C., Choi I. (1985). "Buckling of an Elastic Elliptical Ring Inside a Rigid Boundary." Journal of Applied Mechanics, September, Vol. 52, PP523-528

22. Thepot O. (2001). "The Structural Design of Non-circular Linings." Proceedings of the International Conference on Underground Infrastructure Research, Kitchener, Onrario, 11-13 June, 2001, PP65-74

23. Timoshenko, S.P. and Gere, J.M. (1961). *Theory of Elastic Stability*. 2nd Edition, McGraw-Hill, New York, NY

24. Zhao, Q. (1999). "Finite Element Simulation of Creep Buckling of CIPP Liners under External Pressure." Ph.D. Dissertation, Louisiana Tech University, Ruston, LA

25. Zhao W., Nassar R., and Hall D. E. (2003). "Incorporating reliability into the design of pipeline rehabilitation liners." Proceedings of North American Society for Trenchless Technology, 2003 Conference, Las Vegas, Nevada

26. Zhu, M. (2000). "Computational Investigation of Stress, Contact Condition, and Buckling of Thin-Walled Pipe Liners." Ph.D. Dissertation, Louisiana Tech University, Ruston, LA

APPENDIX A

LINER BUCKLING EXPERIMENTAL DATA

Table A.1 Short-term Circular Liner Buckling Tests by Guice et al. (TTC, 1998)

Test No.	t (in)	D_{mean} (in)	DR	P_{cr} (psi)
12"OD5.5mm1	0.200	11.64	58.22	64
12"OD5.5mm2	0.202	11.65	57.67	60
12"OD5.5mm3	0.197	11.66	59.11	54
12"OD5.5mm4	0.197	11.67	59.17	50
12"OD5.5mm5	0.205	11.68	57.04	36
Average	0.200	11.66	58.24	52.8
12"OD6.5mm1	0.244	11.67	47.90	80
12"OD6.5mm2	0.238	11.67	49.04	86
12"OD6.5mm3	0.232	11.66	50.32	92
12"OD6.5mm4	0.235	11.67	49.69	105
12"OD6.5mm5	0.241	11.65	48.38	98
Average	0.238	11.66	49.07	92.2
12"OD7.5mm1	0.259	11.68	45.12	138
12"OD7.5mm2	0.261	11.67	44.66	127
12"OD7.5mm3	0.263	11.62	44.14	103
12"OD7.5mm4	0.262	11.59	44.20	112
12"OD7.5mm5	0.267	11.59	43.47	139
Average	0.262	11.63	44.32	123.8
8"OD4.5mm1	0.148	7.83	52.99	80
8"OD4.5mm2	0.151	7.82	51.88	86
8"OD4.5mm3	0.150	7.85	52.41	80
8"OD4.5mm4	0.146	7.77	53.42	88
8"OD4.5mm5	0.154	7.86	51.16	78
Average	0.150	7.83	52.37	82.4
8"OD5.5mm1	0.160	7.79	48.65	92
8"OD5.5mm2	0.162	7.74	47.74	105
8"OD5.5mm3	0.165	7.81	47.29	110
8"OD5.5mm4	0.159	7.84	49.23	115
8"OD5.5mm5	0.159	7.81	49.19	112
Average	0.161	7.80	48.43	106.8
8"OD6.5mm1	0.182	7.79	42.78	113
8"OD6.5mm2	0.176	7.83	44.42	115
8"OD6.5mm3	0.176	7.79	44.39	133
8"OD6.5mm4	0.174	7.79	44.73	115
8"OD6.5mm5	0.177	7.77	43.92	113
Average	0.177	7.80	44.05	117.8

Table A.2 Short-term Oval Liner Buckling Tests by Guice et al. (TTC, 1998)

Test No.	t (in)	D_{mean} (in)	DR	OV (%)	P_{cr} (psi)
12"OD0%OV1	0.308	11.65	37.85	n/a	134
12"OD0%OV2	0.293	11.64	39.80	n/a	117
12"OD0%OV3	0.294	11.77	40.06	n/a	125
12"OD0%OV4	0.295	11.66	39.54	n/a	131
12"OD0%OV5	0.302	11.69	38.76	n/a	109
Average	0.298	11.68	39.19	n/a	122.9
12"OD2%OV1	0.296	11.64	39.36	1.94	105
12"OD2%OV2	0.293	11.68	39.91	1.82	105
12"OD2%OV3	0.313	11.65	37.27	1.65	90
12"OD2%OV4	0.306	11.63	38.03	1.62	99
12"OD2%OV5	0.281	11.68	41.54	1.81	98
Average	0.298	11.66	39.17	1.77	99.3
12"OD5%OV1	0.304	11.68	38.46	3.56	75
12"OD5%OV2	0.293	11.66	39.75	4.59	81
12"OD5%OV3	0.291	11.71	40.28	5.35	67
12"OD5%OV4	0.293	11.66	39.77	4.72	74
12"OD5%OV5	0.302	11.62	38.523	4.19	78
Average	0.297	11.67	39.34	4.48	75.0

Table A.3 Long-term Liner Buckling Tests by Guice et al. (1993)

Test No.	*DR*	*G* (%)	*P* (psi)	T_{cr} (hr)
1	51.27	0.4174	75	0.5
2	51.09	0.2553	75	51
4	52.87	0.3408	75	68
5	52.44	0.3491	75	1.5
6	49.34	0.5986	70	33
7	52.96	0.2722	75	54
8	52.24	0.6806	69	0.2
9	53.82	0.6819	70	3
11	51.27	0.3322	70	2
12	52.39	0.4942	65	521
13	54.07	0.4261	70	136
14	52.30	0.5548	65	1056
15	53.27	0.5461	65	528
16	54.72	0.4590	60	2455
17	52.83	0.4604	60	200
18	52.44	0.2989	60	54
19	51.78	0.6722	60	2455
21	53.23	0.5979	60	494
22	52.30	0.5121	55	3272
23	54.02	0.5200	60	1536
24	53.43	0.6837	55	4349
25	55.10	0.4260	55	3384
26	53.82	0.4262	55	455
27	55.71	0.7692	55	144
28	55.90	0.4259	55	2236
29	54.02	0.5118	50	5379
31	53.57	0.4432	50	6013
32	53.86	0.3407	50	10000
33	54.02	0.5118	50	1272
34	53.32	0.4263	50	3302
35	52.83	0.4263	50	3338
36	52.98	0.5978	45	10000
37	53.77	0.5119	45	10000
38	53.18	0.7350	45	10000
39	54.58	0.5283	45	1616

Table A.4 Short-term Test Results for Liners with Ovality (Omara, 1997)

Pipe	Ovality	Ave. Thickness	P_{test} (psi)	Observed Failure Mode
5-1	5%	0.235	55.75	Buckling Failure
5-2	5%	0.231	54.25	Buckling Failure
5-3	5%	0.240	52.50	Buckling Failure
5-4	5%	0.238	49.75	Buckling Failure
5-5	5%	0.235	62.50	Buckling Failure
5-6	5%	0.235	54.50	Buckling Failure
			55.20	Average
			4.05	Standard Deviation
10-1	10%	0.240	39.25	Buckling Failure
10-2	10%	0.222	37.00	Buckling Failure
10-3	10%	0.241	37.50	Buckling Failure
10-4	10%	0.230	33.00	Buckling Failure
10-5	10%	0.236	35.00	Buckling Failure
10-6	10%	0.239	32.50	Buckling Failure
			38.71	Average
			2.43	Standard Deviation
20-1	20%	0.231	16.00	Buckling Failure
20-2	20%	0.242	14.30	Buckling Failure
20-3	20%	0.226	23.90	Buckling Failure
20-4	20%	0.235	16.90	Buckling Failure
20-5	20%	0.237	--	Pipe was leaking
20-6	20%	0.229	18.20	Buckling Failure
			17.86	Average
			3.28	Standard Deviation

Table A.5 BoRSF Short-term Liner Buckling Test Results (Zhu, 2000)

Name	Thickness (in)	ID (in)	Mean Diameter (in)	OD (in)	SDR	Buckling Pressure (psi)
8" Diameter 4.5 mm Liners						
A	0.1478	7.6835	7.8313	7.9792	53.9741	80
B	0.1507	7.6670	7.8177	7.9683	52.8872	86
C	0.1497	7.6965	7.8462	7.9958	53.4243	80
D	0.1455	7.6265	7.7720	7.9175	54.4158	88
E	0.1537	7.7095	7.8632	8.0168	52.1703	78
AVG	0.1495	7.6766	7.8261	7.9755	53.3743	82.4
8" Diameter 5.0 mm Liners						
A	0.1602	7.6335	7.7937	7.9538	49.6597	92
B	0.1622	7.5805	7.7427	7.9048	48.7451	105
C	0.1652	7.6465	7.8117	7.9768	48.2957	110
D	0.1592	7.6785	7.8377	7.9968	50.2419	115
E	0.1587	7.6475	7.8062	7.9648	50.1985	112
AVG	0.1611	7.6373	7.7984	7.9594	49.4282	106.8
8" Diameter 5.5 mm Liners						
A	0.1822	7.6120	7.7942	7.9763	43.7859	113
B	0.1763	7.6550	7.8313	8.0077	45.4121	115
C	0.1755	7.6145	7.7900	7.9655	45.3875	133
D	0.1742	7.6180	7.7922	7.9663	45.7397	115
E	0.1770	7.5960	7.7730	7.9600	44.9153	113
AVG	0.1770	7.6191	7.7961	7.9732	45.0481	117.8

Table A.5 BoRSF Short-term Liner Buckling Test Results (continued)

Name	Thickness (in)	ID (in)	Mean Diameter (in)	OD (in)	SDR	Buckling Pressure (psi)
12" Diameter 5.5 mm Liners						
A	0.2	11.4435	11.6435	11.8435	59.2175	64
B	0.202	11.4480	11.65	11.852	58.6733	60
C	0.1972	11.4585	11.6557	11.8528	60.1158	54
D	0.1973	11.477	11.6743	11.8717	60.1605	50
E	0.2048	11.476	11.6808	11.8857	58.026	36
AVG	0.2003	11.4606	11.6609	11.8611	59.2386	52.8
12" Diameter 6.5 mm Liners						
A	0.2437	11.429	11.6727	11.9163	48.9042	80
B	0.238	11.434	11.672	11.91	50.042	86
C	0.2317	11.4265	11.6582	11.8898	51.323	92
D	0.2348	11.4335	11.6683	11.9032	50.6877	105
E	0.2408	11.4085	11.6493	11.8902	49.3709	98
AVG	0.2378	11.4263	11.6641	11.9019	50.0656	92.2
12" Diameter 7.5 mm Liners						
A	0.2588	11.4180	11.6768	11.9357	46.1133	138
B	0.2612	11.4045	11.6657	11.9268	45.6675	127
C	0.2633	11.36	11.6233	11.8867	45.1392	103
D	0.2623	11.3315	11.5938	11.8562	45.195	112
E	0.2665	11.3195	11.5860	11.8525	44.4747	139
AVG	0.2624	11.3667	11.6291	11.8916	45.318	123.8

Table A.6 BoRSF Flexural Modulus Summary (Zhu, 2000)

Pipe Type	1255 (psi)	1265 (psi)	1275 (psi)	845 (psi)	850 (psi)	855 (psi)
F1	453030	540810	423910	370660	477920	385090
F2	449800	385570	523610	390620	589100	427030
F3	462040	488240	493080	415280	490340	537480
F4	429780	502280	457530	380650	533230	330960
F5	497520	478420	536530	450080	510090	476250
AVG	**459210**	**476090**	**486950**	**400640**	**477920**	**385090**

Table A.7 BoRSF Material Tensile Modulus Summary

Pipe Type	1255 (ksi)	1265 (ksi)	1275 (ksi)	845 (ksi)	850 (ksi)	855 (ksi)
F1	363.1	471.7	465.2	448.5	514.8	396.4
F2	387.8	511.7	484.5	549.9	559.9	443.9
F3	500	496.9	470.5	483.4	551.6	394.3
F4	362.2	439.7	466.4	551.2	503.5	458.1
F5	503.4	476.3	401.6	510.7	424	597.1
AVG	423.3	479.26	457.64	508.74	510.78	457.96

Table A.8 Long-term BoRSF Test Results Summary

Pipe No.	845				850				855			
	SDR	P	Time (hours)	Test Valid	SDR	P	Time (hours)	Test Valid	SDR	P	Time (hours)	Test Valid
1	55.19	39	2826.5	Good	47.59	51	2656.5	Good	44.90	56	6819.0	Bad
2	52.99	39	1051.1	Good	48.46	51	2875.5	Good	44.65	56	2012.8	Bad
3	52.99	39	51.7	Bad	49.68	51	1995.6	Good	45.42	56	1938.8	Good
4	54.44	41	4581.8	Bad	50.95	53	3831.3	Bad	44.40	58		Bad
5	56.77	41	13220.8	Bad	49.99	53	13066.0	Bad	45.16	58	942.6	Good
6	56.37	41	3449.2	Bad	47.88	53	6306.9	Bad	46.75	58	6306.9	Bad
7	54.44	43		Bad	51.28	55	147.0	Bad	46.21	60	804.6	Good
8	53.34	43	304.7	Good	47.88	55	6691.6	Bad	46.21	60	540.2	Good
9	54.07	43	22.3	Bad	51.28	55	901.5	Bad	45.42	60	880.7	Bad
10	51.28	43	13196.8	Bad	51.95	55	3424.5	Bad	45.16	60	963.3	Good
11	55.58	45	2521.4	Bad	49.68	57	488.3	Good	46.48	63	155.0	Bad
12	55.97	45	476.4	Good	47.59	57	488.8	Good	47.03	63	2711.6	Bad
13	55.19	45	419.2	Good	49.06	57	802.5	Good	46.48	63	4486.5	Bad
14	55.97	48	672.3	Good	52.64	60	219.4	Good	44.90	67	184.8	Good
15	55.97	48	881.1	Bad	50.30	60	488.8	Good	46.21	67	727.4	Good
16	54.44	48	314.1	Good	48.17	60	655.8	Good	44.90	67	15.0	Bad
17	54.81	52	25.3	Bad	46.75	64	422.0	Good	45.94	73	211.8	Good
18	55.58	52	854.3	Bad	47.03	64	629.0	Good	45.42	73	515.5	Good
19	54.44	52	209.3	Good	49.06	64	329.2	Good	45.16	73	353.9	Good
20	54.07	55	333.2	Good	48.76	70	329.2	Good	46.48	80	244.7	Good
21	53.70	55	2545.6	Bad	49.37	70	96.0	Good	46.48	80	144.3	Good
22	54.07	55	74.8	Good	50.95	70	92.7	Good	46.75	80	140.3	Good
23	52.64	58	3.0	Good	47.88	77	143.3	Good	48.17	87	46.0	Good
24	54.07	58	253.3	Good	51.95	77	210.8	Good	45.68	87	141.4	Good
25	56.37	58	8.3	Good	49.68	77	0.1	Bad	44.16	87	35.5	Good
AVG	54.59				49.43				45.78			

NOTE: All pressures are in psi.

Table A.8 Long-term BoRSF Test Results Summary (Continued)

Pipe No	1255				1265				1275			
	SDR	P	Time (hours)	Test Valid	SDR	P	Time (hours)	Test Valid	SDR	P	Time (hours)	Test Valid
1	59.20	25	3701.5	Good	50.19	41	2150.7	Good	42.75	56	7313.4	Good
2	55.86	25	1058.4	Good	48.35	41	583.7	Bad	43.53	56	3301.0	Good
3	63.63	26	8070.3	Good	49.77	43	7088.7	Good	42.45	58	10105.8	Good
4	60.40	26	4752.3	Good	48.95	43	782.0	Good	46.25	58	5415.8	Good
5	57.48	27	1198.3	Good	51.49	45	1789.4	Bad	44.02	61	406.5	Bad
6	60.71	27	503.7	Good	49.56	45	668.3	Good	43.69	61	3697.2	Good
7	60.71	27	3694.7	Bad	46.65	45	139.3	Bad	42.60	61	1827.2	Good
8	56.93	29	423.3	Good	51.05	47	692.2	Good	43.06	64	1438.1	Good
9	60.71	29	4693.3	Good	46.83	47	241.5	Good	43.86	64	2895.1	Good
10	58.62	29	2950.7	Good	50.40	47	1840.5	Good	45.36	64	1662.0	Bad
11	60.40	31	1034.5	Good	49.15	50	759.5	Good	43.06	67	1588.0	Good
12	58.33	31	2786.5	Good	47.20	50	434.4	Good	42.30	67	522.4	Good
13	61.02	31	112.8	Good	49.36	50	800.1	Good	43.86	67	2729.4	Good
14	53.36	33	453.3	Good	49.98	53	2528.8	Good	45.36	71	1619.4	Good
15	57.21	33	481.2	Good	50.19	53	794.1	Good	46.25	71	1124.4	Good
16	55.60	33	554.5	Good	49.56	53	103.6	Bad	44.85	71	965.6	Good
17	58.62	35		Bad	46.46	57	145.8	Good	43.38	75	1188.1	Good
18	58.91	35	462.0	Good	48.35	57	117.6	Good	47.35	75	1940.0	Good
19	56.39	35	285.0	Good	47.58	57	107.7	Good	40.98	75	1821.1	Good
20	58.04	37	121.2	Good	47.77	61	379.8	Good	44.18	80	41.8	Good
21	60.10	37	42.6	Good	47.02	61	31.8	Good	45.36	80	255.8	Good
22	60.10	37	82.1	Good	50.19	61	44.8	Good	41.56	80	932.8	Good
23	58.91	41	1.9	Good	48.75	66	23.2	Good	42.91	90	185.7	Good
24	58.33	41	49.2	Good	47.77	66	45.8	Good	43.22	90	99.3	Good
25	55.60	41		Bad	49.36	66	368.8	Good	42.75	90	123.8	Good
AVG	58.61				48.88				43.80			

NOTE: All pressures are in psi.

Table A.9 Material Modulus Summary of Oval Liner Tests (Seeman, 2000)

Pipe Type	Tensile		Flexural	
	5% (ksi)	0% (ksi)	5% (ksi)	0% (ksi)
F1	538	557	463.6	448.5
F2	452.6	512	452.1	497.8
F3	546.9	547	431.7	435.6
F4	474	462	484.2	448.3
F5	492.7	577.0	446.1	485.8
AVG	500.8	531.0	455.5	463.21

Table A.10 Geometry and Buckling Pressure for Oval Liner Tests (Seeman, 2000)

	specimen	SDR	computed Ovality (%)	volume-based gap (inches)	buckling pressure (psi)
0% ovality	1	40.457	0	0.056	134.0
	2	42.641	0	0.051	116.7
	3	42.930	0	0.047	124.7
	4	42.700	0	0.051	130.7
	5	41.476	0	0.052	108.7
	STD DEV	1.050	0	0.003	10.3
	AVG	42.041	0	0.051	123.0
2% ovality	1	42.127	1.94	0.055	105.0
	2	42.742	1.82	0.052	105.0
	3	39.822	1.65	0.055	90.0
	4	40.700	1.62	0.050	98.7
	5	44.542	1.81	0.053	98.0
	STD DEV	1.834	0.13	0.002	6.2
	AVG	41.987	1.77	0.053	99.3
5% ovality	1	41.178	3.56	0.048	75.0
	2	42.552	4.59	0.054	80.7
	3	43.066	5.35	0.063	67.3
	4	42.561	4.72	0.057	74.0
	5	41.229	4.19	0.052	78.0
	STD DEV	0.859	0.66	0.006	5.0
	AVG	42.117	4.48	0.055	75.0

Table A.11 Deform-reform Liner Buckling Tests Results (Chunduru, 1996)

Pipe set (1)	SDR (2)	Average outside diameter, OD_{avg} (mm) (3)	Average thickness, t (mm) (4)	Tests performed (5)	Average short-term buckling pressure, P_w (kPa) (6)	Standard deviation in P_w (kPa) (7)	Remarks (8)
1	32.5	200.7 (7.9)[a]	6.27 (0.243)[a]	20	279.9 (40.6)[b]	10.3 (1.49)	Circular[c]
2	32.5	149.9 (5.9)[a]	4.62 (0.182)[a]	20	202.7 (29.4)[b]	8.27 (1.20)	Circular
3	26	200.7 (7.9)[a]	7.65 (0.301)[a]	20	441.3 (64.0)[b]	8.69 (1.26)	Circular
4	26	149.9 (5.9)[a]	5.77 (0.227)[a]	20	319.9 (46.4)[b]	18.3 (2.65)	Circular
5	32.5	218.4 (8.6)[a]	6.34 (0.249)[a]	5	151.7 (22.0)[b]	11.0 (1.60)	Oval[c]
6	26	218.4 (8.6)[a]	7.85 (0.309)[a]	5	204.1 (29.6)[b]	10.3 (1.50)	Oval

[a] In inches.
[b] In psi.
[c] Liner processed in either circular or oval steel casing pipe.

Table A.12 Long-term HDPE Liner Test Results at Tulane University (Bakeer, 2001)

Chamber number	HDPE Liner: Diameter mm (in.)	HDPE Liner: SDR	HDPE Liner: Thickness mm (in.)	Applied pressure kPa (psi)	Time to Failure in hours: Time	Time to Failure in hours: Average	Time to Failure in hours: Standard deviation
I-1	152 (6)	32.5	5.2 (0.20)	104 (15)	2,832	1,502	1,138
I-2	152 (6)	32.5	5.2 (0.20)	104 (15)	312		
I-3	152 (6)	32.5	5.2 (0.20)	104 (15)	2,640		
I-4	152 (6)	32.5	5.2 (0.20)	104 (15)	1,632		
I-5[a]	152 (6)	32.5	5.2 (0.20)	104 (15)	96		
II-1	152 (6)	26	6.5 (0.26)	172 (25)	96	101	10
II-2	152 (6)	26	6.5 (0.26)	172 (25)	96		
II-3	152 (6)	26	6.5 (0.26)	172 (25)	96		
II-4	152 (6)	26	6.5 (0.26)	172 (25)	120		
II-5[a]	152 (6)	26	6.5 (0.25)	172 (25)	96		
III-1	203 (8)	32.5	6.8 (0.27)	151.7 (22)	144	173	56
III-2	203 (8)	32.5	6.8 (0.27)	148 (21.5)	264		
III-3	203 (8)	32.5	6.8 (0.27)	145 (21)	192		
III-4	203 (8)	32.5	6.8 (0.27)	138 (20)	96		
III-5[a]	203 (8)	32.5	6.8 (0.27)	172 (25)	167		
IV-1	203 (8)	26	8.4 (0.33)	224 (32.5)	1,104	2,318	1,386
IV-2	203 (8)	26	8.4 (0.33)	221 (32)	2,712		
IV-3	203 (8)	26	8.4 (0.33)	221 (32)	4,536[b]		
IV-4	203 (8)	26	8.4 (0.33)	221 (32)	2,640		
IV-5[a]	203 (8)	26	8.4 (0.33)	221 (32)	599		

[a]Liner pipe was filled with water.
[b]Failure was induced to prepare the chambers for test Group B.

Table A.13 Properties of HDPE Liner Long-term Test Chambers (Bakeer, 2001)

Property	Pipe Standard Diameter Ratio (SDR): SDR 32.5	SDR 26	SDR 32.5	SDR 26
Inner-diameter of steel pipe	152 mm (6 in.)	152 mm (6 in.)	203 mm (8 in.)	203 mm (8 in.)
Thickness of HDPE liner	5.18 mm (0.20 in.)	6.48 mm (0.26 in.)	6.81 mm (0.27 in.)	8.43 mm (0.33 in.)
Inner-diameter of HDPE liner	142 mm (5.59 in.)	140 mm (5.49 in.)	190 mm (7.464 in.)	186 mm (7.34 in.)
Length of steel pipe	1.83 m (72 in.)	1.83 m (72 in.)	2.44 m (96 in.)	2.44 m (96 in.)
Test chamber length after flaring	1.84 m (72.41 in.)	1.84 m (72.51 in.)	2.45 m (96.54 in.)	2.46 m (96.66 in.)
Volume of test chamber	0.03 m^3 (1,778.27 $in.^3$)	0.03 m^3 (1,716.41 $in.^3$)	0.07 m^3 (4,223.86 $in.^3$)	0.07 m^3 (4,085.64 $in.^3$)
Initial water weight in test chamber[a]	29,081 g (64.11 lb)	28,069 g (61.88 lb)	68,951 g (152.01 lb)	66,692 g (147.03 lb)

[a]Based on water density of 9.81 kN/m^3 (62.3 pcf) at 22°C (71°F).

APPENDIX B

TYPICAL ABAQUS INPUT FILES

B.1 General 3D Model Input File

```
*heading
Input file for the liner buckling analysis with the following parameters
Diameter = 8"
ovality = 3%
liner thickness = 0.178
Gap = 0.0176
#
# node generation
#
*node, input = layer_outer.inp, nset = bottom
**top end node number generation
** 1000*(Half of length)*(1ft=12inch)/((one quater of liner circumference)/10)
** 1000*(3*12)*10
*ncopy, new set = top, old set = bottom, shift, change number = 30000
0.0, 0.0, 10
0.0, 0.0, 0.0, 0.0, 0.0, 1.0, 0.0
**10/0.3
*nfill
bottom, top, 30, 1000
*element, type = s9r5
1, 1, 2001, 2003, 3, 1001, 2002, 1003, 2, 1002
**320, 639, 2639, 2641, 641, 1639, 2640, 1641, 640, 1640
*ELgen, elset = cylinder
1, 10, 2,1, 15, 2000, 1000
*Ngen, nset = mid
1, 30001, 1000
*ngen, nset = crown
21, 30021, 1000
*shell section, elset=cylinder, material = mat_1, offset = 0.5
0.178
*material, name = mat_1
*elastic
459000, 0.3
*node, input = hostpipe_g1.inp, nset = host_bottom
*ncopy, new set = host_top, old set = host_bottom, shift, change number = 30000
0.0,0.0, 10
0.0, 0.0, 0.0, 0.0, 0.0, 1.0, 0.0
*nfill
host_bottom, host_top, 30, 1000
*element, type = r3d4
501, 501, 2501, 2503, 503
*elgen, elset = host_cylinder
501, 10, 2,1, 15, 2000, 1000
**shell general section, elset=cylinder
```

```
*rigid body, elset = host_cylinder, ref node = 501
*surface definition, name = Host_inner_surf
host_cylinder, spos
*surface definition, name = liner_outer_surf
cylinder, sneg
*CONTACT PAIR,INTERACTION=smooth
 liner_outer_surf, host_inner_surf
*SURFACE INTERACTION,NAME=smooth
*boundary
501, encastre
mid, 2,6
crown,  1
crown,  3, 6
top, 3, 5
bottom, 3, 5
*RESTART,WRITE,FREQ=1
*STEP,NLGEOM,INC=1000
*STATIC
0.1,1.,1.E-15,1.E-1
*DLOAD
cylinder, p ,600
*contact print,slave=liner_outer_surf,master=host_inner_surf,freq=500
*contact print,slave=liner_outer_surf,freq=500
 CFN
*END STEP
```

B.2 Input File for 3D Modeling of Thickness Variations

```
*heading
Input file for the liner buckling analysis with the following parameters
Diameter = 8"
ovality = 3%
liner thickness = 0.178
Gap = 0.0176
#
# node generation
#
*node, input = layer_outer.inp, nset = bottom
**top end node number generation
** 1000*(Half of length)*(1ft=12inch)/((one quarter of liner circumference)/10)
** 1000*(3*12)*10
*ncopy, new set = top, old set = bottom, shift, change number = 24000
0.0, 0.0, 1.256
0.0, 0.0, 0.0, 0.0, 0.0, 1.0, 0.0
**20/0.3
*nfill
bottom, top, 24, 1000
*element, type = s9r5
1, 1, 2001, 2003, 3, 1001, 2002, 1003, 2, 1002
*ELgen, elset = cylinder
1, 60, 2,1, 12, 2000, 1000
*Ngen, nset = mid
1, 24001, 1000
*Ngen, nset = crown
121, 24121, 1000
*shell section, elset=cylinder, material = mat_1, nodal thickness, offset=0.5
*nodal thickness, input=thickness.inp
*material, name = mat_1
*elastic
459000, 0.3
*node, input = hostpipe_g1.inp, nset = host_bottom
*ncopy, new set = host_top, old set = host_bottom, shift, change number = 24000
0.0,0.0, 1.256
0.0, 0.0, 0.0, 0.0, 0.0, 1.0, 0.0
*nfill
host_bottom, host_top, 24, 1000
*element, type = r3d4
501, 501, 2501, 2503, 503
*elgen, elset = host_cylinder
501, 60, 2,1, 12, 2000, 1000
**shell general section, elset=cylinder
*rigid body, elset = host_cylinder, ref node = 501
```

```
*surface definition, name = Host_inner_surf
host_cylinder, spos
*surface definition, name = liner_outer_surf
cylinder, sneg
*CONTACT PAIR,INTERACTION=smooth
 liner_outer_surf, host_inner_surf
*SURFACE INTERACTION,NAME=smooth
*nset, nset = top
24001, 24121,1
*boundary
501, encastre
mid, 2
mid, 4
mid, 6
crown,  1
crown, 5,6
top, 3, 5
bottom, 3, 5
*RESTART,WRITE,FREQ=1
*STEP,NLGEOM,INC=1000
*STATIC
0.1,1.,1.E-15,1.E-1
*DLOAD
cylinder, p ,200
*contact print,slave=liner_outer_surf,master=host_inner_surf,freq=500
*contact print,slave=liner_outer_surf,freq=500
 CFN
*END STEP
```

B.3 Input File for Modeling 3D Circular Defects

```
*heading
Input file for the liner buckling analysis with the following parameters
Diameter = 8"
ovality = 3%
liner thickness = 0.178
Gap = 0.0176
#
# node generation
#
*node, input = layer_outer.inp, nset = bottom
**top end node number generation
** 1000*(Half of length)*(1ft=12inch)/((one quarter of liner circumference)/10)
** 1000*(3*12)*10
*ncopy, new set = top, old set = bottom, shift, change number = 48000
0.0, 0.0, 10
0.0, 0.0, 0.0, 0.0, 0.0, 1.0, 0.0
**20/0.3
*nfill
bottom, top, 48, 1000
*element, type = s4r5
1, 1, 1001, 1002, 2
**320, 639, 2639, 2641, 641, 1639, 2640, 1641, 640, 1640
*ELgen, elset = cylinder
1, 30, 1,1, 48, 1000, 1000
*Ngen, nset = mid
1, 48001, 1000
*ngen, nset = crown
31, 48031, 1000
*shell section, elset=cylinder, material = mat_1, offset=0.5
0.178
*material, name = mat_1
*elastic
229500, 0.3
*node, input = hostpipe_g1.inp, nset = host_bottom
*ncopy, new set = host_top, old set = host_bottom, shift, change number = 48000
0.0,0.0, 10
0.0, 0.0, 0.0, 0.0, 0.0, 1.0, 0.0
*nfill
host_bottom, host_top, 48, 1000
*element, type = r3d4
501, 501, 1501, 1502, 502
**320, 639, 2639, 2641, 641, 1639, 2640, 1641, 640, 1640
*elgen, elset = host_cylinder
501, 30, 1,1, 48, 1000, 1000
```

```
**shell general section, elset=cylinder
*rigid body, elset = host_cylinder, ref node = 501
*surface definition, name = Host_inner_surf
host_cylinder, spos
*surface definition, name = liner_outer_surf
cylinder, sneg
*CONTACT PAIR,INTERACTION=smooth
 liner_outer_surf, host_inner_surf
*SURFACE INTERACTION,NAME=smooth
*boundary
501, encastre
mid, 2
mid, 4
mid, 6
crown,  1
crown, 5,6
top, 3, 5
bottom, 3, 5
*RESTART,WRITE,FREQ=1
*STEP,NLGEOM,INC=1000
*STATIC
0.1,1.,1.E-15,1.E-1
*DLOAD
cylinder, p ,200
*contact print,slave=liner_outer_surf,master=host_inner_surf,freq=500
*contact print,slave=liner_outer_surf,freq=500
 CFN
*END STEP
```

APPENDIX C

TYPICAL C++ Code to Generate Host-pipe and Liner Geometry

C.1 C++ Code for Generating Liner Nodal Coordinates

```
# include <iostream.h>
# include <fstream.h>
# include <math.h>

void main()
{

   const int size = 20;
   double x[size+1], y[size+1];
   double Rmin, Rmax, diameter, Oval, thickness;
   cout << "Please input the liner Diameter and Ovality ( seperate in space)::"<< endl;
   cin >> diameter >> Oval;
   //cout << "\nPlease input the Gap value::" << endl;
   //cin >> gap;
   cout << endl;
   Rmin = ((1 - Oval)* diameter)/2;
   Rmax = diameter - Rmin;
   cout <<"the smaller radius of the liner is " << Rmin << endl;
        cout << "the larger radius of the liner is   " << Rmax << endl;
        cout << "Please input the CIPP linear thickness::" << endl;
   cin >> thickness;
   double a=Rmax-thickness*0/4;
        double b=Rmin-thickness*0/4;
        double a2=a*a;
        double b2=b*b;
        cout <<"thickness" << thickness<< endl;


   ofstream outFile("layer_outer.inp", ios::out);  // open the data file
   if ( !outFile )                  // can't open file
   {
        cerr << "File not exist or could not be opened.\n"
           <<endl;
        return;
   }


   for(  int i=0; i<=size; i++)
        {
        double cta=(90.0/size)*i*3.14159/180;
        double tg =tan(cta);
        double x1= pow(tg, 2);
        double x4= 1/(b2+a2*x1);
        double x5= pow(x4, 0.5);
```

```
        double actg=pow(1/tg, 2);
        double x7=1/(b2*actg + a2);
        double x8=pow(x7, 0.5);

        x[i]= a*b*x5;
        y[i]= a*b*x8;

   outFile << i+1<< ',' << x[i] << ',' << y[i] << endl;

        }
}
```

C.2 C++ Code for Generating Host-pipe Nodal Coordinates

```
# include <iostream.h>
# include <fstream.h>
# include <math.h>

void main()
{

  const int size =20;
  double x[size+1], y[size+1];
  double Rmin, Rmax, diameter, Oval, thickness, gap, HostRmin, HostRmax ;
  cout << "Please input the liner Diameter and Ovality ( seperate in space)::"<< endl;
  cin >> diameter >> Oval;
  cout << "\nPlease input the Gap value::" << endl;
  cin >> gap;
  cout << endl;
  Rmin = ((1 - Oval)* diameter)/2;
  Rmax = diameter - Rmin;
  cout <<"the smaller radius of the liner is " << Rmin << endl;
       cout << "the larger radius of the liner is   " << Rmax << endl;
       cout << "Please input the CIPP linear thickness::" << endl;
  cin >> thickness;
       cout <<"thickness" << thickness<< endl;
  double a=Rmax-thickness*4/4;
       double b=Rmin-thickness*4/4;
       HostRmin = Rmin + gap;
       HostRmax = ((1+Oval)/(1-Oval))*HostRmin;
       double a2=pow(HostRmax, 2);
       double b2=pow(HostRmin, 2);
       cout << "test" << HostRmax << " " << HostRmin << endl;


  ofstream outFile("hostpipe_g1.inp", ios::out);  // open the data file
  if ( !outFile )                  // can't open file
  {
      cerr << "File not exist or could not be opened.\n"
         <<endl;
      return;
  }


  for(  int i=0; i<=size; i++)
       {
       double cta=(90.0/size)*i*3.14159/180;
       double tg =tan(cta);
```

```
        double x1= pow(tg, 2);
        double x4= 1/(b2+a2*x1);
        double x5= pow(x4, 0.5);
        double actg=pow(1/tg, 2);
        double x7=1/(b2*actg + a2);
        double x8=pow(x7, 0.5);

        x[i]= HostRmin*HostRmax*x5;
        y[i]= HostRmin*HostRmax*x8;

   outFile << i+501<< ',' << x[i] << ',' << y[i] << endl;

        }

}
```

C.3 C++ Code for Generating Nodal Thickness for the Model with Thickness Variation in Both the Circumferential and Longitudinal Directions

```
# include <iostream.h>
# include <fstream.h>
# include <math.h>

void main()
{

   const int size = 900;
   double thickness[size];
   double T, deltaT, number_rows, number_col, beginning_phase_cir,
beginning_phase_long;
   cout << "Please input the liner thickness T::"<< endl;
   cin >> T;
   cout << "\nPlease input the maximum thickness variation deltaT::" << endl;
   cin >> deltaT;
        cout << "\nPlease input the number of nodes on circumference::" << endl;
   cin >> number_rows;
        cout << "\nPlease input the number of nodes on length::" << endl;
   cin >> number_col;
        cout << "\nPlease input the beginning_phase of circumferential direction::" <<
endl;
   cin >> beginning_phase_cir;
        cout << "\nPlease input the beginning_phase of longitudinal direction::" << endl;
   cin >> beginning_phase_long;
   cout << endl;


   ofstream outFile("thickness.inp", ios::out);  // open the data file
   if ( !outFile )                 // can't open file
   {
        cerr << "File not exist or could not be opened.\n"
           <<endl;
        return;
   }


   for(  int i=0; i<number_rows; i++)
        {
                double sum =0;
                double alfa_cir;
                alfa_cir = beginning_phase_cir+12*3.14159/(number_rows-1)*i;

                for (int j = 0; j < number_col; j++)
```

```
                {
                        double alfa_long;
                        alfa_long = beginning_phase_long+ 1*3.14159/(number_col-1)*j;
                        thickness[j] = T + deltaT * sin(alfa_cir+ alfa_long);

                        sum += thickness[j];


                }
                for (int x = 0; x < number_col; x++)
                {
                        double thick;
                        thick  = T*number_col*thickness[x]/sum;
                        outFile<< i +1  + x * 1000 << ',' << thick << endl;


                }

                outFile << endl;

        }

}
```

C.4 C++ Code for Generating Nodal Thickness of Models with Circular Thickness Defects

```
# include <iostream.h>
# include <fstream.h>
# include <math.h>

void main()
{

   const int size = 3000;
        double Length;
        cout << "Input the LENGTH of the model::" << endl;
        cin >> Length;
   double thickness[size];
        double d = 8.0;
        double num_nodes_long, num_nodes_cir;
        cout << "Input the NUMBER of nodes along length::" << endl;
        cin >> num_nodes_long;
        cout << "Input the NUMBER of nodes along circumference::" << endl;
        cin >> num_nodes_cir;
        double weak_point_dia_fra;
        cout << "Input the FRACTION of the weak point diameter to liner diameter::" <<
endl;
        cin >> weak_point_dia_fra;
        double T;
        T = 0.178;
        double deltaT, deltaT_fra;
        cout << "Input the maximum THICKNESS VARIATION::" << endl;
        cin >> deltaT_fra;
        deltaT = T * deltaT_fra;
        int num_element_long = (num_nodes_long -1) ;
        double element_length = Length/num_element_long;
        int num_element_cir = (num_nodes_cir-1);
        double element_wideth = 3.14*d/4.0/num_element_cir;

        double beginning_phase_cir, beginning_phase_long;
        beginning_phase_cir = 0;
        beginning_phase_long = 0;

  ofstream outFile("thickness.inp", ios::out);  // open the data file
        ofstream outFile1("weakpoint_nodes.inp", ios::out);
  if ( !outFile )                  // can't open file
  {
       cerr << "File not exist or could not be opened.\n"
```

```
            <<endl;
        return;
    }

        int count = 10;
    for( int i=0; i<num_nodes_long; i++)
        {


                int max_points_cir = ceil(d*weak_point_dia_fra/element_wideth);
                int max_points_long = ceil(d*weak_point_dia_fra/element_length);

                for (int j = 1; j <= num_nodes_cir; j++)
                {

                        double dis_cir = (num_nodes_cir -j) * (element_wideth);
                        double dis_long = i *element_length;
                        double dis;
                        dis = sqrt ( dis_cir*dis_cir + dis_long * dis_long);
                        if (dis <= d*weak_point_dia_fra/2.0){
                                double ratio = dis / (d*weak_point_dia_fra/2.0);
                                double alfa;
                                alfa = -1.57+ratio * (1.57);
                                thickness[j] = T + deltaT*sin(alfa);


                                outFile << j  + i * 1000 << ',' << thickness[j] << endl;



                        }
                        else outFile << j + i*1000 << ',' << 0.178 << endl;

                }


        }


}
```

C.4 C++ Code for Generating Nodal Coordinates of Models with Circular Material Defects

```
# include <iostream.h>
# include <fstream.h>
# include <math.h>

void main()
{

   const int size = 3000;
        double Length;
        cout << "Input the LENGTH of the model::" << endl;
        cin >> Length;
   double thickness[size];
        double d = 8.0;
        double num_nodes_long, num_nodes_cir;
        cout << "Input the NUMBER of nodes along length::" << endl;
        cin >> num_nodes_long;
        cout << "Input the NUMBER of nodes along circumference::" << endl;
        cin >> num_nodes_cir;
        double weak_point_dia_fra;
        cout << "Input the FRACTION of the weak point diameter to liner diameter::" <<
endl;
        cin >> weak_point_dia_fra;
        double T;
        T = 0.178;
        int num_element_long = (num_nodes_long -1) ;
        double element_length = Length/num_element_long;
        int num_element_cir = (num_nodes_cir-1);
        double element_wideth = 3.14*d/4.0/num_element_cir;




        double beginning_phase_cir, beginning_phase_long;
        beginning_phase_cir = 0;
        beginning_phase_long = 0;


   ofstream outFile("weak_point.inp", ios::out);  // open the data file
        ofstream outFile1("normal_area.inp", ios::out);
   if ( !outFile )                  // can't open file
   {
        cerr << "File not exist or could not be opened.\n"
```

```
            <<endl;
        return;
    }

        int count = 10;
        int wp_ele_count =1;
        int na_ele_count =1;
    for( int i=1; i<=num_nodes_long; i++)
        {


                int max_points_cir = ceil(d*weak_point_dia_fra/element_wideth);
                int max_points_long = ceil(d*weak_point_dia_fra/element_length);

                for (int j = 2; j <= num_nodes_cir; j++)
                {

                        double dis_cir = (num_nodes_cir -j) * (element_wideth);
                        double dis_long = i *element_length;
                        double dis;
                        dis = sqrt ( dis_cir*dis_cir + dis_long * dis_long);
                        if (dis <= d*weak_point_dia_fra/2.0){


                                outFile << (j-1)  + (i-1) * 1000  ;
                                if (wp_ele_count % 16 ==0) outFile << endl;
                                else outFile << ',';
                                wp_ele_count++;

                        }
                        else{
                                outFile1 << (j-1) + (i-1)*1000  ;
                                if (na_ele_count % 16 ==0) outFile1 << endl;
                                else outFile1 << ',';
                                na_ele_count++;
                        }
                }

        }
}
```

APPENDIX D

SAS PROGRAM

D.1 SAS Input Program for One-variable Regression of 12-inch Liners with a DR of 55

```
// EXEC SAS
//SAS.SYSIN DD *
OPTIONS NOCENTER;
DATA ONE;
INPUT P T;
LP = LOG10 (P);
LT = LOG10 (T);
CARDS;
25 3701.5
25 1058.4
26 8070.3
26 4752.3
27 1198.3
27 503.7
29 423.3
29 4693.3
29 2950.7
31 1034.5
31 2786.5
31 112.8
33 453.3
33 481.2
33 554.5
35 462.0
35 285.0
37 121.2
37 42.6
37 82.1
41 1.9
41 49.2
*  10000
;
PROC GLM;
MODEL LP =LT/ CLI;
OUTPUT OUT=NEW H=LEVERAGE COOKD = D DFFITS=DF COVRATIO =
COVR;
PROC PRINT DATA=NEW;
PROC GLM;
MODEL LP = LT/ CLI;
OUTPUT  OUT = NEW1 RESIDUAL = RES PREDICTED = PRED STUDENT=S;
PROC STANDARD STD = 1.0;
VAR RES;
PROC RANK NORMAL = BLOM;
```

```
VAR RES;
RANKS NSCORE;
PROC PLOT;
RANKS NSCORE;
PROC PLOT;
PLOT RES*PRED='+';
PLOT RES*NSCORE = '$';
PLOT PRED*S = '&';
```

D.2 SAS Input Program for Two-variable Regression of 12-inch Liners

```
// EXEC SAS
//SAS.SYSIN DD *
DATA LINER;
*INFILE 'G:\RESEARCH\STATISTICS\SAS-DATA.TXT';
OPTIONS NOCENTER;
DATA LINER;
INPUT DR P T;
LP = LOG10 (P);
LT  = LOG10(T);
CARDS;
58.65 25 3701.5
58.65 25 1058.4
58.65 26 8070.3
58.65 26 4752.3
58.65 27 1198.3
58.65 27 503.7
58.65 29 423.3
58.65 29 4693.3
58.65 29 2950.7
58.65 31 1034.5
58.65 31 2786.5
58.65 31 112.8
58.65 33 453.3
58.65 33 481.2
58.65 33 554.5
58.65 35 462.0
58.65 35 285.0
58.65 37 121.2
58.65 37 42.6
58.65 37 82.1
58.65 41 49.2
48.85 41 2150.7
48.85 43 7088.7
48.85 43 782.0
48.85 45 668.3
48.85 47 692.2
48.85 47 241.5
48.85 47 1840.5
48.85 50 759.5
48.85 50 434.4
48.85 50 800.1
48.85 53 2528.8
48.85 53 794.1
```

```
48.85 57 145.8
48.85 57 117.6
48.85 57 107.7
48.85 61 379.8
48.85 61 31.8
48.85 61 44.8
48.85 66 23.2
48.85 66 45.8
48.85 66 368.8
43.78 56 7313.4
43.78 56 3301.0
43.78 58 5415.8
43.78 61 3697.2
43.78 61 1827.2
43.78 64 1438.1
43.78 64 2895.1
43.78 67 1588.0
43.78 67 522.4
43.78 67 2729.4
43.78 71 1619.4
43.78 71 1124.4
43.78 71 965.6
43.78 75 1188.1
43.78 75 1940.0
43.78 75 1821.1
43.78 80 41.8
43.78 80 255.8
43.78 80 932.8
43.78 90 185.7
43.78 90 99.3
43.78 90 123.8
;
PROC REG DATA = LINER;
  MODEL LT = LP DR /I CORRB COVB XPX INFLUENCE;
OUTPUT OUT = TEMP PREDICTED = PTIME RESIDUAL = RES;
PROC STANDARD STD = 1.0;
  VAR RES;
PROC RANK NORMAL = BLOM;
PROC STANDARD STD = 1.0;
  VAR RES;
PROC RANK NORMAL = BLOM;
   VAR RES;
RANKS NSCORE;
PROC PLOT;
   PLOT RES*PTIME='+';
   PLOT RES*NSCORE = '$';
```